University of Alberta

Achieving High Rates and High Uniformity in Copper Chemical Mechanical Polishing

by

Lucy Marjorie Nolan

A thesis submitted to the Faculty of Graduate Studies and Research in partial fulfillment of the requirements for the degree of

Doctor of Philosophy

in

Materials Engineering

Department of **Chemical and Materials Engineering**

© Lucy Marjorie Nolan
Spring 2012
Edmonton, Alberta

Permission is hereby granted to the University of Alberta Library to reproduce single copies of this thesis and to lend or sell such copies for private, scholarly or scientific research purposes only. Where the thesis is converted to, or otherwise made available in digital form, the University of Alberta will advise potential users of the thesis of these terms.

The author reserves all other publication and other rights in association with the copyright in the thesis, and except as hereinbefore provided, neither the thesis nor any substantial portion thereof may be printed or otherwise reproduced in any material form whatever without the author's prior written permission.

Dedication

To my wonderful husband Chris, who makes every day better than the last ...

And to my parents, Jane and Ossie, and my siblings, Jessica, Patrick and Belinda. With you in my heart, I am never too far from home.

Abstract

The chemical mechanical polishing of Copper (Cu-CMP) is a complex and poorly understood process. Despite this, it is widely used throughout the semiconductor and microelectronics industries, and makes up a significant portion of wafer processing costs. In these contexts, desirable polishing outcomes such as a high rate of removal from the copper surface, and high removal rate uniformity, are achieved largely by trial-and-error. In this study, the same outcomes are pursued through a systematic investigation of polishing lubrication characteristics and abrasive and oxidiser concentrations in the polishing slurry. A strong link between lubrication characteristics, quantified by the dimensionless Sommerfield number, and the uniformity of polishing is demonstrated. A mechanism for the observed relationship is proposed, based on an adaptation of hydrodynamic lubrication theory. The overall rate of removal is maximised by polishing in a slurry containing oxidiser and abrasives in a synergistic ratio. Polishing away from this ratio has additional effects on the overall quality of the surface produced. Transport of slurry across the polishing pad is investigated by using tracers; the results demonstrate that slurry usage can be

reduced in many circumstances with no impact on overall polishing outcomes, reducing overall processing costs. These findings are combined to design a polishing process, with good results.

Acknowledgements

No man, or woman, is an island, and this thesis was not produced in isolation. I would like to gratefully acknowledge my supervisor, Dr Kenneth Cadien, for his assistance, encouragement and patience. I would also like to thank the faculty, staff and students of the Department of Chemical and Materials Engineering. My fellow students have been a constant source of support, relief and new ideas. Lily Laser, Randy Reichardt, Kevin Heidebrecht and Les Dean all provided fundamental administrative and technical assistance to me. Finally, I am very grateful to the staff of NanoFab, the Integrated Nanosystems Research Facility (INRF) and Micralyne, particularly Les Schowalter, Shiau-Yin Wu and Dean Spicer. Without their expertise, this would have never made it off the drawing board. I would additionally like to acknowledge the financial assistance I received from the Natural Sciences and Engineering Research Council of Canada, Alberta Innovates - Technology Futures and the University of Alberta.

Contents

1 Introduction **1**

1.1 Problem Statement 1

1.2 Literature Review 4

1.2.1 The Preston Equation 4

1.2.2 Cook's "Chemical Tooth" 6

1.2.3 Current Research in Cu-CMP 7

1.3 Goals of This Work 11

1.4 Outline of this Thesis 11

2 Experimental Procedures **13**

2.1 Wafer Preparation and Polishing 13

2.1.1 Wafer Preparation 15

2.1.2 Slurry Preparation 16

2.2 Pad and Wafer Rotational Velocity 18

2.3 Friction Measurement 22

2.4 Additional Characterisation Techniques 26

2.4.1 Atomic Force Microscopy (AFM) 26

2.4.2 Transmission Electron Microscopy (TEM) 26

3 Polish Rate Uniformity as a Function of Lubrication **28**

3.1 Introduction 28

3.1.1 Lubrication, the Sommerfield Number and the Stribeck Curve 28

3.1.2 Lubrication Theory in Cu-CMP Research 32

3.1.3 Previous Studies of Within-Wafer-Non-Uniformity (WI-WNU) 39

3.2 Experimental Procedures 42

3.3 Results and Discussion 43

3.3.1 Modeled Film Thickness, Wafer Tilt and Radial Pressure Distribution 43

3.3.2 MRRNU as a Function of Lubrication 46

3.3.3 Hydrodynamic Pressure and the MRR Profile 51

3.4 Conclusions 59

3.4.1 Future Work 59

4 Polish Rate as a Synergistic Interaction of Mechanical Abrasion and Chemical Reaction Rate 61
4.1 Introduction 61
4.1.1 Slurry Components and Their Roles in CMP 61
4.1.2 Slurry Component Interactions 65
4.1.3 Effect of Abrasive Concentration on Material Removal Rate 70
4.2 Experimental Procedures 72
4.3 Results and Discussion 74
4.3.1 Material Removal Rate MRR 74
4.3.2 Coefficient of Friction CoF 84
4.4 Conclusions 84
4.4.1 Future Work 86

5 Optimal Delivery of Slurry to the Polishing Interface 88
5.1 Introduction 88
5.1.1 Slurry Utilization in CMP 89
5.2 Experimental Procedures 94
5.2.1 Flow Field Characterisation (Ink Tests) 94
5.2.2 Polishing Tests 96
5.3 Results and Discussion 97
5.3.1 Flow Field Characteristics (Ink Tests) 97
5.3.2 Impact of Flow Rate on Polishing Outcomes 111
5.4 Conclusions 113

6 Maximising Rate and Uniformity in Cu-CMP 115
6.1 Introduction 115
6.2 Design Method 116
6.2.1 Slurry Chemistry 116
6.2.2 Applied Pressure and Velocity - MRRNU 117
6.2.3 Slurry Flow Rate q_{input} 118
6.3 Experimental Method 119
6.4 Results and Discussion 119
6.5 Conclusions 121

7 Conclusions 125
7.1 Future Work 127

Bibliography 129

Appendices

A MATLAB Code for Relative Velocity Calculations 135

B Motor and Gearbox Data Sheets 138

C MATLAB Code for Evaluating Model of Pressure Distribution **142**

List of Tables

2.1 Slurry components used in this work 17

3.1 Comparison of model results for a wafer with a dome height of 10μm, polished with an applied pressure of 7 psi at a relative linear velocity of 0.314 m/s in a fluid of viscosity 21.4 mPa.s. . . 39
3.2 Summary of polishing conditions 43
3.3 Slurry composition 43
3.4 Sommerfield number So for each set of polishing conditions described in table 3.2 45

4.1 Slurry components and their roles 64
4.2 Concentrations of H_2O_2 and SiO_2 for polishing conditions A0 to F5. Each set of polishing experiments was carried out at an applied pressure of 4 psi and rotational speed of 60rpm (1.07 m/s), and the slurry additionally contained 1 wt% glycine, 1mM BTA, and sufficient citric acid to adjust the pH to 3.55. 73

5.1 Summary of polishing conditions 96
5.2 Slurry composition used at 200mL/min and diluted as described at higher flow rates 97
5.3 Summary of polishing conditions 114

6.1 Slurry composition 116
6.2 Polishing conditions used in this study, including mean measured wafer dome heights h_D and corresponding calculated slurry film thicknesses. 120

List of Figures

1.1 Schematic diagram of a rotary CMP apparatus, showing the a) top view and b) side view of the tool. 2
1.2 Step-by-step schematic of the Copper damascene process (reproduced from [1] with permission). 3
1.3 Cross section of an eight-layer device (reproduced from [1] with permission). CMP is used to planarize each level before the next is constructed. 3
1.4 MRR vs. PxV data for copper CMP. All polishing was conducted using the same pad and slurry, with the exception that the abrasive diameter was approximately 120nm for Series A, 20nm for Series B, and 85nm for Series C and D. The Preston equation is fit to the data in a), and linear or sublinear curves are fit to the data in b). 9

2.1 Axus 372M Polisher 14
2.2 Schematic of the 9-point film thickness measurement jig. 17
2.3 Comparison of particle sizes and distributions for SP599 silica particles analysed using a) transmission electron microscopy and b) dynamic light scattering. 19
2.4 Velocity field across the wafer surface for four combinations of pad and wafer speeds. The centre-to-centre offset distance is 0.17m in these simulations, and the wafer radius is 50mm. 21
2.5 Schematic diagram of the tool and data collection system used in this work. 24

3.1 Modes of load transfer between the pad and wafer during polishing. The applied pressure can be transferred by direct contact between the pad and wafer (a), through the polishing fluid (c), or by a combination of both (b). This figure is drawn to scale using actual profilometry data from a polishing pad. The abrasives are drawn with a diameter of 150nm. 29
3.2 Schematic Stribeck curve, showing three distinct zones of lubrication; boundary lubrication (a), mixed lubrication (b) and hydrodynamic lubrication (c). 31

3.3 Experimentally-obtained Stribeck curves for polishing interlayer dielectrics with a variety of pads at a slurry abrasive loading of a) 2.5% and b) 25% (from [2], ©2003 The Japan Society of Applied Physics). 33
3.4 Experimentally-obtained Stribeck curves for polishing copper with a concentrically-grooved and flat pad (as labeled) (from [3], reproduced by permission of ECS - The Electrochemical Society). 34
3.5 Schematic representation of a convex wafer, in which the centre of the wafer protrudes past its edges into the pad / wafer interface. 38
3.6 Measured pressure distributions for non-rotating (a) and rotating (b) wafers during CMP (from [4]). 39
3.7 Relationship between measured dome height h_D and modeled values of h_m and α. The relationship between h_D and α is projected onto the x-y plane for clarity. 44
3.8 Radial pressure distribution for all wafers, labeled by polishing conditions used. 45
3.9 Radial pressure distributions for wafers M4-02 and M4-4, with dome heights of 270nm and 1255nm respectively. 46
3.10 Radial MRR distribution for all polishing conditions given in Table 3.2. 47
3.11 Radial MRR distributions, re-plotted in order from most to least lubricating. The Sommerfield numbers for each set of polishing conditions are also shown. 49
3.12 MRRNU vs. *So* for a) the polishing conditions outlined in Table 3.2 and b) the polishing conditions outlined in Table 3.2, and similar studies carried out with abrasives of diameter D=120nm and D=20nm, and with a commercial Cabot® slurry. 50
3.13 Plot of the slope of the MRRNU - *So* curve against abrasive particle diameter for slurries with otherwise identical compositions. 52
3.14 MRR profile and modeled pressure distribution for polishing at conditions a) M3, b) N1 and c) N3. The Preston coefficient for each point is also shown. The shaded regions indicate regions of hydrodynamic lubrication. 53
3.15 The MRR profiles shown in Figure 3.11, with the suppression, hydrodynamic and edge zones indicated. 54
3.16 TEM micrographs of abrasive particles a) prior to polishing (250,000x); particle sizes are labeled and range from 30nm to 80nm b) after polishing (250,000x); particle dimensions are 230nm by 185nm and small 'studs' of a second material are present on the abrasive, and c) a close-up of b) (500,000x), showing the 'studs' in more detail. 56

3.17 Distribution of MRR for oxide polishing, showing considerable MRRNU, obtained by Shan, Zhou and coworkers (from [5], ©[2001] IEEE). Their data were obtained at a constant pressure a velocities ranging from 0.2m/s (representing a low Sommerfield number)to 0.7m/s (representing a high Sommerfield number). 58

4.1 Schematic diagram of the passivation-abrasion mechanism proposed by Kaufman et al [6] for the removal of material in metal CMP (adapted from [1]). 62
4.2 Pourbaix diagrams for the copper-BTA system with a) no BTA, b) {a_{BTA}}=10^{-4}, and c) {a_{BTA}}=10^{-4} (from [7]) 63
4.3 Structural formulae for benzotriazole (BTA), glycine and citric acid. 64
4.4 Potentiodynamic scans of copper in a buffered, pH 4 solution of 10g/L of Na_2SO_4 (open circles) and 10g/L of Na_2SO_4 with 3 vol% H_2O_2 (from [8]). 66
4.5 Removal rates of copper by varying concentrations of H_2O_2, in static (etch rate) and polishing conditions (from [9]). 67
4.6 Anodic current transient (0.1V) of copper in 3 wt% solution of nitric acid. 0.02M of BTA is added at the point indicated; the anodic current immediately drops (from [10]). 67
4.7 AFM images of the copper surface after polishing with 30 wt% H_2O_2 and Rodel® XJFW8099 slurry mixed in a a) 1:1 ratio and b) 1:4 ratio (from [11]). 70
4.8 Effect of particle concentration on a) W-CMP (from [12]) and b) Cu-CMP (replotted from [13]). 71
4.9 Effect of SiO_2 concentration on MRR, without the presence of H_2O_2. 74
4.10 AFM images and sections for copper films polished in a slurry containing 11.8 wt% colloidal SiO_2 particles, polished at a) an applied pressure of 4psi and rotational speed of 30rpm (relative velocity = 0.53m/s), and b) an applied pressure of 8psi and rotational speed of 60rpm (relative velocity = 1.07m/s). Each scan is $10\mu m \times 10\mu m$ 76
4.11 AFM image of a wafer in the as-sputtered condition. 77
4.12 Effect of H_2O_2 concentration on MRR, without the presence of abrasives. 78
4.13 Optical image of a wafer polished with an applied down pressure of 6 psi and a rotational speed of 30rpm (relative velocity = 0.53m/s) in a solution containing 1mM BTA, 1 wt% glycine and citric acid as indicated, and 1 wt% H_2O_2. 79

4.14 Surface plot of measured polishing rate for varying concentrations of H_2O_2 and abrasives. The colour bar represents material removal rate, MRR, in nm/min. All results were obtained at an applied pressure of 4 psi and a rotational speed of 60rpm (1.07m/s). 80
4.15 Contour map of polishing rate at all concentrations of H_2O_2 and abrasives. The colour bar represents material removal rate, MRR, in nm/min. 81
4.16 Schematic representation of abrasion-dominated, passivation dominated and synchronised polishing mechanisms. 83
4.17 AFM images of wafers polished at a) location A, b) location B and c) location C in figure 4.15. All scans are 1μm × 1μm. . . . 85
4.18 Map of measured CoF, represented by the colour bar, for varying concentrations of H_2O_2 and abrasives. No strong trends were observed. 86
4.19 Correlation between MRR and CoF for a) conditions A0 to F5 in this work and b) Li, Ina and coworkers [14]. 87

5.1 Variation of slurry utilization with flow rate for four combinations of high and low relative linear velocity, and high and low applied pressure (redrawn from [15]). 91
5.2 Variation of slurry flow rate in the pad/wafer interface with input flow rate with an applied pressure of 2psi. 92
5.3 Photograph of the wafer carrier during polishing, with the bow wave indicated. 93
5.4 Sample data point for Pad 1, 30rpm, 400mL/min, approximately one second after ink was injected into the slurry stream. The frame has been overlaid with a polar grid and the position of the ink tracer noted. 95
5.5 θ(t) data for a) pad 1 at 30rpm and b) pad 1 at 60rpm. All data are shown on the same axes to aid comparison. 99
5.6 θ(t) data for c) the bare platen (plane) at 30rpm and d) pad 2 at 60rpm. All data are shown on the same axes to aid comparison. 100
5.7 r(t) data for the bare platen at a) 30rpm and b) 60rpm. The axes are the same on both plots to allow for comparison. 101
5.8 r(t) data for Pad 1 at a) 30rpm and b) 60rpm. The axes are the same on both plots to allow for comparison. 102
5.9 r(t) data at 30rpm for a) Pad 2: Plane and b) Pad 2: Groove. The axes are the same on both plots to allow for comparison. . . 103
5.10 r(t) data at 60rpm for a) Pad 2: Plane and b) Pad 2: Groove. The axes are the same on both plots to allow for comparison. . . 104
5.11 Initial radial velocity $v_{r,0}$ as a function of flow rate at a) 30rpm and b) 60rpm. 106

5.12 Radial acceleration a_r as a function of flow rate at a) 30rpm and b) 60rpm. 107
5.13 Shear force τ across the pad surface, normalised by the film thickness t. 110
5.14 Schematic of alternative slurry paths, demonstrating the incursion of fresh or old slurry into the polishing interface. 112

6.1 Contour map of MRRNU at varying concentrations of H_2O_2 and abrasives. The colour bar represents MRRNU. All results were obtained as outlined in Chapter 4. 117
6.2 Polish rate profiles obtained for conditions T1 and T2. The error bars represent ± 1 standard deviation. 122
6.3 MRRNU vs. $\log So$ for conditions T1, T2 and D4. The line shown is a logarithmic fit to the data, with a correlation coefficient of 0.86. 123

1

Introduction

1.1 Problem Statement

Chemical Mechanical Polishing, or CMP, is a technique used by the semiconductor industry to planarize surfaces and remove material from them. In it, a wafer to be polished is rotated and pressed against a rotating polishing pad, while a polishing slurry is fed on to the pad. This is shown schematically in Figure 1.1. The slurry contains chemicals which modify the wafer surface, and small abrasives which mechanically remove it. The combined chemical and mechanical action of the system is the basis of the polishing action.

Copper CMP (Cu-CMP) is the chemical mechanical polishing of copper surfaces. It is used primarily in the damascene fabrication of interconnects. These are formed by depositing an overburden of copper on to a patterned substrate and using CMP to remove the excess, leaving copper in the trenches only. This is shown schematically in Figure 1.2. The use of Cu-CMP allows multi-layer devices to be fabricated, such as the device shown in Figure 1.3.

Successful polishing requires rapid and uniform copper removal. Expanded use of this technique required fundamental insight into the mechanisms behind removal, to allow Cu-CMP protocols to be designed *a priori*. This thesis addresses the development of non-uniform polishing rates across the surface

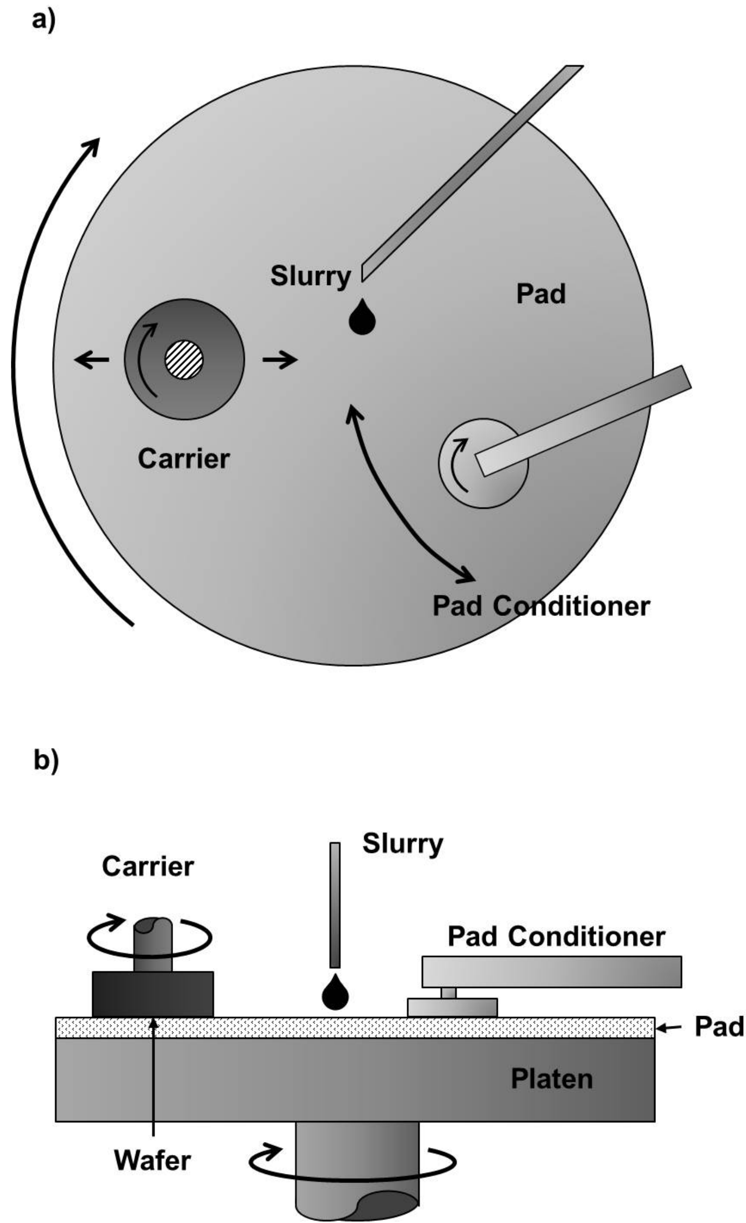

Figure 1.1: Schematic diagram of a rotary CMP apparatus, showing the a) top view and b) side view of the tool.

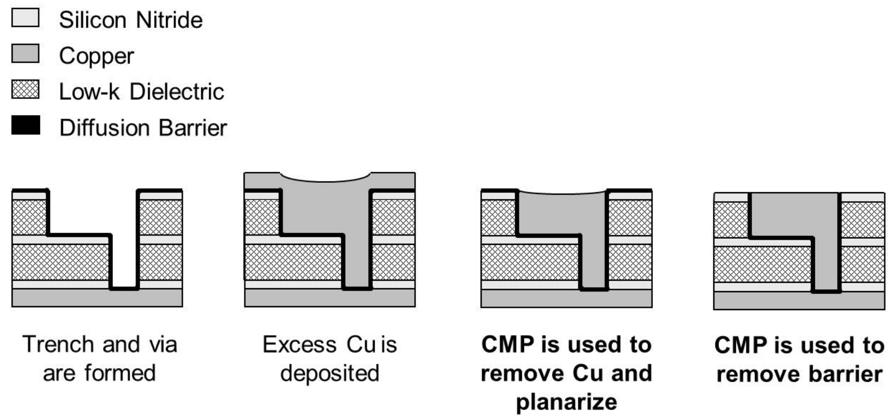

Figure 1.2: Step-by-step schematic of the Copper damascene process (reproduced from [1] with permission).

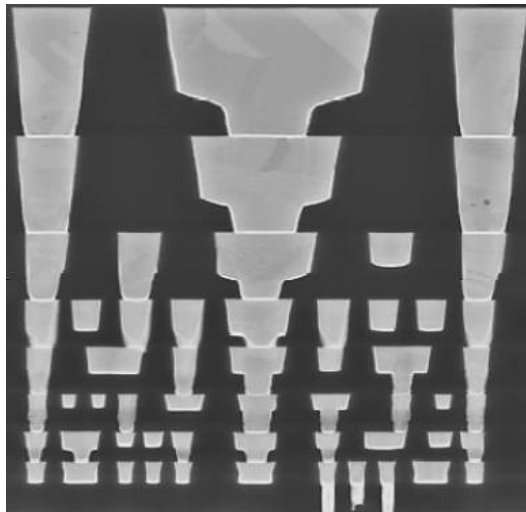

Figure 1.3: Cross section of an eight-layer device (reproduced from [1] with permission). CMP is used to planarize each level before the next is constructed.

of a wafer, and the interaction of the chemical and mechanical components of the slurry to maximise the overall polishing rate. Utilization of slurry during polishing is also addressed.

1.2 Literature Review

Chemical Mechanical Polishing was introduced into semiconductor manufacturing in 1983 as an adaptation of silicon substrate polishing [16]. At the time, it was developed to planarise wafers following a re-flown glass technique for isolating areas of the wafer from each other. This technique was never adapted commercially, but the CMP process was shown to be successful and was introduced into other areas of manufacture. Perhaps as a legacy from its beginnings as a glass processing technique, CMP research has been heavily influenced by the glass industry. Preston's 1927 treatment of glass polishing [17] and Cook's 1990 model of glass removal by a "chemical tooth" [18] have formed the basis for much of the research surrounding CMP, both for glassy materials such as silicon oxide, and for metals such as copper. Neither of these works have proven satisfactory in explaining the more complex behaviour of metal CMP, sparking a large number of alternative theories, none of which have achieved wide acceptance. However, due to the importance of both the Preston and Cook models in informing Cu-CMP research, they are both discussed here in detail. Current research is then examined, and several of the proposed models for removal are also discussed.

1.2.1 The Preston Equation

Preston's seminal paper on glass polishing [17] proposed the following relationship between the polish rate and the pressure and relative linear velocity applied to the polishing couple:

$$MRR = K_p \times PV \tag{1.1}$$

In this equation, known as the Preston equation, the material removal rate MRR is proportional to the product of the pressure P and velocity V. The constant of proportionality, K_p, is experimentally determined and encompasses all other parameters that may influence polishing, such as the composition of the polishing slurry or the relative hardness of the surfaces involved. This simple relationship is based on the principle that the amount of material removed from the surface is proportional to the amount of mechanical work done on that surface. Notably, this relationship implies that the rate of material removal is zero unless mechanical work is done on the surface.

The Preston equation has a number of limitations which hinder its usefulness and applicability, especially in the special case of Copper CMP. Preston did not, in his paper, cite any experimental evidence as to the veracity of Equation 1.1. The paper deals mainly with the distribution of work on glass surfaces in industrial glass polishing apparatus, with the assumption that, given Equation 1.1, an even distribution of work would result in even polishing. Moreover, in the apparatus he is concerned with, the glass is placed on the bottom of the polishing couple and is the larger of the two surfaces, taking the place of the polishing pad in CMP apparatus. Polishing is therefore the result of intermittent contact with the upper surface (the "runner" in Preston's work, or the wafer in CMP). This is in contrast to CMP, where the surface of interest is in constant contact with the pad and is continuously polished. Finally, he offers no insight into the value of the constant K_p, except that it is constant for a given apparatus, and is related to the coefficient of friction μ. It is therefore implicit in Equation 1.1 that μ is constant. The validity

or otherwise of this assumption will be discussed in more detail in Chapter 3. In practice, K_p must be determined experimentally for each combination of CMP tool, polishing slurry, polishing pad and wafer material that is used. This prohibits the use of Equation 1.1 for *a priori* design of CMP processes, limiting its use to the adjustment of existing processes only.

Despite this, Preston's equation is widely used in CMP of both oxide and metallic materials, with a variety of proposed modifications. A number of these will be examined in section 1.2.3.

1.2.2 Cook's "Chemical Tooth"

Cook reexamined the glass polishing process in 1990. Unlike Preston's investigation of polishing, which is mechanical in nature, Cook [18] postulates in his work that polishing is due to a combination of mechanical and chemical factors. This makes it one of the first true chemical-mechanical models of polishing. In his work, the discrepancies between values of K_p predicted by contact mechanics and those actually observed are first demonstrated. Cook then notes the strong correlation between polish rate and the density of chemically active sites on the surface of various abrasives. From this, a mechanism for material removal is proposed in which the glass surface is softened and hydrolysed by the pH of the slurry and the presence of hydroxyl groups. Individual silica tetrahedra are then removed from the surface as they make contact with, and chemisorb on to, abrasive particles. The efficacy of polishing is therefore dependent on the formation of chemical bonds between the abrasives and the polished surface, and the strength of those bonds being sufficient to remove the adsorbed material when the particle moves away from the surface. This process is termed "chemical tooth", implying that both mechanical and chemical phenomena are necessary to achieve polishing.

Cook's model addresses many of the shortcomings of the Preston equation. By including dissolution processes, which are a function of the slurry chemistry, in the chemical action of polishing, there is no longer the requirement that the polish rate is zero when either the pressure or velocity are zero. The notion of "Chemical tooth" also allows for the possibility that material is redeposited on to the polished surface. This effect is countered in practice by introducing chemical species that chelate strongly with the hydrated silica removed during polishing to prevent it from redepositing, with good results. Similar behaviour has been observed in Cu-CMP, with redeposited cuprous oxides and hydroxides found on polished surfaces [19]. Chelating agents are also an important part of Cu-CMP slurries, and have been shown to increase polishing rates substantially [20, 21, 22]. Cook's model initiated an intense interest in the surface chemistry in Cu-CMP, including surface adhesion effects [23, 24], colloidal effects [25] and surfactants [26].

While greatly enhancing our understanding of polishing processes, the "Chemical Tooth" model is qualitative in nature and cannot be used to predict or calculate the polishing rate. It was also developed for glass polishing, and does not take into account the electrochemical aspects of polishing copper or other metals.

1.2.3 Current Research in Cu-CMP

As mentioned in section 1.2.1, a major limitation of the Preston equation is the implication that the polishing rate is zero at zero applied pressure or relative linear velocity. Removal rate vs. PxV data for Cu-CMP is shown in Figure 1.4. The line that best fits the data and passes through the origin is also shown in part a) of the plot, along with the corresponding Preston coefficient K_p. It is apparent that the Preston equation breaks down at either $P=0$ or $V=0$, and

that the fit to the data is poor at low values of PxV. A better fit to the data intercepts either the x-axis, in the case of Series B and Series D, or the y-axis, in the case of Series A and Series C. It may also be sublinear, in the case of Series A and Series C.

Several modifications for the Preston equation that take these deviations into account have been proposed. The static etch rate of copper, R_c, is used as the y-intercept for the line of best fit in a model proposed by Luo, Ramarajan and Babu [27]. The material removal rate in this case is expressed as:

$$MRR = (KP + B)V + R_c \tag{1.2}$$

The constants K, B and R_c are determined experimentally. This model allows a non-zero removal rate when either P or V is zero, and in fact predicts that material removal is enhanced by increasing the relative velocity even when no pressure is applied to the polishing couple. This is consistent with the proposed dependence on static etch rate R_c, which would also be enhanced in a real polishing situation by increased exposure to reactants.

For conditions described by Series C in Figure 1.4, Zhao and Shi propose an alternative mechanism in which the x-intercept of the curve is defined as a threshold pressure P_{th} [28]. Below this pressure, no polishing occurs. Zhao and Shi additionally predict a sublinear relationship between MRR and pressure. The removal rate is therefore given by:

$$MRR = \begin{cases} K(P^{\frac{2}{3}} - P_{th}^{\frac{2}{3}})V & \mathrm{P} > \mathrm{P}_{th} \\ 0 & \mathrm{P} < \mathrm{P}_{th} \end{cases} \tag{1.3}$$

The authors postulate that the onset of polishing coincides with the transition from rolling abrasive motion to sliding abrasive motion, and use contact mechanics to predict that transition in terms of the pad and abrasive properties. In contrast to Luo, Ramarajan and Babu, the model described in Equation 1.3

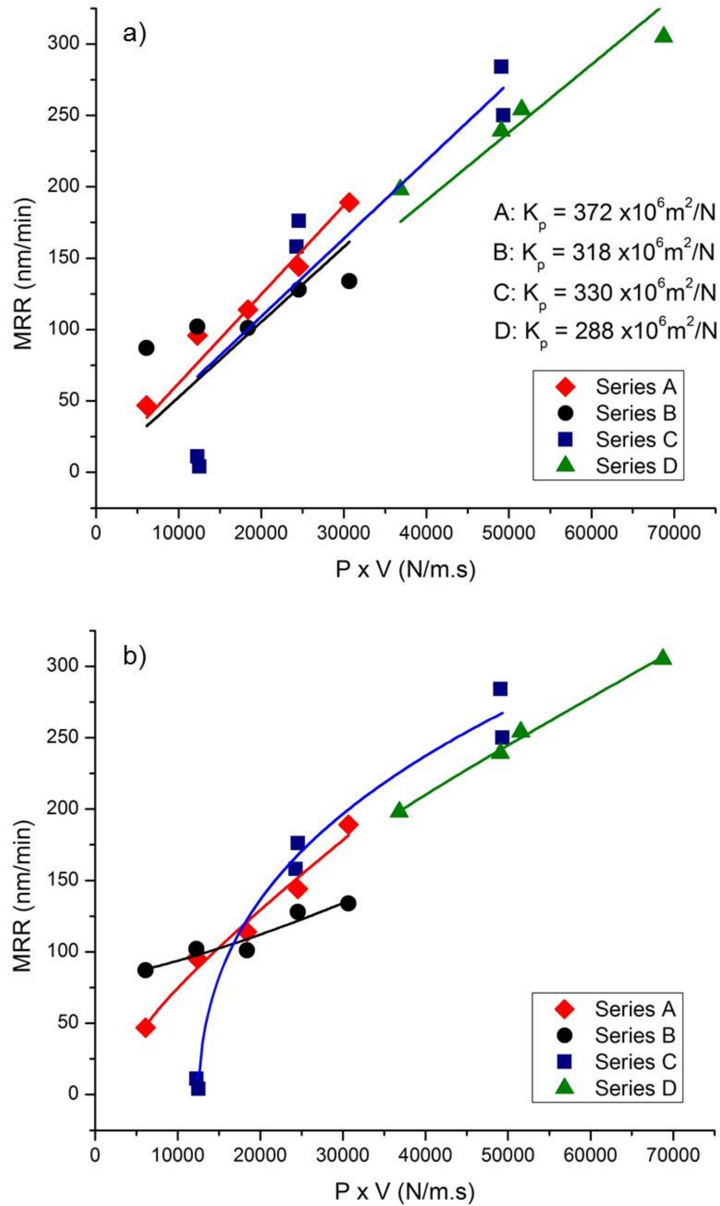

Figure 1.4: MRR vs. PxV data for copper CMP. All polishing was conducted using the same pad and slurry, with the exception that the abrasive diameter was approximately 120nm for Series A, 20nm for Series B, and 85nm for Series C and D. The Preston equation is fit to the data in a), and linear or sublinear curves are fit to the data in b).

implies that no material removal occurs without some relative motion between the wafer and the pad.

While both of these relationships are intuitively satisfactory, they do not account for each other, and hence neither one can describe the complete set of polishing results shown in Figure 1.4, in which both a static etch rate R_c and threshold pressure P_{th} are observed. They additionally suffer from the same limitation as the Preston equation, namely that they require the use of experimentally-determined constants and cannot be used for *a priori* process design.

To that end, a number of models have been proposed that aim to determine MRR from first principles. The scratch intersection model of Che, Guo et al [29] postulates that material is removed from the wafer surface only when the deformation tracks of two particles intersect. In this model, the penetration depth and detachment length of each particle under a given wafer pressure are calculated. The polishing velocity is then used to calculate the frequency of intersections, which are then summed to give a net material removal rate. In order to use this model, some geometric constants must be determined from finite element modeling of the pad as a series of elastic cells.

Almost all of these include a statistical treatment of either the pad roughness or particle size distribution, or both, and techniques such as finite element analysis. The diversity of these models is a product of the diverse fields from which they come, encompassing statistics, mechanical and fluid engineering, electrochemistry and tribology. This indicates that CMP research is an open and multidisciplinary field, reflecting the complexity of the process itself.

1.3 Goals of This Work

This work demonstrates that polishing rate within-wafer non-uniformity (WIWNU) is a function of the degree of lubricity experienced by the polishing couple, for a given chemistry. The degree of non-uniformity is controlled entirely by the initial non-uniformity of the wafer, and the pressure and velocity selected by the operator. It also demonstrates that a synergistic peak in removal rate is observed at certain abrasive:oxidiser ratios in the slurry. Further, the extent of this peak is largely independent of the actual component concentrations. A method for optimising the use of slurry is also presented, which in combination with removal rate peak observed, may allow for slurry use, and hence the cost-of-ownership for CMP, to be significantly reduced.

1.4 Outline of this Thesis

An introduction to the field of CMP research is presented in this chapter, along with an outline of the specific problems considered in this work.

Chapter 2 outlines the experimental techniques used to explore these problems.

Chapter 3 presents the relationship between the lubricity of the polishing couple and the WIWNU developed. Experimental results pertaining to this relationship are presented and discussed, then conclusions regarding this relationship are drawn.

Chapter 4 discusses the synergistic interaction of the abrasives and oxidiser, and presents experimental results which demonstrate the presence of a peak in polish rate at certain ratios of abrasive to oxidiser. The ramifications of this for understanding the mechanisms behind material removal in Cu-CMP are discussed.

Chapter 5 examines the delivery of slurry to the polishing interface, and the effect of slurry delivery on polishing. A method of optimising the use of slurry is presented.

Chapter 6 demonstrates the use of the principles outlined in Chapters 3, 4 and 5. It describes the application of these principles to actual polishing processes, and shows that significantly better outcomes can be achieved by doing so.

The overall conclusions of this work are summarised in Chapter 7. Recommendations for Cu-CMP processes and suggestions for future work are also made.

2

Experimental Procedures

This chapter outlines the methods used to prepare and polish copper surfaces using CMP. It also details the characterization techniques used to quantify polishing parameters and outcomes.

2.1 Wafer Preparation and Polishing

All polishing was carried out on an Axus 372M polisher, pictured in Figure 2.1. This instrument polishes wafer on a 0.5m diameter polishing platen, with wafer and platen rotational speeds of up to 125 rpm and 175 rpm respectively, and a maximum applied pressure of 60 psi for 100mm-diameter wafers. In this work, rotational speeds of up to 90 rpm and polishing pressures of up to 8 psi were used, as these ranges are typical for industrial CMP processes.

During processing, polishing slurry is fed on to the platen by peristaltic pumps at a rate of 20mL/min to 500mL/min. The pad is conditioned with a diamond-grit conditioner that sweeps back and forth across the pad surface. This is usually carried out continuously during polishing. A schematic of this arrangement is shown in the previous chapter, in Figure 1.1.

The pads used in polishing are considered consumables and must be replaced periodically. In the course of this work, Cabot Microelectronics® IC1000 and NexPlanar® E7450-30S and E7070-30S pads were used. The first of these

Figure 2.1: Axus 372M Polisher

is concentrically grooved, while the latter two are both radially and concentrically grooved.

2.1.1 Wafer Preparation

All polishing was carried out silicon wafers with a blanket coating of copper. These were prepared from 100mm (4") diameter p- or n-doped prime silicon wafers in the {100} orientation that had been polished on one side. The wafers were first thermally oxidized at 950°C for time taken for the furnace temperature to reach this temperature, and an additional 15 minutes. This produced a silicon dioxide (SiO_2) layer approximately 150nm thick, with a non-uniformity of around 4%. The polished surface of the wafer was then coated with a 20nm adhesion layer of either chromium or tantalum, and approximately 1.5μm of copper. These metals were applied using DC magnetron sputtering systems located at the University of Alberta. Regardless of the adhesion layer or sputtering tool used, the Argon (working) pressure was maintained at 5mTorr, and base pressures of 1.8×10^{-6} or lower were used.

The thickness of the copper coating on the wafers was measured after deposition, and before and after polishing, using a 4-point probe. The probe measures the sheet resistance of the film, which can be used to determine its thickness by the following relationship:

$$\frac{\pi}{ln(2)} R_s = \frac{\rho}{d} \tag{2.1}$$

where ρ is the resistivity of the film and d is its thickness. The term $\frac{\pi}{ln(2)}$ is a correction factor applied to account for the fact that the film is not infinite in extent, and is accurate to within 3% provided that the measurement is not taken within a distance of four probe spacings from the edge of the film [30]. All the measurements in this work were made with either a Jandel® probe

with a Keithley® Sourcemeter® (model 2400), or a Veeco® (model FPP-5000) probe, both with probe spacings of 1.575mm. An edge exclusion of 10mm from the edge of the wafer was used, to avoid the need to apply additional geometric correction factors.

In order to accurately quantify the film thickness using Equation 2.1, the resistivity of the film must be known. This was determined by depositing calibration films on glass microscope slides at the same time as the wafers. The calibration slides contained blank regions, or 'steps', where the film was partially removed after deposition to allow its thickness to be measured by profilometry. The film resistivity was then calculated using Equation 2.1 and the film thickness d determined by profilometry. Resistivity values for the films used in this work ranged from 2.13 to 2.72 $\mu\Omega$.cm, depending on the sputtering conditions used. These values are higher than the published value for bulk copper at 20°C of 1.6730$\mu\Omega$.cm [31], illustrating the need for calibration. The thickness of copper deposited on each wafer was measured at three or 9 locations across the wafer surface. In order to ensure consistent measurement positions, jigs were constructed from polyvinyl sheet to be placed over the wafer as a 'mask' for measurement. The 9-location jig is shown schematically in Figure 2.2. Each position, designated A-H, J, occupies a unique radial and tangential coordinate such that readings are taken at 5mm and $\frac{\pi}{4}$ radial and tangential intervals. The probe was placed manually on the wafer to take measurements. With the use of jigs, the positional accuracy of the measurements is estimated to be $\pm$ 2mm and 3°.

2.1.2 Slurry Preparation

Polishing slurries were mixed from their constituents no more than 24 hours before use. They consisted of hydrogen peroxide as an oxidiser, glycine and

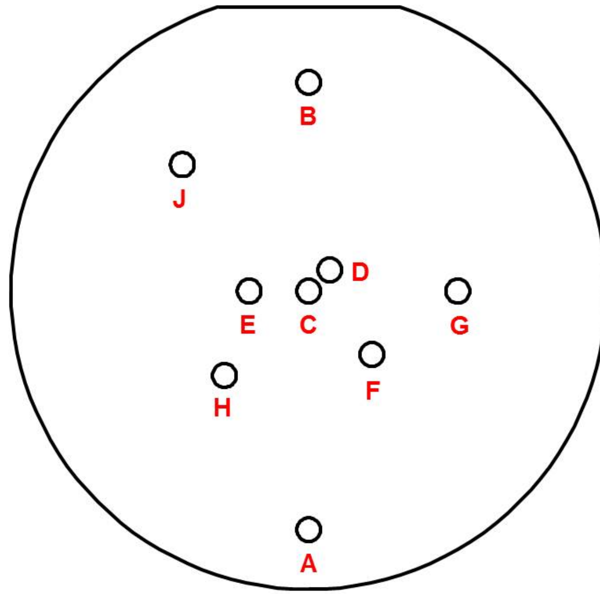

Figure 2.2: Schematic of the 9-point film thickness measurement jig.

Table 2.1: Slurry components used in this work

Component	Grade	Supplier	Concentration Range
Hydrogen Peroxide	Electrical	Ricca Chemical	0 - 4wt%
Glycine	Reagent	Fisher Chemical	1wt%
Citric Acid	Reagent ACS 99.5%	Acros Organics	As required
Benzotriazole	98%	Acros Organics	1mMol
Colloidal Silica	Bindzil	AkzoNobel	0 - 20wt%

citric acid as chelating agents (with citric acid also being used to adjust pH), and benzotriazole as a corrosion inhibitor. Colloidal silica was used as the abrasive. The balance of the slurry was deionised or demineralised water. The grade of each component and its range of concentration in the slurry is given in Table 2.1.

Different sizes of silica abrasive were used in this work, as both their size and size distribution have been shown to significantly impact polishing rate [12]. Particle characteristics can be measured using a number of techniques, all

with different advantages and limitations [32]. The most frequently used abrasive here is Bindzil® SP599. For this abrasive, the manufacturers determined the specific surface area to be 80 m^2/g by titration, and the mean particle diameter to be 34.1 nm. The particle size distribution cannot be determined from techniques based on surface area. Measurement by dynamic light scattering (DLS) was performed at the University of Alberta using a Brookhaven ZetaPALS instrument and a refractive index for colloidal silica of 1.45. This gave the mean particle diameter as 84.6nm with a distribution half width of 45.6nm, indicating a wide particle size distribution. Direct measurement of the diameter of 97 particles in two perpendicular directions by transmission electron microscopy (TEM) gave the de Brouckere mean diameter as 88nm, with a distribution half-width of around 40nm. The de Brouckere mean is used according to the guidelines of the U.K. National Physical Laboratory to provide a volume-based mean that can be compared with the volume-dependent data obtained using DLS analysis [33]. Further details of the TEM characterization are given in section 2.4.2. The DLS measurements are used in this work as they were performed for every size of abrasive, allowing direct comparison. The particle size distributions obtained using TEM and DLS for SP599 particles are shown in Figure 2.3.

Following mixing, all the slurries used in polishing were agitated thoroughly by hand. They were further agitated during use with a motorized stirrer (for large quantities) or magnetic stir bar (for smaller quantities) when the polishing period extended ten minutes.

2.2 Pad and Wafer Rotational Velocity

Both the wafer and the polishing pad corotate during polishing, with speeds that can be independently set. The offset between the centre of the pad and

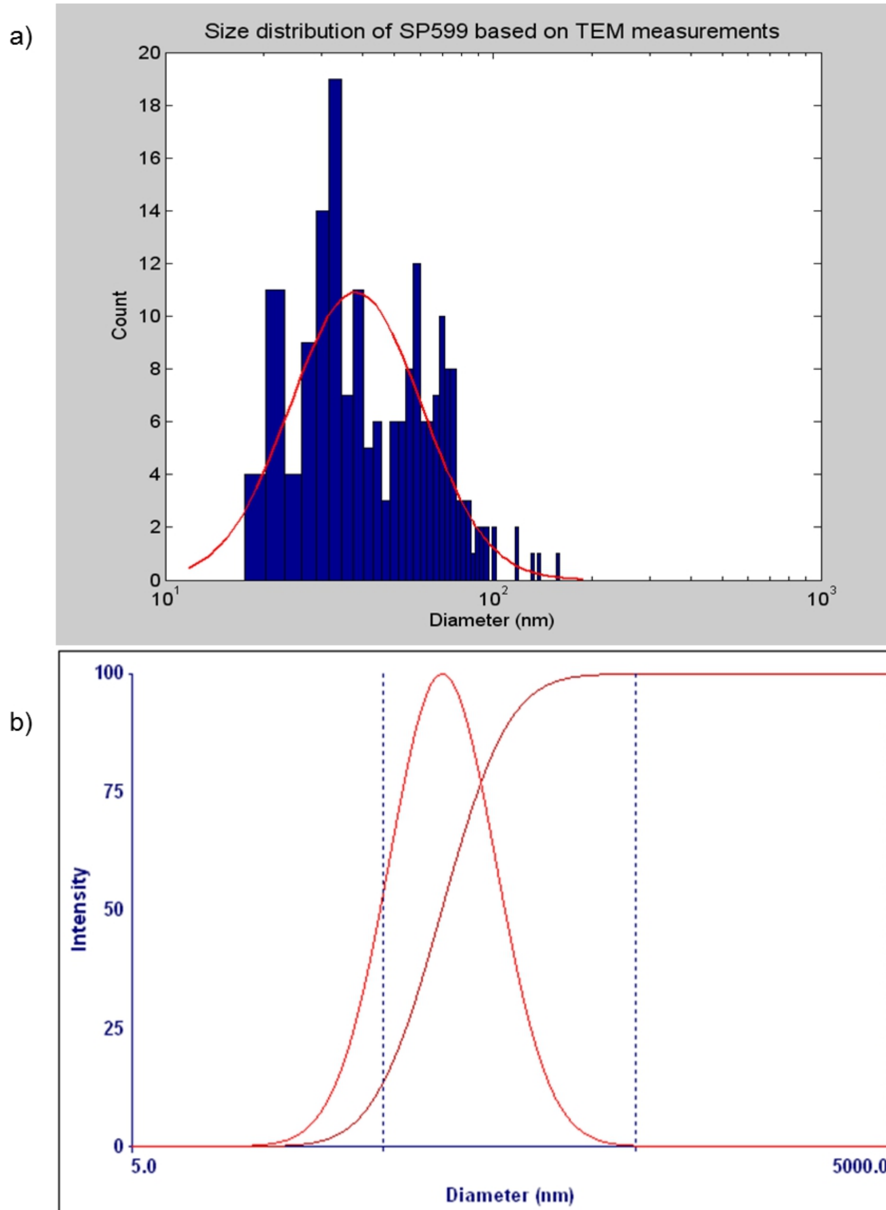

Figure 2.3: Comparison of particle sizes and distributions for SP599 silica particles analysed using a) transmission electron microscopy and b) dynamic light scattering.

the centre of the wafer can also be set by the user. These rotational speeds and the offset distance determine the magnitude and direction of the relative linear velocity (henceforth referred to as velocity V) between the wafer and the pad. If the pad and wafer have the same rotational speed (i.e. if $\omega_{pad} = \omega_{wafer}$), the velocity between them is constant at all points across the wafer surface, and equal to the product of the rotational speed and the offset distance:

$$V = \omega \times e \tag{2.2}$$

where V = relative linear velocity (m/s), ω = rotational velocity of the pad and wafer (rad/s) and e = offset distance between the pad and wafer centres (m). Additionally, the direction of the relative velocity is constant, and perpendicular to the vector joining the centres of the pad and wafer. This is indicated by the arrows in Figure 2.4a) and b).

A varying velocity profile across the wafer surface can be created by rotating the pad and wafer at different speeds (i.e. $\omega_{pad} \neq \omega_{wafer}$). The degree of variation depends on both the difference in the pad and wafer rotational speeds, and whether the wafer or pad rotates faster. As an example, the magnitude and direction of the velocity field is shown in Figure 2.4c) and d) for different pad and wafer rotational speed combinations. The code used to calculate the velocity field in MATLAB® is given in Appendix A.

In this work, all polishing was carried out under the condition that $\omega_{pad} = \omega_{wafer}$. However, the offset between the pad and wafer was varied during polishing to reduce wear on the pad. The offset oscillated between 150mm and 190mm with a speed of 7mm/s. Thus while the velocity between the wafer and the pad was constant across the wafer at any given time, it varied in magnitude by ±12% from the mean value during polishing. The centre position, at which

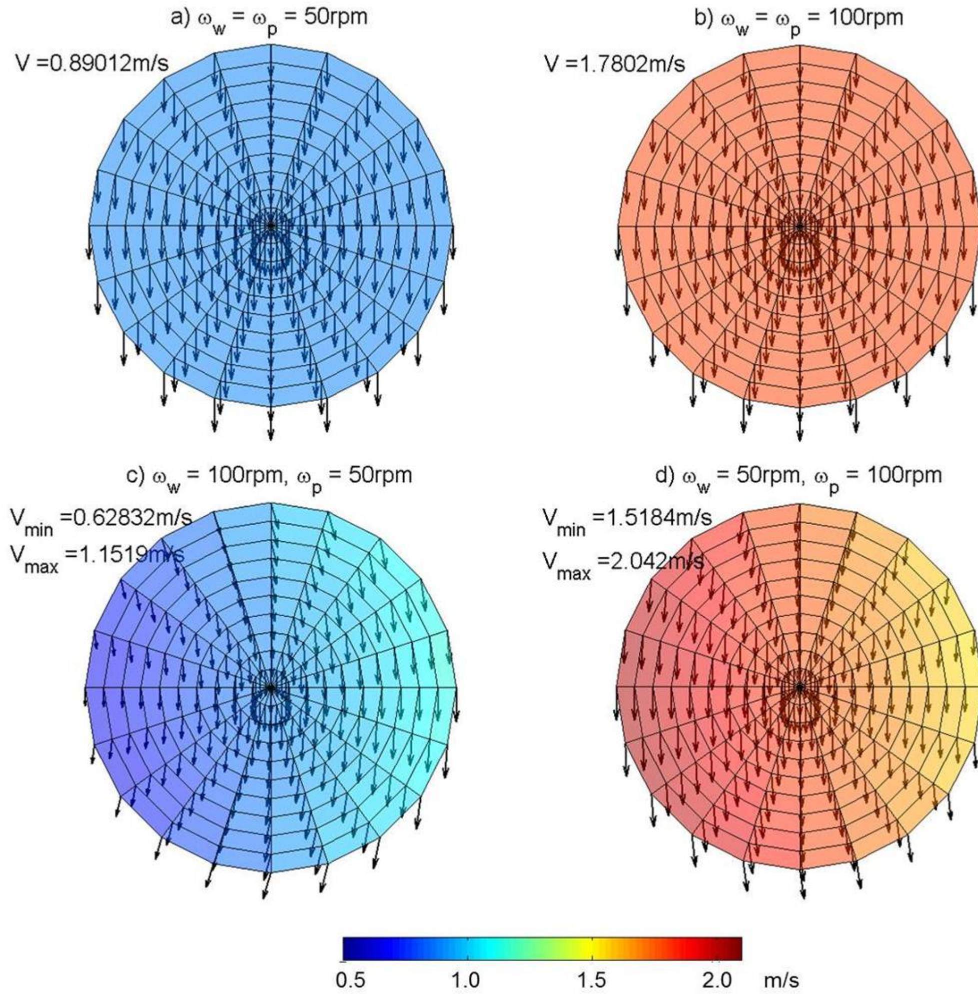

Figure 2.4: Velocity field across the wafer surface for four combinations of pad and wafer speeds. The centre-to-centre offset distance is 0.17m in these simulations, and the wafer radius is 50mm.

the offset equals 170mm, was used to calculate the mean velocity.

2.3 Friction Measurement

Measuring the friction force between the pad and the wafer during polishing is an important part of tribological analysis. On small, bench top-scale instruments, this is often achieved by disengaging the platen mechanism from the wafer-carrying mechanism and placing the platen on a shear table (as in [15], for instance). The table is used to directly measure the lateral force of the platen with respect to the wafer that is generated during polishing. For larger instruments, such as the one used in this work, this approach is not feasible. In these cases, the friction is measured either directly by the placement of load cells on the carrier shaft (e.g. [5]), or indirectly by the measurement of either the wafer carrier or platen motor current. Xie and Boning [34] measured the platen motor current during polishing and found it to be directly proportional to the friction generated during polishing. Tamai, Morinaga and coworkers [35] also measured the platen current during polishing, and used this data along with the observed temperature changes to calculate a mechanical energy balance for the polishing system. In this work. the friction force was quantified from the current drawn by the motor powering the wafer carrier.

On the Axus 372M, the power supplied to the wafer carrier motor is used to overcome the carrier's internal friction and rotate the wafer at the speed set by the user. This can be performed with the carrier raised off the pad, or disengaged, or with the carrier and pad in contact, or engaged. This latter state is used for polishing. The motor control has a tachometer and feedback loop to ensure that more or less power is drawn by the motor as required to maintain the set speed. When polishing, the frictional force between the pad and the wafer tends to promote the rotation of the wafer, reducing the power

required by the motor to maintain the set speed. The difference between the power required to rotate the wafer at the set speed when the pad and wafer are disengaged and when engaged can therefore be equated to the friction force, using the carrier motor characteristics and the tool geometry.

The carrier motor is a DC electric permanent magnet motor with a constant operating voltage of 90V (Leeson® model number C42D17FK7), connected to the carrier shaft by a gearbox (MorseLeeson® model number 18SF15) that reduces its output speed by a factor of 15. Data sheets for each of these components are included in Appendix B. The feedback loop for maintaining the correct output speed incorporates a 10A shunt resistor, across which the voltage varies from 0 to 100mV depending on the motor current. An acquisition system was designed and constructed by the Department of Chemical and Materials Engineering instrument shop to record this voltage and hence the current drawn by the motor.

The feedback loop in the polisher is isolated from ground, and hence operates at a floating voltage. A compatible floating-voltage data acquisition card, or DAQ (National Instruments® model number NI9261-USB) records input voltage from 0 to 10V, rather than the 0-100mV range that is the output of the shunt. The voltage signal from the shunt was therefore passed through a similarly isolated circuit that amplified it by a factor of 100 prior to being recorded by the DAQ. The DAQ output was then converted to current, recorded and displayed using LabView® software installed on the computer to which the DAQ was connected. The amplification circuit was calibrated using a FLUKE® 725 process calibrator and an Agilent® 3458A 8 1/2 digit multimeter, and found to have a full-scale error of less than 0.4%. To reduce electrical noise, shielded cable was used to connect the amplification circuit to the shunt and the DAQ. The signal was also filtered through a 500Hz low-

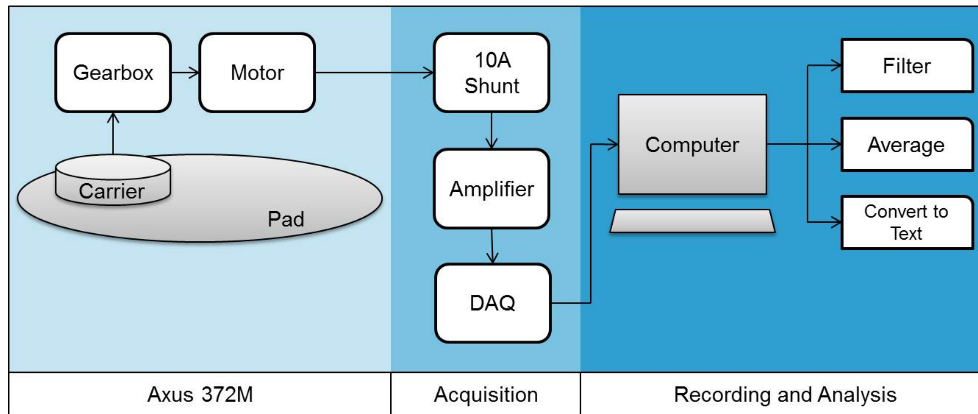

Figure 2.5: Schematic diagram of the tool and data collection system used in this work.

pass filter prior to use in calculation. The effect of noise was further reduced through the data collection protocol. Software modules to average the data and convert it to text for analysis with other software were also created. A schematic of the tool and data collection system is shown in Figure 2.5.

As the friction between the wafer and the pad tends to assist the wafer rotation, the current drawn by the motor with the pad and wafer engaged is less than that drawn with the surfaces disengaged. To quantify the friction force generated during polishing, the carrier motor current was recorded during polishing and again immediately before or after polishing with the surfaces disengaged. During this step, the current was recorded at six speeds to allow the construction of a power curve for the motor. This was done for each friction measurement to minimise the effect of noise on the measurements. Following recording, the root-mean-square averaged value of the current was calculated using the LabView® software. All polishing was carried out for 90 seconds. However, only the final 60s of current data was used when calculating the average; the first 30s were discarded as the applied pressure ramped up during this time. Similarly, current data was collected for the power curves over 60 to

90 seconds at each speed, and the average found over 60s. The power curves generated were fit with a second-order polynomial using MATLAB®. This was used to calculate the equivalent speed of the carrier during polishing, which is the speed at which the carrier would rotate if powered by the same current with the pad and wafer disengaged. As discussed, the geometry of the tool promotes rotation of the wafer during polishing, reducing the current drawn. The equivalent speed of the carrier during rotation is therefore less than the set speed. The quantities established in this process are:

- i_{set}, i_{eng}: the current drawn by the motor at the set speed with the pad and wafer disengaged and engaged (polishing), respectively
- i_f: the current replaced by friction (i_{set} - i_{eng})
- ω_{set}, ω_{eng}: the set carrier rotation speed and the equivalent rotation speed during polishing
- V: the motor voltage of 90V as specified by the manufacturer
- G: the gear ratio of 15 as specified by the manufacturer, and
- η: the product of the gearbox and motor efficiencies given by the manufacturers (0.57 for this combination)

Using the relationships

$$P = Vi$$

$$P = T\omega$$

where P is the power of the motor and T is the torque produced, the collected data was used to calculate the torque due to friction only, T$_f$ using the following relationship:

$$T_f = \eta VG(\frac{i_f}{\omega_{set}} + \frac{i_{eng}}{\omega_{set}} - \frac{i_{eng}}{\omega_{eng}}) \tag{2.3}$$

The values for the coefficient of friction determined using this method were between 0.25 and 0.75. This is consistent with the values measured by other workers (such as in [14, 36] using direct methods of friction measurement.

2.4 Additional Characterisation Techniques

2.4.1 Atomic Force Microscopy (AFM)

A Digital Instruments/Veeco® Dimension 3100 atomic force microscope was used to characterise the surface quality of the wafers before and after polishing. This instrument was located on a structurally isolated floor pad in a basement laboratory, and was further isolated from vibration by an air table. All measurements were taken in tapping mode, using Veeco® TESP n-type (Antimony-doped) probes. Scans were made from 500nm to 10μm in width, with scan rates of 0.5Hz to 2Hz.

2.4.2 Transmission Electron Microscopy (TEM)

Samples of both used and unused slurry were analysed using a JEOL® 2010 TEM equipped with a LaB6 electron gun and a 4pi® EDS system. Images and EDS spectra of the slurry components were captured, and where tilt contrast indicated crystallinity, diffraction patterns and dark field images were also collected.

Samples were prepared by placing small droplets of slurry on either nickel or copper grids with a Formvar® support and a 200 mesh. EDS was only carried out for samples on nickel grids, as the copper of the grids swamps the signal of any copper present in the samples due to polishing. The slurry was placed on the samples using a fine-tip disposable plastic pipette. Used slurry was removed from the polishing pad during polishing from immediately behind the trailing edge of the wafer. A fine-tip pipette or a clean room swab was used to

lift the slurry and transfer it on to the grid. After depositing the slurry, the grids were dried in a desiccator or clean petri dish for a minimum of 4 hours.

3

Polish Rate Uniformity as a Function of Lubrication

This chapter describes the relationship between the lubrication of the pad / wafer polishing couple, characterised by the Sommerfield number So, and the uniformity of the polish rate across the wafer.

3.1 Introduction

3.1.1 Lubrication, the Sommerfield Number and the Stribeck Curve

During polishing, the pressure applied to the polishing couple can be transferred between the pad and the wafer through direct contact with the pad, through the intervening slurry, or through a combination of both. These modes are illustrated in Figure 3.1.

Intuitively, each of these modes of contact promotes different mechanisms of material removal from the wafer surface, and additionally have different friction characteristics, making the determination of the mode of load transfer an important question in CMP research.

The mode of load transfer is characterised in tribology by the construction of a Stribeck curve. This is a plot of the dimensionless Sommerfield number, So, against the measured coefficient of friction CoF for a given polishing couple,

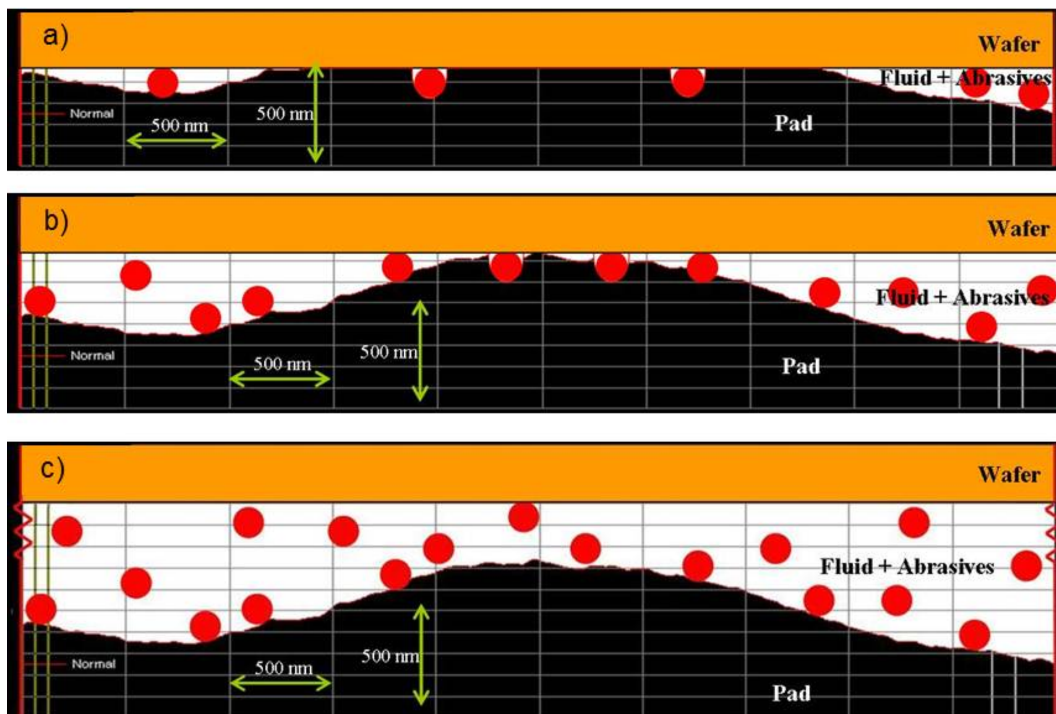

Figure 3.1: Modes of load transfer between the pad and wafer during polishing. The applied pressure can be transferred by direct contact between the pad and wafer (a), through the polishing fluid (c), or by a combination of both (b). This figure is drawn to scale using actual profilometry data from a polishing pad. The abrasives are drawn with a diameter of 150nm.

and was originally developed to characterise the performance of bearings [37]. The Sommerfield number is defined as:

$$So = \frac{\mu V}{\delta P} \tag{3.1}$$

where μ is the viscosity of the fluid, V is the relative velocity between the two surfaces, δ is the thickness of the fluid between the two surfaces and P is the pressure.

A schematic Stribeck curve is shown in 3.2. Three distinct regions are apparent; the first, at low Sommerfield numbers, is termed the boundary lubrication regime. From Equation 3.1, this regime corresponds to low relative velocities and high applied pressures. It is characterised by a high, constant CoF and is the result of contact between the two surfaces, corresponding to Figure 3.1a). It is also characterised by high wear rates in bearings [38]. The third region, at high Sommerfield numbers, is the hydrodynamic regime, in which the motion of the fluid between the two surfaces induces sufficient pressure to fully separate them. The coefficient of friction in this regime is significantly lower, as expected, but increases with increasing velocity (and hence So) due to fluid drag. This regime corresponds to Figure 3.1c) and is typified by low wear, making it the desired regime for the operation of bearings. Between the two, there exists a transitional region where there is partial contact between the two surfaces, illustrated in 3.1b). This is, appropriately, the mixed lubrication regime and is typified by rapidly decreasing CoF.

The transition from one regime to another is not related to a particular value of So, and is rather a system-specific parameter that depends on the characteristics of the surfaces and fluid involved. For systems where the surfaces are very rough, or the viscosity of the fluid is low, there may be only

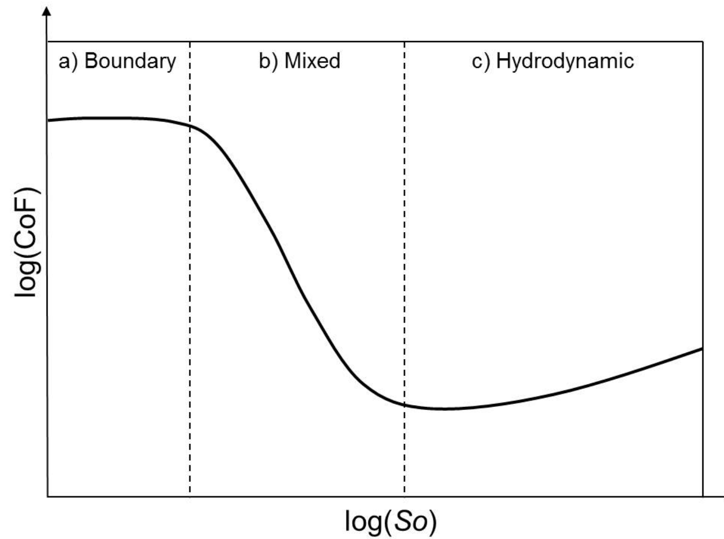

Figure 3.2: Schematic Stribeck curve, showing three distinct zones of lubrication; boundary lubrication (a), mixed lubrication (b) and hydrodynamic lubrication (c).

boundary lubrication. Such systems are described as 'anti-lubricating'.

Clearly, the degree of contact between the pad and wafer during polishing has a significant influence on the removal of material from the wafer. The Stribeck curve has thus been widely adopted in the CMP community, as will be illustrated in the next section. However, there two major limitations on its use in CMP. The first of these is that, from Equation 3.1 the thickness of the fluid film between the pad and the wafer must be known in order to evaluate So, and there are great practical difficulties associated with measuring this directly. Secondly, the Stribeck curve, like the CoF it depicts, can describe only the overall response of a polishing couple and cannot give spatially-resolved information about the polishing interface. This chapter describes the adaptation of lubrication theory for investigating one such spatially-dependent phenomenon, the development of non-uniform polish rates across the wafer surface.

3.1.2 Lubrication Theory in Cu-CMP Research

Stribeck curves have been developed for numerous CMP systems, and have been used to examine the effect of pads, slurries and wafers on the lubrication characteristics of the polishing system. Two examples are shown in Figures 3.3 and 3.4.

Philipossian and Olsen [2] measured friction coefficients to create Stribeck curves while polishing interlayer dielectrics with seven different pads, at low and high abrasive slurry loadings, shown in Figures 3.3a) and b) respectively. They illustrate that the lubrication characteristics of the polishing couple are not greatly influenced by the amount of abrasive particles present in the slurry, with little difference in either the magnitude or shape of the curves. However, the pads themselves have a significant effect on the lubrication characteristics of the system. The authors attribute this to the degree of grooving on the pad surface, and the ability of the grooves to drain slurry away from polishing interface. For pads without grooves (IC-1000 and FX-9 flat pads), a transition from boundary to mixed lubrication is observed at a Sommerfield number of approximately 1×10^{-2}. A transition to mixed lubrication is also observed for pads with topography that does not drain fluid effectively, such as the IC-1000 and FX-9 perforated pads, and the IC-1000 x-y pad. A fully-developed hydrodynamic response was not observed under any conditions. For pads with significant and effective drainage, such as the IC-1000 and IC-1400 k-grooved pads, no transition was observed over the tested range, and the wafer remains in the boundary lubrication regime. These pads are therefore anti-lubricating for the pressure and velocity conditions considered. Philipossian and Olsen postulate that polishing under boundary lubrication may reduce the variation of removal rates across the surface of the wafer, or within-wafer-non-uniformity

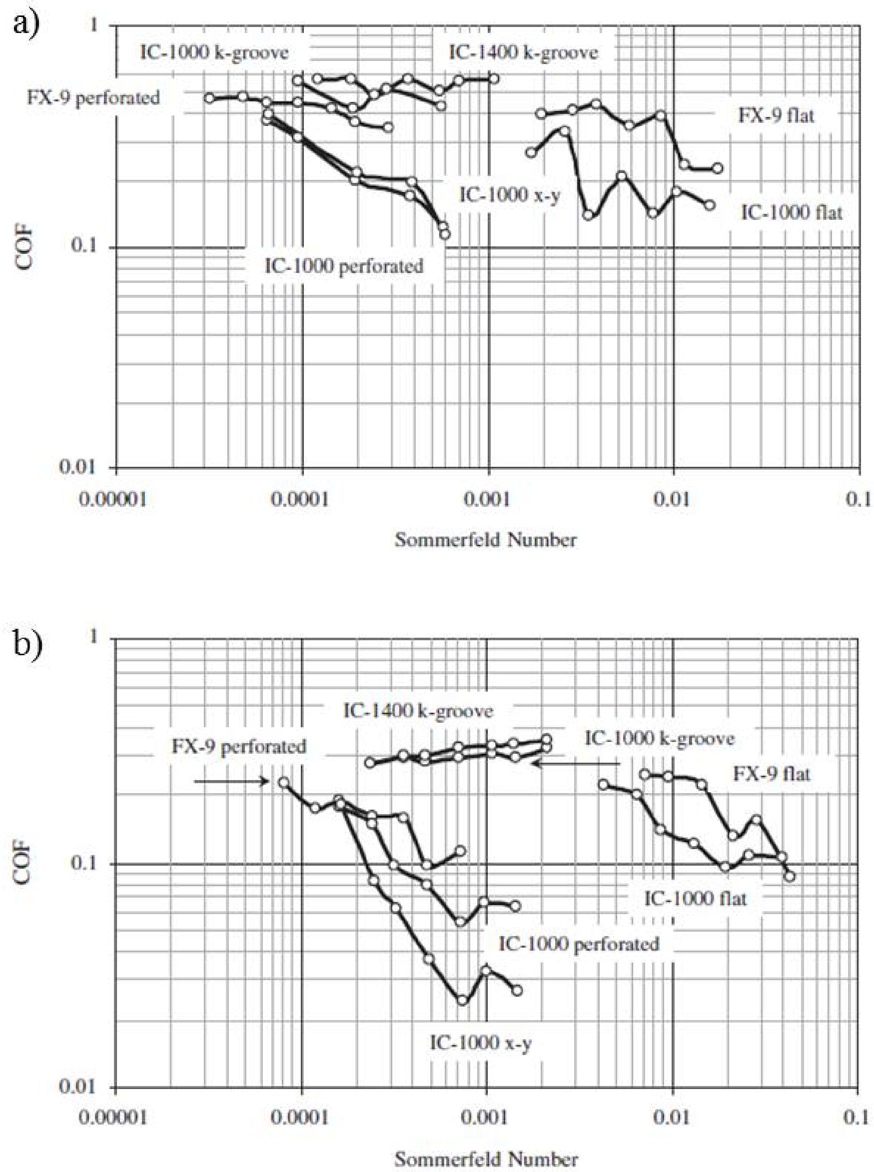

Figure 3.3: Experimentally-obtained Stribeck curves for polishing interlayer dielectrics with a variety of pads at a slurry abrasive loading of a) 2.5% and b) 25% (from [2], ©2003 The Japan Society of Applied Physics).

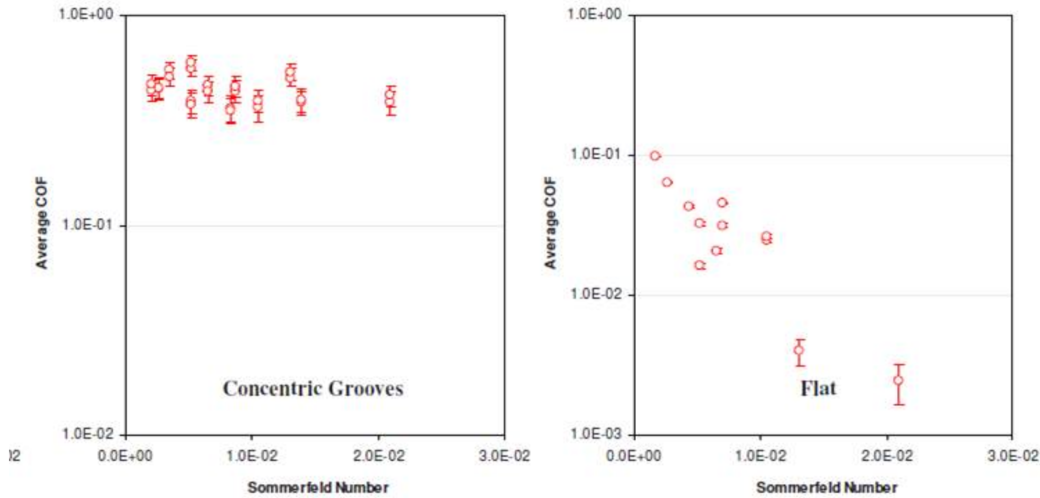

Figure 3.4: Experimentally-obtained Stribeck curves for polishing copper with a concentrically-grooved and flat pad (as labeled) (from [3], reproduced by permission of ECS - The Electrochemical Society).

(WIWNU); however they do not directly measure WIWNU in this study.

A similar study was conducted by Rosales-Yeomans and coworkers for polishing copper surfaces [3], shown in Figure 3.4. The results obtained are similar to those for interlayer dielectric polishing, with mixed lubrication observed for a flat (ungrooved) pad, and boundary lubrication for a concentrically grooved pad. The magnitude of the CoF recorded is also similar, with values of around 0.2 for the interlayer dielectric and 0.5 for the copper surface. This suggests that the overall lubrication response of a polishing system does not depend strongly on the type of surface being polished. Despite this, the magnitude of the Sommerfield numbers under investigation varies considerably between the two studies, even though the authors using similar pressure and velocity conditions. This may appear to indicate underlying differences in the lubrication characteristics of the systems. However, closer investigation reveals that this is more likely due to differences in the techniques used to estimate the thickness of the slurry film. Rosales-Yeomans and coworkers approximated

the film thickness as the average surface roughness of the pad R_a. A similar technique was used by Philipossian and Olsen, except that they averaged the film thickness in the grooves (as the groove depth) and on the plane of the pad (as the roughness R_a) by the relative area of each. These techniques yield values of film thickness of around 20μm and 60μm respectively, accounting for the difference in So observed.

Approximations of this nature are used because measuring the thickness of the film between the wafer and the pad during polishing is technically difficult. Measurements have been made using slurries containing fluorescing dyes, where the wafer is replaced by a transparent glass surface and the dye in the slurry is stimulated using dual-emission light induced fluorescence (DELIF) [39] or dual-emission UV-enhanced fluorescence (DEUVEF) [40]. Measured film thicknesses of 15μm to 30μm were reported in the first of these studies, and 60μm to 75μm in the second.

An alternative method of determining the film thickness is to use modeling techniques. The most common method for doing so is to approximate the polishing couple as a hydrodynamic bearing, the fluid mechanics of which are well-established and relatively simple [41]. This approximation is valid when the reduced Reynolds number Re^*, given by Equation 3.2, is substantially less than unity:

$$Re^* = \frac{Ul}{\nu}\left(\frac{h}{l}\right)^2 \ll 1 \tag{3.2}$$

In this expression, U is the fluid velocity, taken as equal to the relative linear velocity between the pad and wafer, l is the length of interest, taken as the diameter of the wafer, ν is the kinematic viscosity of the slurry, conservatively taken as the viscosity of water, and h is the thickness of fluid film separating the wafer and pad, conservatively taken as 75μm as reported in [40]. At a

relative linear velocity of 1.84m/s, the highest used in this study, the value of Re* is approximately 1x10^{-4}, which satisfies this criterion. At a wafer diameter of 300mm (12"), Re* is approximately 3.5x10^{-2} and Equation 3.2 is still satisfied, implying that modeling the polishing couple as a hydrodynamic bearing is scalable up to large wafer sizes.

Such models additionally give information on the pressure distribution across the wafer surface and the tilt of the wafer during polishing [42, 43, 44], and may also take into account the compression of the pad [45]. One of the simplest of these hydrodynamic models is that developed by Chen and Fang [44]. In this model, the Navier-Stokes equations for the fluid in the pad / wafer interface are simplified considerably by assuming that the flow is laminar, and further that the pressure distribution in the film is radially symmetric about the centre of the wafer. With the assumption of suitable boundary conditions, an ordinary differential equation can be formulated to describe the pressure gradient, and hence pressure, along the radius of the wafer. However, as noted previously, there is strong evidence to suggest that polishing is not in fact a hydrodynamic process. Models which account for the transfer of some of the load directly from the wafer to the pad [46], and from the wafer to particles to the pad [47], have also been developed in response to this. Despite the differences in technique, both classes of model predict similar film thicknesses and wafer tilts. An important feature of all these models is that they are able to give spatially-resolved information regarding the film thickness and hydrodynamic pressure, and hence may offer insights into the causes and occurrence of WIWNU. An outline of current research dedicated specifically to the question of WIWNU is given in the next section.

Verifying the accuracy of any of these models is hampered by similar practical concerns as the measurement of film thickness, and as a result the literature

dedicated to this question is patchy and difficult to directly compare with modeled scenarios. However, from the studies that have been made, the following conclusions can be drawn:

- When the wafer has a convex profile (i.e. the centre of the wafer protrudes past the edges into the pad / wafer interface), the pressure that develops is positive with respect to the atmosphere [48, 5]. This is in agreement with the models cited above. This configuration, which describes all the wafers polished in this work, is shown in Figure 3.5.

- When the wafer is flat or concave (i.e. the centre of the wafer is recessed from the edges), the wafer tilt is negative. The pressure that develops is negative with respect to the atmosphere, or mostly negative, across the surface of the wafer [46, 5]. This is also in agreement with the models cited above.

- Many of the models mentioned predict a pressure distribution that is not symmetrical about the centre of the wafer. Several experimental measurements of pressure also suggest that the pressure distribution is asymmetrical [46, 5]. However, closer investigation reveals that the experiments that measure asymmetrical pressure distributions were conducted with a rotating pad and a stationary wafer, leading to a non-uniform velocity across the interface as described in section 2.4. Where the wafer was also permitted to rotate while pressure was measured, the pressure distribution was found to be radially symmetric [4, 49], or close to radially symmetric [48]. A comparison of the measured pressure distributions under rotating and non-rotating conditions is shown in Figure 3.6. Regardless of whether or not the pressure distribution is instantaneously symmetrical, the pressure experienced by the wafer is always symmetrical in the time-averaged

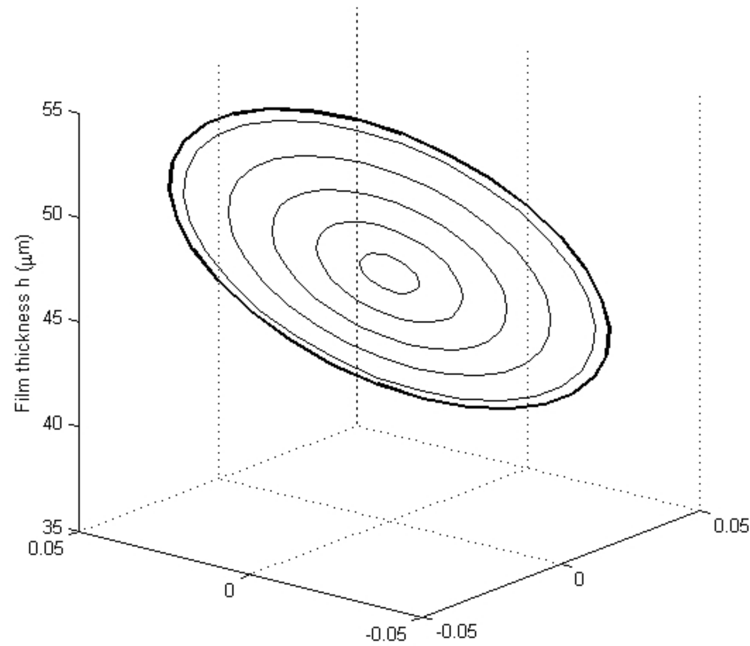

Figure 3.5: Schematic representation of a convex wafer, in which the centre of the wafer protrudes past its edges into the pad / wafer interface.

sense due to its rotation, as noted by Cho and coworkers [43]. This validates the work of Chen and Fang [44], who assume radial symmetry in their model.

In this work, the model of Chen and Fang [44] was used as a tool to predict the hydrodynamic characteristics of the fluid film between the pad and wafer. This model uses the assumption of laminar fluid flow and a radially symmetrical pressure distribution to reduce the Navier-Stokes equations to Equation 3.3.

$$\begin{aligned} \frac{\partial p}{\partial r} &= \mu \frac{\partial^2 v_r}{\partial h^2} \\ \frac{1}{r}\frac{\partial p}{\partial \theta} &= \mu \frac{\partial^2 v_\theta}{\partial h^2} \end{aligned} \tag{3.3}$$

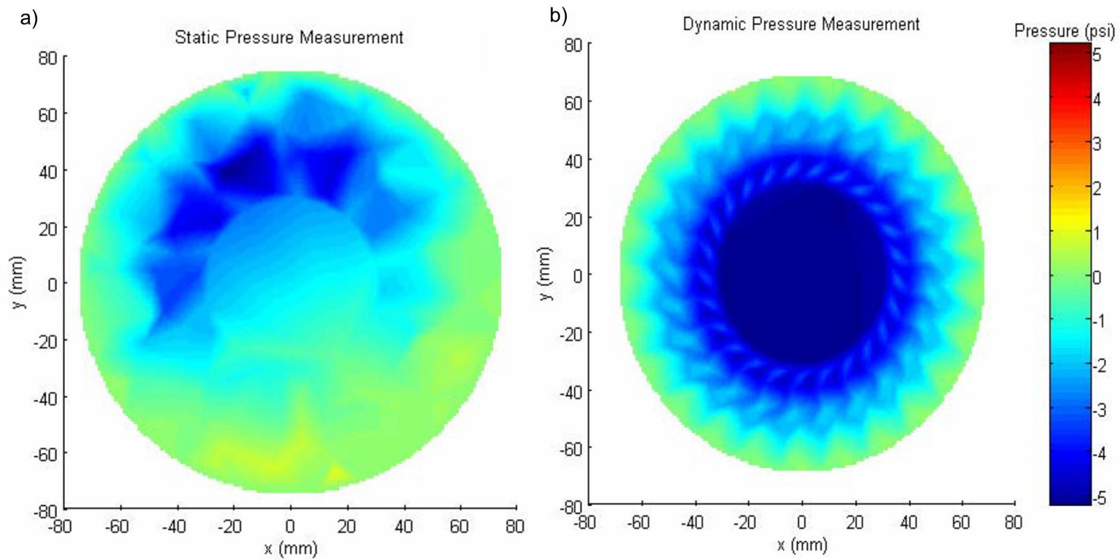

Figure 3.6: Measured pressure distributions for non-rotating (a) and rotating (b) wafers during CMP (from [4]).

Table 3.1: Comparison of model results for a wafer with a dome height of 10μm, polished with an applied pressure of 7 psi at a relative linear velocity of 0.314 m/s in a fluid of viscosity 21.4 mPa.s.

Parameter	Runnels and Eyman [42]	Cho et al [43]	Chen and Fang [44]
Minimum film thickness h_m	63 μm	35.5 μm	41.24 μm
Wafer tilt α	0.01°	-	0.0103°

The model was numerically evaluated using MATLAB®. The code used to evaluate the model is included in Appendix C. The results obtained using this method are similar to those given by the other models cited here, as shown in Table 3.1, with the exception of the prediction of a radially symmetric pressure distribution. However, the validity of this assumption is borne out by experimental results shown in Figure 3.6, and hence it is adopted here.

3.1.3 Previous Studies of Within-Wafer-Non-Uniformity (WIWNU)

Within-wafer-non-uniformity (WIWNU) is defined as the standard deviation of the film thickness remaining after polishing, divided by the mean film thickness, as shown in Equation 3.4.

$$WIWNU = \frac{\sqrt{\frac{\sum_{f=1}^{n}(x_f - x_f)^2}{n}}}{x_f} \tag{3.4}$$

Several authors have examined the effect of polishing conditions on WIWNU in an attempt to elucidate its causes. Guo, Lee and coworkers [50], and Park, Oh and Jeong [51] both attributed WIWNU in oxide polishing to pad effects. Guo, Lee and coworkers found that the width of the pad grooves affected the wafer WIWNU. They postulated that this was due to slurry flow effects in grooves of different sizes, with narrow grooves restricting slurry movement and wider ones encouraging it, although the connection between such an effect and the observed differences in WIWNU is not stated in the study. Park, Oh and Jeong examined the role of conditioning and pad wear in the occurrence of WIWNU. They found that the degree of wear of the pad, related to the length of conditioning it had undergone, did indeed have an effect on the oxide WIWNU and the overall MRR, but were not able to find a correlation between pad wear and WIWNU, pad wear and MRR, or MRR and WIWNU. They did however note the importance of pad conditioning, and found that conditioned pads exhibited slightly lower MRR and WIWNU than unconditioned, glazed pads.

For copper CMP, WIWNU has been examined as function of the slurry chemistry by Miranda, Imonigie and Moll [52], Yi, Yuling and coworkers [53], and Lee, Park and Jeong [54]. The work of Miranda and coworkers takes the form of a statistical Design of Experiments study. They found a strong correlation between the interaction of slurry pH and hydrogen peroxide (H_2O_2) content, and the overall material removal rate, and a weaker but still significant correlation between the same interaction and WIWNU. They did not attempt to describe possible mechanisms for such a correlation, but rather focussed

on the suitability of Design of Experiments as a CMP optimisation technique. Yi, Yuling and coworkers performed a more comprehensive study of polishing parameters on WIWNU and found a slight, linearly increasing relationship between WIWNU and both polishing speed and slurry abrasive content. A stronger, linearly decreasing relationship between WIWNU and polishing pressure was observed. The concentration of H_2O_2 and an unspecified chelating agent had the greatest impact on WIWNU. Both of these factors were shown to affect the WIWNU in complex ways, with both WIWNU-concentration curves displaying minima at intermediate concentrations. Lee, Park and Jeong performed a systematic analysis of the role of citric acid, H_2O_2, benzotriazole and silica abrasive concentration on both MRR and WIWNU. In contrast to the work of Yi, Yuling and coworkers, this group found that the concentrations of citric acid, benzotriazole and abrasives used had a far greater impact on WIWNU than H_2O_2 concentration.

In the more general sense, Xin [55] suggests that non-uniformity in material removal across the wafer is due to the "coffee stain ring effect" enhancing slurry evaporation at the wafer edges, resulting in localized microfluidic flows that increase material removal rate. The mechanism is proposed for polishing of any type of surface. This paper provides a theoretical treatment only and does not include any direct experimental evidence.

Obviously, any change in WIWNU that occurs during polishing must be the result of a difference in removal rates across the wafer, and hence the key to understanding the development of WIWNU is understanding non-uniformity of MRR. This phenomenon is mentioned in passing in several studies [56], including those cited above, but not quantitatively investigated. The difference in MRR that occurs during polishing is quantified here for the first time. The quantity MRRNU, or material-removal-rate-non-uniformity, is defined in

Equation 3.5:

$$MRRNU = \frac{\Delta MRR}{\overline{MRR}} \tag{3.5}$$

The denominator of this expression is the mean MRR, $\overline{MRR}$, while the quantity ΔMRR is the difference between the lowest and highest material removal rates observed across the wafer surface. A positive value of ΔMRR, and hence MRRNU, indicates that the centre of the wafer polishes more quickly than the outside, resulting in wafer-scale dishing, while negative values indicates doming.

Having defined this quantity, the mechanisms behind it are examined in terms of experimental analysis and lubrication theory.

3.2 Experimental Procedures

Thirty-six wafers were polished using eight different polishing conditions, M1-M4 and N1-N4. Either four or five wafers were polished under each set of conditions, and are designated M1-01, M1-02 and so on. These conditions represent a range of applied pressures and velocities, slurry flow rates and conditioning protocols, described in Table 3.2. All polishing was conducted on 4" wafers with a blanket Cu coating on the polishing side. The polishing apparatus and wafer preparation procedures were as described in section 2.1. The pad used for polishing was a Nexplanar® E7070-30S with both concentric and radial grooving. The composition of the slurry used for all wafers is as described in Table 3.3, except when used at a flow rate of 500mL/min; in those cases, it was diluted in a 2:3 ratio with deionised water so that the flow rate of reactants on to the pad was the same as for the slurry used at 200mL/min.

During the experiments, the wafers were each polished for 90 seconds. Be-

Table 3.2: Summary of polishing conditions

Conditions	Pressure (psi)	Velocity (m/s)	Flow Rate (mL/min)	Conditioning Protocol
M1	5	1.38	150	In situ
M2	5	1.84	150	In situ
M3	7	1.38	150	In situ
M4	7	1.84	150	In situ
N1	5	1.07	500	Ex situ
N2	5	1.07	200	Ex situ
N3	2	1.07	500	Ex situ
N4	2	1.07	200	Ex situ

Table 3.3: Slurry composition

Component	Concentration
Colloidal Silica, mean diameter 84nm	3wt%
Hydrogen peroxide	1wt%
Glycine	1wt%
BTA	1mM
Citric Acid	To adjust pH to 3.55
Deionised water	Balance

fore and after each polish, the thickness of the copper film was measured at nine points at 5mm intervals along the radius using a four-point probe, as described in 2.1.1. From this data, the initial non-uniformity of the wafer was determined by finding the difference between the highest and lowest point on the profile. This value was then used as the dome height h_D in the Chen and Fang model, along with the pressure and velocity described in Table 3.2, to calculate the slurry film thickness, wafer tilt and radial pressure distribution. The code used to evaluate the model in MATLAB® is given in Appendix C.

3.3 Results and Discussion

3.3.1 Modeled Film Thickness, Wafer Tilt and Radial Pressure Distribution

The dome heights (h_D) measured for the wafers were all positive, and ranged from 87nm to 1255nm. Using this information, the film thicknesses (h_m), wafer tilts (α) and pressure distributions for each wafer were calculated using the

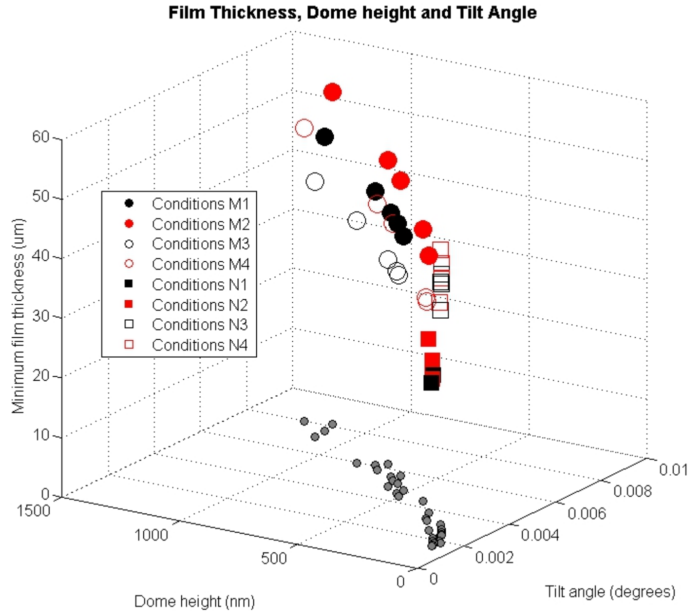

Figure 3.7: Relationship between measured dome height h_D and modeled values of h_m and α. The relationship between h_D and α is projected onto the x-y plane for clarity.

hydrodynamic model of Chen and Fang [44]. The film thicknesses obtained range from 28μm to 56μm, with wafer tilt angles of 0.0017° to 0.0082°. Generally, higher applied pressures and smaller dome heights resulted in thinner films and smaller angles of tilt. The relationship between h_D, h_m and α for all the wafers analysed is shown in Figure 3.7.

The Sommerfield number for each set of polishing conditions can then be calculated using the mean modeled film thickness for each wafer polished. These range from 4x10^{-4} to 14x10^{-4}. From this data, the polishing conditions used can be arranged in order from 'most lubricating' to 'least lubricating', as shown in Table 3.4. For the purposes of this study, the actual lubrication regime for each set of conditions is not important and hence a Stribeck curve was not constructed.

The calculated hydrodynamic pressure distribution $P(r)$ for each wafer is

Table 3.4: Sommerfield number So for each set of polishing conditions described in table 3.2

Conditions (in order of increasing So)	$So \times 10^{-4}$
M3	4.2
M1	5.1
M4	5.2
M2	6.3
N2	7.8
N1	8.1
N4	13.3
N3	13.7

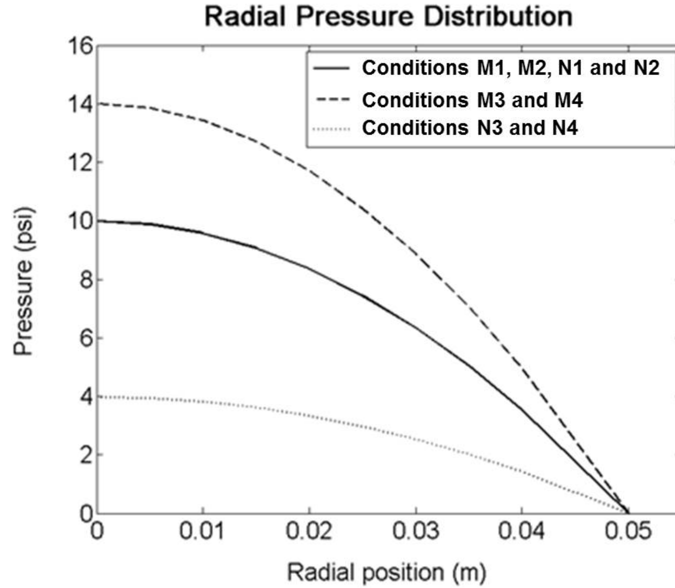

Figure 3.8: Radial pressure distribution for all wafers, labeled by polishing conditions used.

shown in Figure 3.8. From this figure, it is evident that the pressure distribution depends almost entirely on the applied pressure, with wafer dome height and polishing velocity having only a minor effect. To illustrate the effect of dome height, a segment of the $P(r)$ profile is shown in Figure 3.9 for wafers M4-02 and M4-4, with dome heights of 270nm and 1255nm respectively.

As the model used here is based on hydrodynamic fluid characteristics, it is only applicable under hydrodynamic conditions. The limits of its validity with respect to the polishing experiments performed are explored in the next

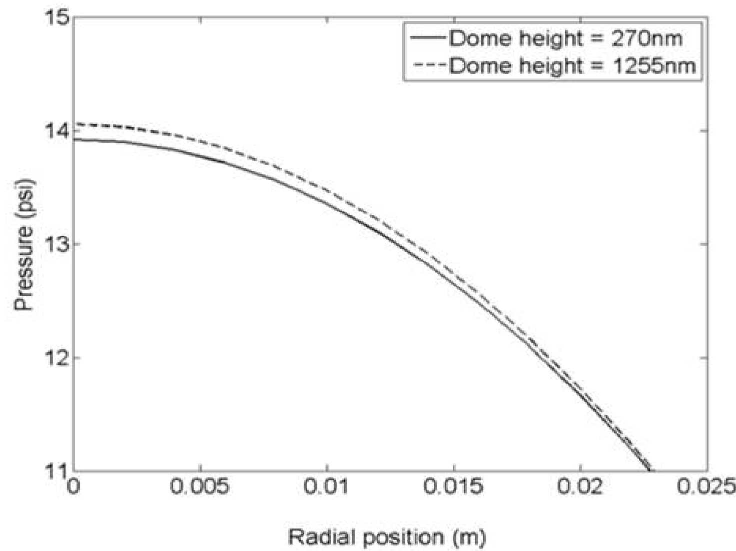

Figure 3.9: Radial pressure distributions for wafers M4-02 and M4-4, with dome heights of 270nm and 1255nm respectively.

section.

3.3.2 MRRNU as a Function of Lubrication

The average material removal rate at each of the measurement points along the wafer radius is shown in Figure 3.10. Removal rates of between 100nm/min and 500nm/min were obtained. It is clear from these profiles that MRR varies significantly across the wafer radius, depending on the polishing conditions used.

To inspect the shapes of these MRR curves, they are re-plotted in Figure 3.11 in order of Sommerfield number. For clarity, the curves are transposed along the y-axis and hence no units for MRR are shown. It is apparent that, as the polishing conditions become more lubricating, the shape of the MRR profile changes; at low values of So, polishing is suppressed in the centre of the wafer, while at higher So values the reverse is true. This can be quantified as a transition from negative to positive values of MRRNU. MRRNU is

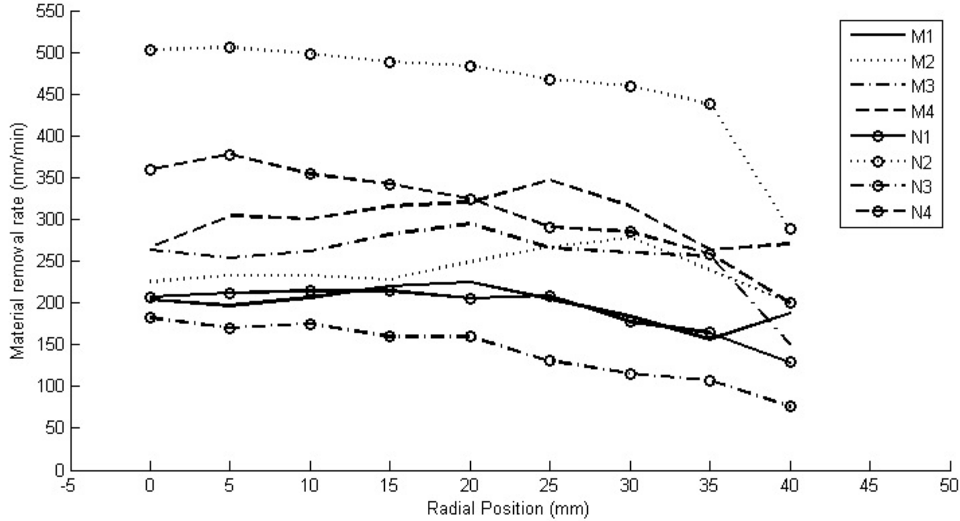

Figure 3.10: Radial MRR distribution for all polishing conditions given in Table 3.2.

plotted against log(So) in Figure 3.12a). The correlation coefficient between the logarithmic fit shown and the data is 0.9, indicating good agreement. To confirm the apparent relationship between the degree of lubrication and MR-RNU, three additional sets of polishing data were plotted on the same axes, as shown in 3.12b). The first two of these were obtained using the same slurry described in Table 3.3 but with abrasives of mean diameter 20nm and 120nm. The velocity for each of these data sets was held constant at 0.89m/s, while pressure was varied from 1psi to 5psi. The third set of data was obtained using a commercial Cu-CMP slurry, iCueC7092 from Cabot Microelectronics®. This slurry had a pH of 8.62, compared with 3.55 for the other slurries used. For all three sets of conditions, the slurry flow rate was 150mL/min, the pad used was the same NexPlanar E7070-30S model, and conditioning was conducted *in situ* during polishing. As was the case for conditions M1-M4 and N1-N4, the dome height was determined by measurement and the film thickness calculated using the Chen and Fang model. Logarithmic fit lines are shown for

this data also, and similarly indicate good agreement.

As well as indicating a correlation between the degree of lubrication (expressed as the Sommerfield number) and the MRRNU, the data presented also has the following important features:

- The same pad was used for all the experiments conducted, and thus the data trends shown are specific to this polishing pad. Future work should include the effects of different pads on MRRNU, especially in light of the relationship between pad type and lubrication response discussed in section 3.1.2, and between pad wear and WIWNU noted in section 3.4. Additionally, as different slurry flow rates and conditioning protocols were used for conditions M1-M4 and N1-N4 but the same trend was observed, the relationship between MRRNU and So is independent of slurry flow rate and conditioning method.

- The slope of the data is dependent on both the size of the particles used in the slurry, and the slurry chemistry. The relationship between particle size and the slope of the MRRNU - So curve is shown in Figure 3.13. The slope of the MRRNU - So curve increases linearly with increasing particle diameter, suggesting that smaller particles may be used to reduce the sensitivity of MRRNU to So. The relationship between slurry chemistry and the slope of the MRRNU - So curve is less clear as only two distinct chemistries were examined. However it is apparent that chemistry strongly affects the slope, and can even reversed it, as is the case here for the wafers polished using iCueC7092. More specific conclusions are difficult to draw as the composition of the iCueC7092 slurry is proprietary information, but the difference between the pH of this slurry (8.62) is significantly different from the pH of the slurry used in the other stud-

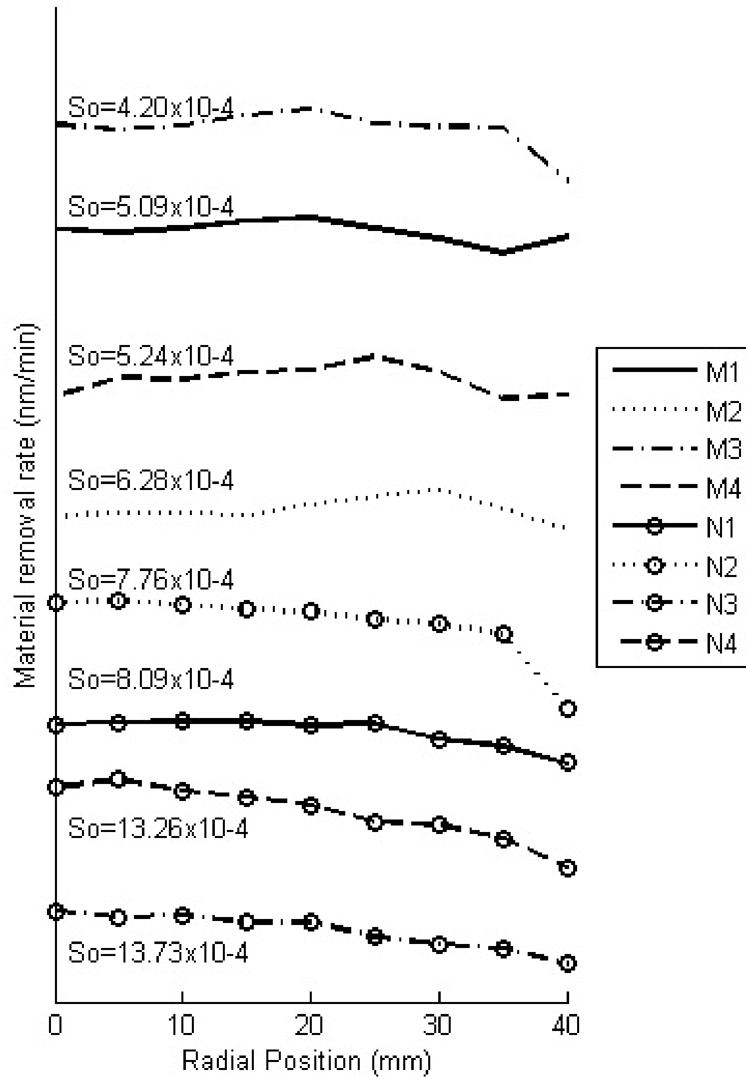

Figure 3.11: Radial MRR distributions, re-plotted in order from most to least lubricating. The Sommerfield numbers for each set of polishing conditions are also shown.

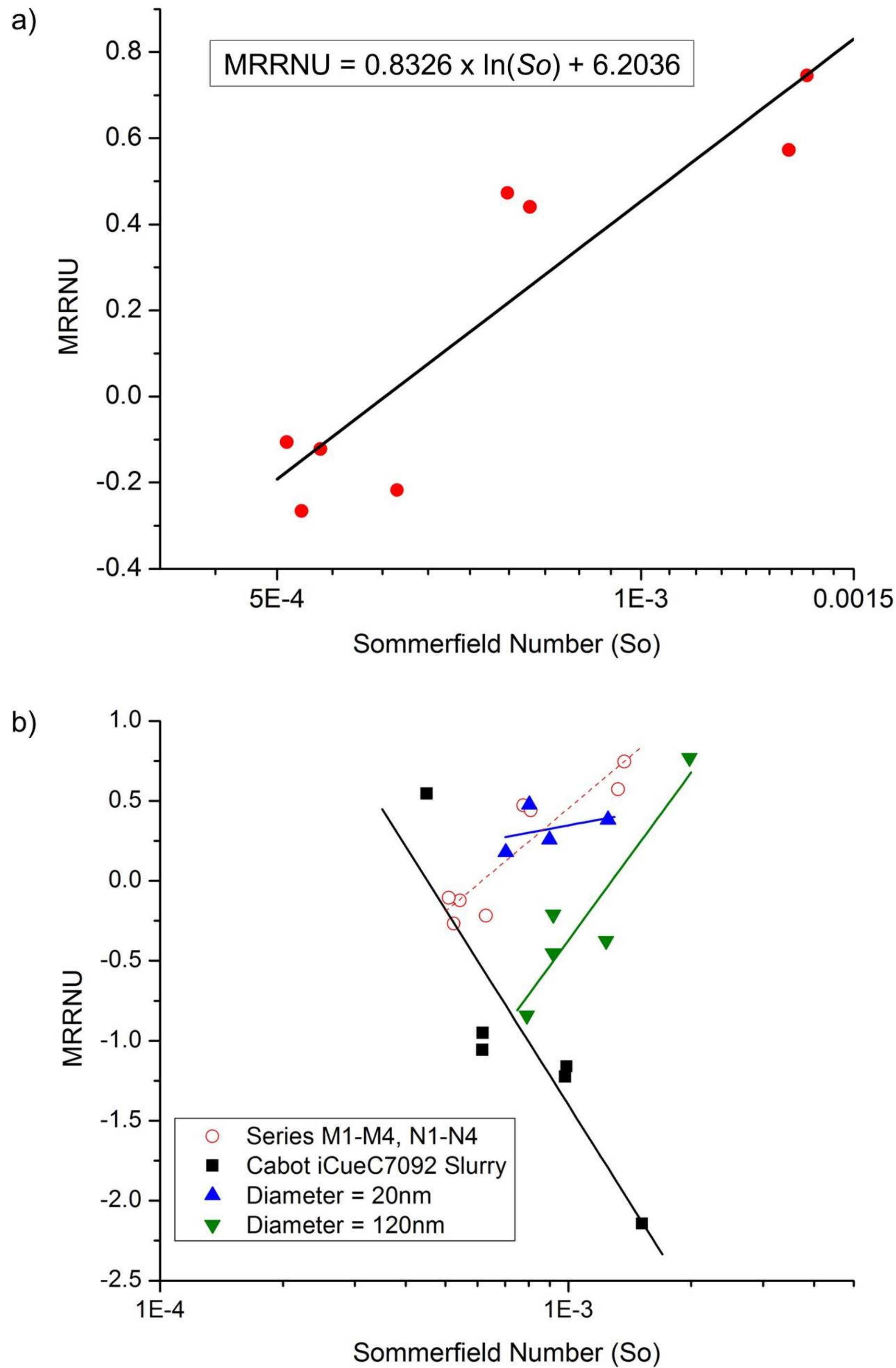

Figure 3.12: MRRNU vs. *So* for a) the polishing conditions outlined in Table 3.2 and b) the polishing conditions outlined in Table 3.2, and similar studies carried out with abrasives of diameter D=120nm and D=20nm, and with a commercial Cabot® slurry.

ies (3.55), suggesting that the compositions may be very different as well. The strong but erratic correlation between slurry chemistry and WIWNU reported by Yi, Yuling and coworkers [53] is consistent with very different MRRNU - So relationships for different chemistries. Further examination of the effect of chemistry on the MRRNU - So curve is warranted.

- Most importantly, the data sets analysed contain both negative and positive values of MRRNU. The trends obtained could therefore be used to design a polishing process to achieve a specific MRRNU. For instance, if the user was to polish copper films that are highly uniform initially, he or she could select polishing conditions that have a zero value of MRRNU to maintain the copper profile. Most importantly, the user could do so based on only the dome height of the wafers to be polished, and without the need for any supplementary information. Conversely, a polishing process may also be designed to correct initial non-uniformities in the copper thickness, if required.

3.3.3 Hydrodynamic Pressure and the MRR Profile

The MRR profiles for conditions M3, N1 and N3, representing low, moderate and high Sommerfield numbers, are compared to their modeled hydrodynamic pressure distributions in 3.14. The corresponding Preston coefficients, determined from Equation 1.1 using the modeled pressure at each radial point, are also shown.

Upon inspection, it is apparent that in all three profiles, a region exists in which the modeled hydrodynamic pressure is proportional to the material removal rate, as predicted by the Preston equation. In this zone, shaded in Figure 3.14, the Preston coefficient is constant, or close to constant. The size of

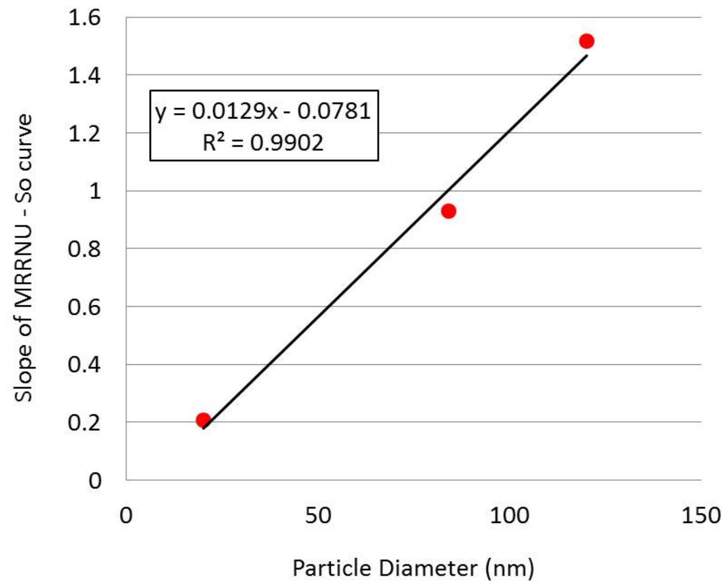

Figure 3.13: Plot of the slope of the MRRNU - *So* curve against abrasive particle diameter for slurries with otherwise identical compositions.

this zone expands as the Sommerfield number increases, and as the conditions experienced by the polishing couple become more hydrodynamic in nature. The hydrodynamic zone initially occurs in the central part of the radius, then expands outwards to the edge of the wafer, then inwards until in encompasses the entire polishing interface at high Sommerfield numbers. Towards the centre of the wafer from the hydrodynamic zone, the MRR is suppressed. Conversely, towards the edge of the wafer from the hydrodynamic zone, the polish rate is enhanced. The hydrodynamic, suppression and edge zones for all the polishing conditions noted in Table 3.2 are indicated in Figure 3.15. From this figure it is apparent that the zones identified in the MRR profiles of M3, N1 and N3 can be applied to all the conditions examined here.

This indicates that a series of mechanisms are responsible for material removal during Cu-CMP, and that these mechanisms can co-exist, depending on the lubrication characteristics of the polishing system. This is a novel approach

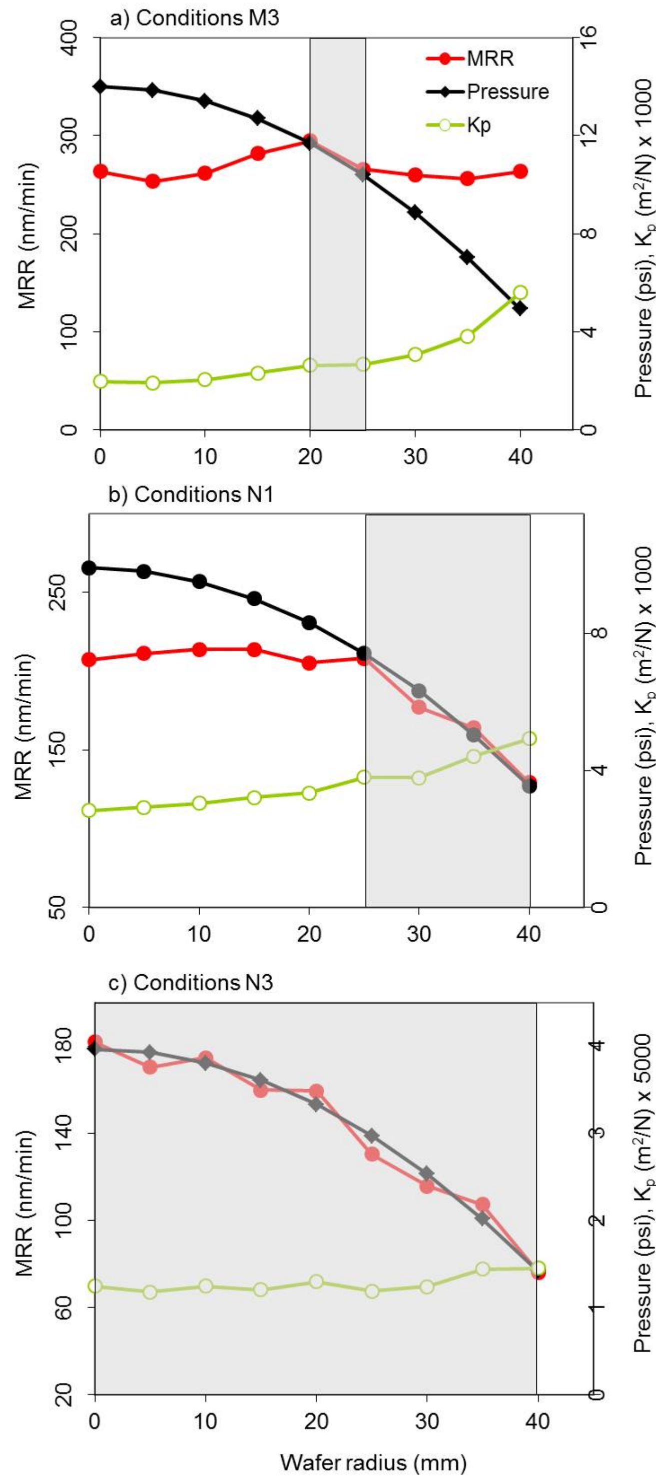

Figure 3.14: MRR profile and modeled pressure distribution for polishing at conditions a) M3, b) N1 and c) N3. The Preston coefficient for each point is also shown. The shaded regions indicate regions of hydrodynamic lubrication.

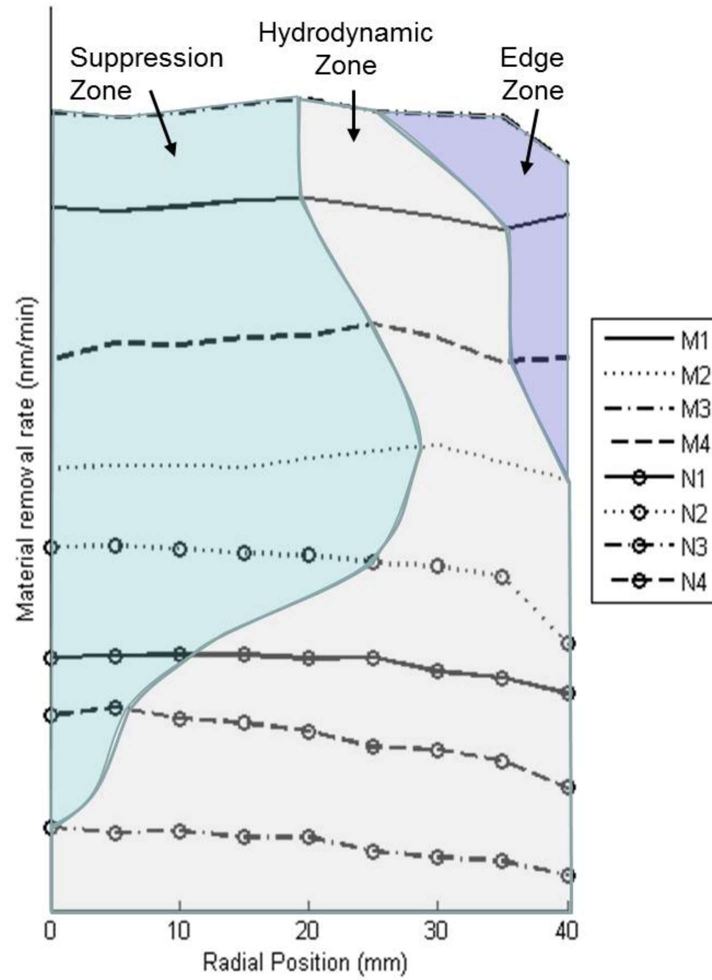

Figure 3.15: The MRR profiles shown in Figure 3.11, with the suppression, hydrodynamic and edge zones indicated.

to understanding CMP; although the presence of different polishing regimes has been suggested previously [45], their coexistence has not. Importantly, such a conclusion can unify much of the contradictory experimental results regarding CMP in the current literature. Suggested mechanisms for material removal in each zone are as follows:

Hydrodynamic Zone

Material removal in the hydrodynamic zone may occur by a process of 'chemical tooth', as suggested by Cook [18] and described in section 1.2.2. In this process, abrasive particles collide with the wafer surface and bond, then shear away from the surface, leading to its gradual attrition. Evidence for this is seen in TEM micrographs of slurry particles recovered from the polishing pad during CMP, such as those shown in Figure 3.16. These show that prior to polishing, the particles are smooth and small. After polishing, the particles are larger and studded with small particles of a material with a different density, such as copper or copper oxide, as evidenced by tilt contrast. Elemental analysis of such particles was not performed as the samples were deposited on copper grids, leading to high levels of background copper that would swamp the signal of any copper in the sample itself.

Interestingly, the Preston Equation discussed in section 1.2.1 was found to hold true in the hydrodynamic zone, as evidenced by the relatively constant value of the Preston coefficient observed. Closer examination of Preston's work reveals that typical conditions for the glass polishing he describes involve relative velocities of around 5m/s, due to the large scale of the apparatus. This is far higher than the velocities used in any of the work described here, and would correspond to much greater Sommerfield numbers. Additionally, his investigation involved the use of ungrooved, felt-covered runners. These two

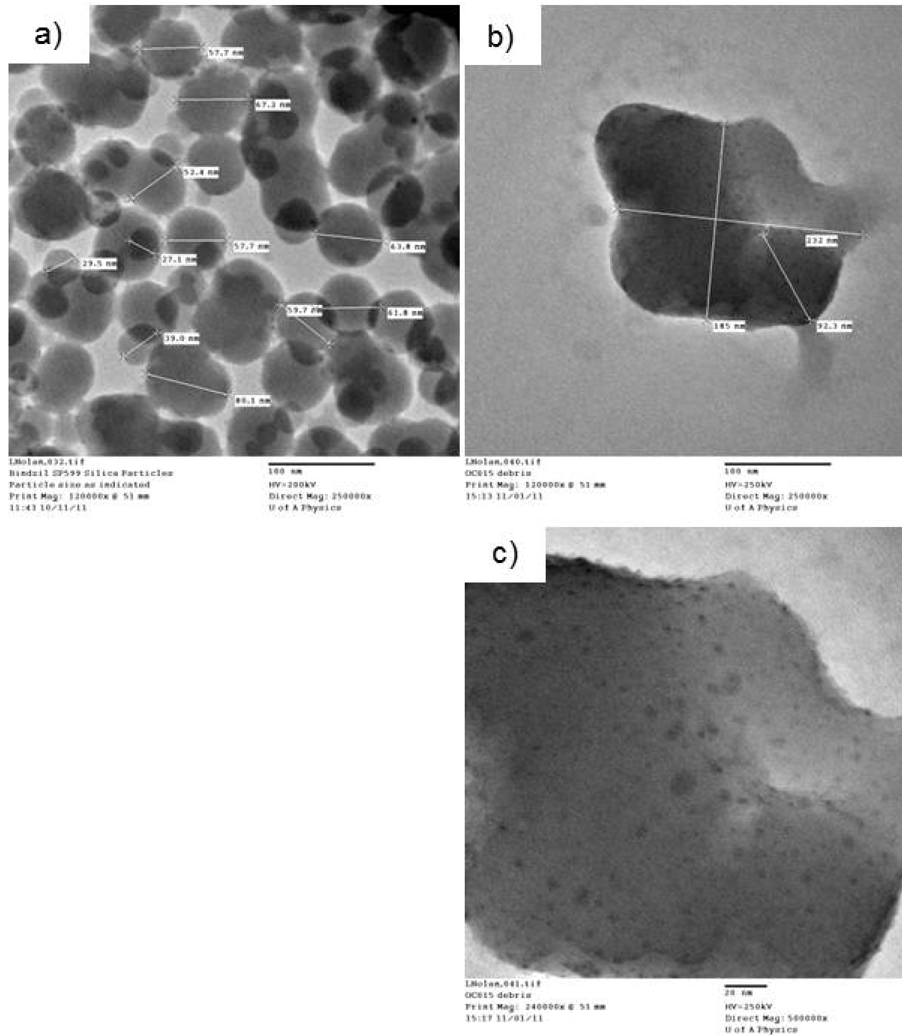

Figure 3.16: TEM micrographs of abrasive particles a) prior to polishing (250,000x); particle sizes are labeled and range from 30nm to 80nm b) after polishing (250,000x); particle dimensions are 230nm by 185nm and small 'studs' of a second material are present on the abrasive, and c) a close-up of b) (500,000x), showing the 'studs' in more detail.

conditions suggest that the glass polishing he describes is likely fully hydrodynamic, and that the Preston equation is a good model of polishing behaviour under hydrodynamic conditions.

Edge Zone

Edge effects in polishing have been noted by a number of authors, and have been attributed to a number of causes. Many of these relate to stresses, such as the Von Mises stress [57] or the contact stress [58, 59] generated during polishing, both around the wafer edge and around features in wafer. As discussed in section 3.4, microfluidic action due to the "coffee stain ring" effect has also been proposed as a mechanism for enhanced material removal at the wafer edge.

The results obtained in this work support the notion of a contact stress-related mechanism. At higher Sommerfield numbers, where the contact between the pad and the wafer is reduced by the hydrodynamic separation of the two surfaces, the edge zone is observed to recede.

Suppression Zone

The majority of workers in the CMP field quantify the material removal rate at the centre of the wafer only (for example [26]), or by the mass lost during polishing [21], and therefore do not provide a radial distribution of MRR that can be compared with the results obtained here. One exception is the work of Shan, Zhou and coworkers [5] for oxide polishing. While they do not quantify or consider the effect of lubricity in their work, they conduct a series of polishing experiments at a constant pressure of 2.9psi while varying the relative linear velocity from 0.2m/s to 0.7m/s, effectively examining MRRNU over a range of Sommerfield numbers. Their results, presented in Figure 3.17, are in excellent agreement with those obtained in this work, and clearly demonstrate

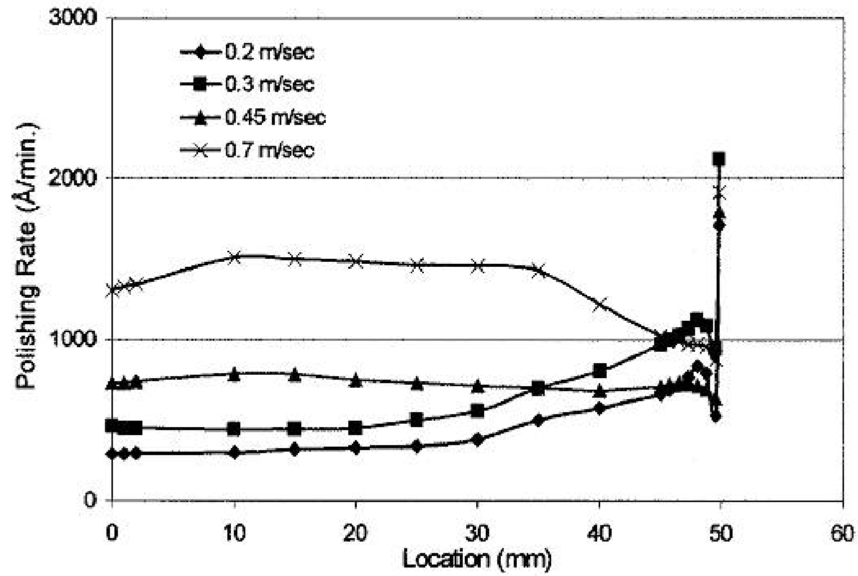

Figure 3.17: Distribution of MRR for oxide polishing, showing considerable MRRNU, obtained by Shan, Zhou and coworkers (from [5], ©[2001] IEEE). Their data were obtained at a constant pressure a velocities ranging from 0.2m/s (representing a low Sommerfield number)to 0.7m/s (representing a high Sommerfield number).

the presence of the hydrodynamic , edge and suppression zones illustrated in Figure 3.15. The agreement between these results, obtained for polishing silicon oxide, and the ones presented in this thesis suggest that the relationship between MRRNU and So is inherent to CMP.

At higher Sommerfield numbers, the authors attribute the enhanced material removal rate in the centre of the wafer to the presence of a region of subambient pressure developed there. Such a region would induce contact between the pad and the wafer, as the wafer surface is 'sucked' against the pad, increasing the rate of wear. However, they do not speculate as to the causes of the polish rate suppression noted at lower Sommerfield numbers. It may be the result of limited slurry penetration to the centre of the wafer, however further investigation of this phenomenon is required.

3.4 Conclusions

The presence of different zones of material removal explains the relationship between MRRNU and the lubrication conditions of the polishing couple as expressed by *So*. For the acidic slurry chemistry used in this work, polishing at less lubricating conditions (typified by lower Sommerfield numbers) results in high, negative values of MRRNU due to the presence of the edge and suppression zones in the pad / wafer interface. Polishing under highly lubricating conditions (typified by high Sommerfield numbers) results in high, positive values of MRRNU as the polishing couple becomes fully hydrodynamic and the material removal rate is proportional to the hydrodynamic pressure developed. An intermediate value of Sommerfield number with zero MRRNU can be deduced from the MRRNU vs. *So* curves produced.

The relationship between MRRNU and Sommerfield number described here may also explain apparently contradictory experimental results presented in the literature, such as those shown in Figure 1.4. It may also clarify the applicability of the Preston equation to CMP processes.

3.4.1 Future Work

Further investigation of the phenomena described in this chapter could clarify the link between lubrication regime and non-uniformity in polishing. The work carried out here utilised only one polishing pad and a limited range of slurry compositions, but was sufficient to indicate that these factors have a significant impact on the relationship between lubrication conditions and MRRNU. Systematic quantification of these effects would clarify the relationship, expanding the relevance of the MRRNU - *So* curves to the CMP community.

Further work should also be carried out to elucidate the mechanisms be-

hind the hydrodynamic, edge and suppression zones described in 3.3.3. An improved understanding of polishing behaviour in these zones could lead to greatly improved modeling methods for Cu-CMP.

4

Polish Rate as a Synergistic Interaction of Mechanical Abrasion and Chemical Reaction Rate

The last chapter dealt primarily with the distribution of material removal rates across a wafer during polishing, and did not consider the overall magnitude of that rate. In this chapter, maximising the Cu-CMP polishing rate by the synergistic interaction of chemical reaction and mechanical abrasion is examined.

4.1 Introduction

4.1.1 Slurry Components and Their Roles in CMP

Chemical mechanical polishing was initially developed to planarise silicon and silicon oxide [16]. However, changing process requirements led to its adaptation to metal surfaces such as tungsten. Kaufman, Thompson and coworkers proposed a now widely-accepted mechanism for W-CMP involving cyclical passivation and abrasion [6]. In this process, the tungsten surface is passivated by the chemical components of the slurry, halting further reaction. The passivated layer is then removed by mechanical abrasion, exposing fresh tungsten which is then passivated, beginning the cycle again. This is shown schematically in

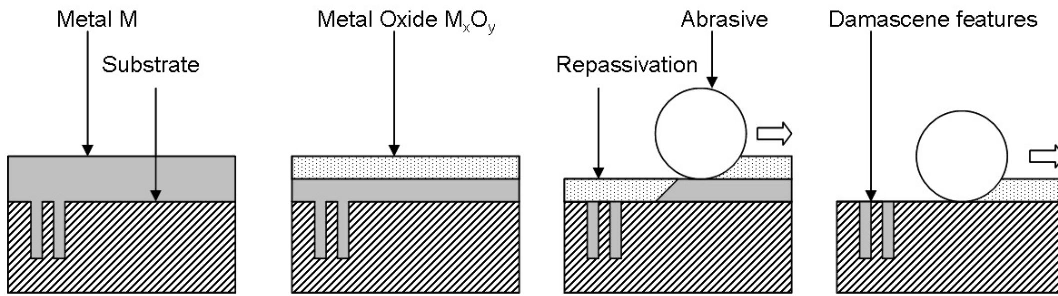

Figure 4.1: Schematic diagram of the passivation-abrasion mechanism proposed by Kaufman et al [6] for the removal of material in metal CMP (adapted from [1]).

figure 4.1 for the fabrication of damascene (inlaid) features.

The advantage of such a mechanism is that removal of the passive film by abrasion does not occur, or does not occur quickly, until the passive film comes into contact with the polishing pad. Low-lying regions of the surface are thus protected while protruding regions are removed, producing highly planar films. This is especially important as the size of features patterned on to wafers using optical lithography decreases; resolution of very small features is only possible with a very small depth of focus, requiring a highly planar surface. It is estimated that using CMP to produce highly planar surfaces has greatly prolonged the useful life of optical lithography [1].

Although this mechanism was proposed for W-CMP, it has found wide acceptance as a model for most metal CMP processes, including copper. Accordingly, the copper surface is passivated by the slurry chemistry during CMP. Inspection of the Pourbaix diagrams for copper in water, pictured in figure 4.2a), shows that oxidation occurs in neutral to basic pH in a narrow range of potentials. However, the oxide formed is not naturally passivating; in practice, a stable passivating film is achieved by adding an oxidiser and film stabiliser (usually referred to as a corrosion inhibitor) to the slurry. A common combination of oxidiser and inhibitor is hydrogen peroxide (H_2O_2) and benzotriazole

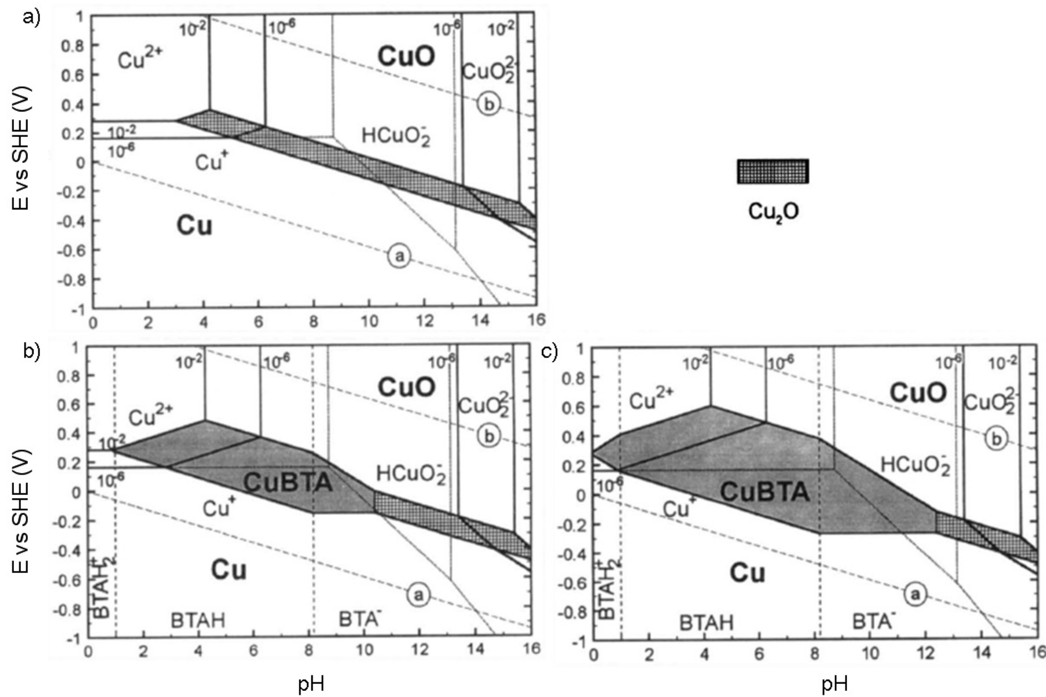

Figure 4.2: Pourbaix diagrams for the copper-BTA system with a) no BTA, b) $\{a_{BTA}\}=10^{-4}$, and c) $\{a_{BTA}\}=10^{-4}$ (from [7])

(BTA). The presence of BTA greatly expands the passivation range of copper, as shown in figure 4.2b) and c).

Chelating agents are also added to Cu-CMP slurries to prevent the redeposition of copper back on to the wafer surface following its removal. Commonly used chelating agents in Cu-CMP are glycine and citric acid, although a wide range of organic acids have been examined [21]. The structural formulae of BTA, glycine and citric acid are shown in figure 4.3.

The second part of Kaufman's model involves the abrasive removal of the passive film. The effects of particle size and concentration have been indirectly examined through their effects on material removal rate for tungsten [60, 12]. When polishing was carried out in a chemically active slurry the removal rate was found to increase with increasing particle concentration, up to a limit beyond which there was no further improvement. The removal rate

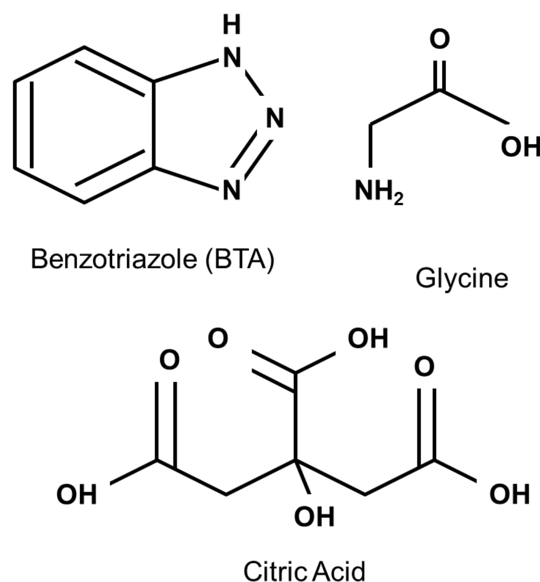

Figure 4.3: Structural formulae for benzotriazole (BTA), glycine and citric acid.

Table 4.1: Slurry components and their roles

Component Type	Specific Chemical
Oxidiser	Hydrogen Peroxide
Corrosion Inhibitor	Benzotriazole
Chelating Agent	Glycine; Citric Acid
Abrasive	Colloidal Silica

was also found to decrease with increasing particle size. However, it is not known whether this was a consequence of the particle size itself, or related to the smaller number of particles and lower specific surface area of the larger abrasives when used at the same weight or volume concentration. A comprehensive study of the interaction of abrasive particles with slurry chemistry in Cu-CMP has not been conducted.

The typical classes of components used in Cu-CMP slurries and the specific chemistries used in this study are shown in table 4.1. These slurries are aqueous.

4.1.2 Slurry Component Interactions

The interactions of the slurry components are complex, and difficult to examine in isolation. Electrochemical techniques have been employed to examine specific chemical combinations, while their overall effects on polishing are assessed through their impact on material removal rate. Electrochemical analyses of the behaviour of the chemicals described in table 4.1 are described here.

Copper, Hydrogen Peroxide and Abrasives

Potentiodynamic scans of copper in water with and without H_2O_2 at a pH of 4, such as those shown in figure 4.4, indicate that without H_2O_2, copper dissolves rapidly in water at potentials of 0.15V (vs. SCE) or higher. This is in agreement with the Pourbaix diagram. The addition of H_2O_2 provides a very limited amount of passivation by the formation of an oxide layer, as indicated by the 'shoulder' in the potentiodynamic curve for this chemistry, but the anodic potential is increased to 0.25V and rapid dissolution does not occur until the potential reaches 0.5V.

When copper is abraded with a fixed-abrasive pad in the presence of H_2O_2 at a pH of 4, the anodic copper reaction rate increases by a factor of three [61]. This indicates that H_2O_2 promotes the formation of a passive film, and that mechanical action removes the film formed. A similar phenomenon was observed when copper was exposed to alumina abrasives and varying concentrations of H_2O_2 in both static and actual polishing conditions [9], as shown in figure 4.5. The addition of small (1 to 2 vol%) amounts of H_2O_2 to the system significantly increased the copper dissolution rate, but further additions of H_2O_2 reduced it, indicating the formation of a passive film. The polish rate achieved in this experiment was an order of magnitude higher than the static etch rate, suggesting that the reaction kinetics are accelerated under the action

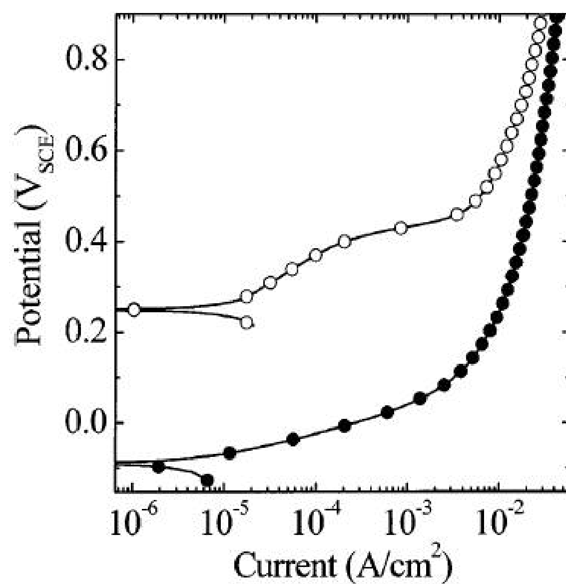

Figure 4.4: Potentiodynamic scans of copper in a buffered, pH 4 solution of 10g/L of Na_2SO_4 (open circles) and 10g/L of Na_2SO_4 with 3 vol% H_2O_2 (from [8]).

of abrasive and fluid motion, but that abrasion does not entirely prevent the formation of a passive film.

Copper, BTA and Abrasives

Addition of BTA to a solution of oxidiser in water stabilizes the copper oxide layer formed, reducing the reaction rate and hence the anodic current transient. This is shown for copper in a 3 wt% solution of nitric acid, another common oxidiser, in figure 4.6. Upon the addition of 0.02M BTA, indicated by the arrow, the anodic current transient decreases immediately.

It is also apparent from figure 4.6 that while the effect of BTA is immediate, it is not particularly rapid, requiring 3.5 minutes to reduce the dissolution rate of the copper by a factor of 10. This is around the same length of time as an entire CMP process, suggesting that BTA's effectiveness may be limited by slow reaction kinetics. BTA is known to act far more quickly in the presence of

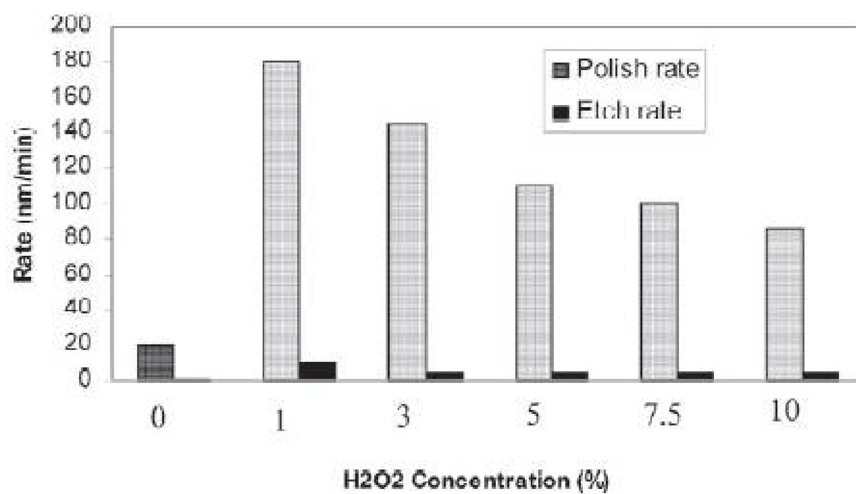

Figure 4.5: Removal rates of copper by varying concentrations of H_2O_2, in static (etch rate) and polishing conditions (from [9]).

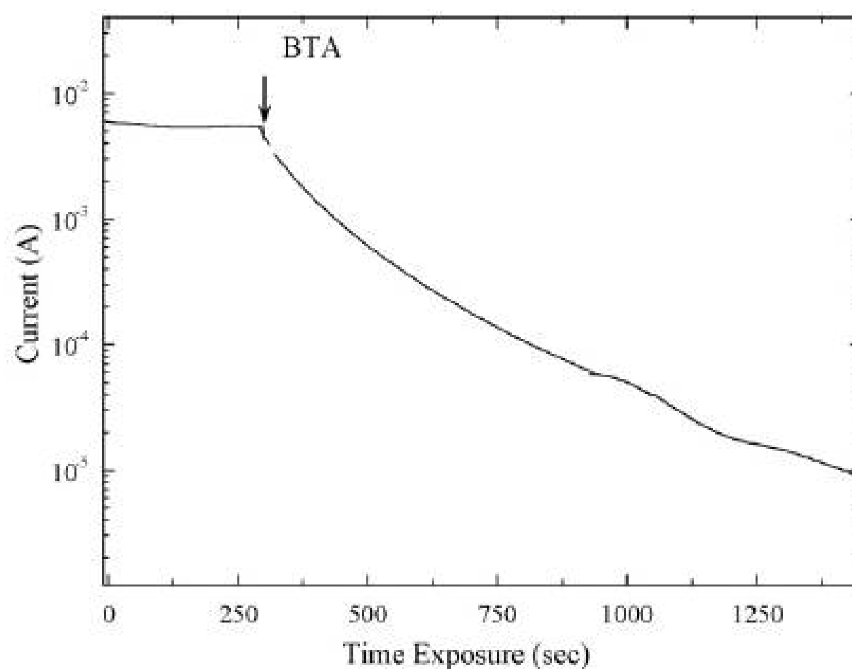

Figure 4.6: Anodic current transient (0.1V) of copper in 3 wt% solution of nitric acid. 0.02M of BTA is added at the point indicated; the anodic current immediately drops (from [10]).

chloride ions [7], however these are typically excluded from Cu-CMP processes as they have been linked to pitting in copper [62].

Copper, Glycine, Hydrogen Peroxide and Abrasives

Glycine on its own has little impact on the dissolution of copper, and is largely unaffected by abrasion by polishing pads and abrasives over a pH range of 4 to 9 [63]. However, the addition of H_2O_2 increased the reaction rate by an order of magnitude at polarization voltages of 0.5V and higher without abrasion, and 0.3V and higher with abrasion by a polishing pad [21]. This indicates firstly that a passive film is formed by the combination of glycine and H_2O_2 at this pH, and secondly that this film is removed by abrasion. This is confirmed by polishing and static etch rate tests at pH=4, at constant glycine concentration and a range of H_2O_2 concentrations. As in figure 4.5, the addition of small amounts of H_2O_2 increased the copper removal rate while larger amounts promoted the formation of a passive film and reduced copper dissolution. However, the presence of glycine reduces the amount of H_2O_2 necessary to form such a film from 1 to 2 vol% H_2O_2 to less than 0.5 vol% H_2O_2, regardless of the degree of abrasion [64]. Glycine is therefore a strong promoter of passive film formation in Cu-CMP.

Copper, Citric Acid, Hydrogen Peroxide and Abrasives

A similar effect is observed when copper is exposed to citric acid solutions containing H_2O_2 in static and dynamic fluids. In electrochemical experiments [65], increasing the concentration of H_2O_2 in the presence of citric acid under static conditions increased the rate of copper dissolution until a steady state was obtained, and the dissolution rate remained unchanged with further increases in the H_2O_2 concentration. Introducing fluid motion by rotating the electrode resulted in significantly higher dissolution rates at low H_2O_2 concen-

tration, compared with a static electrode. At higher H_2O_2 concentrations, the dissolution rate decreased, and at low rotation speeds again reached a steady state. At high rotation speeds, no such state was achieved over the range of H_2O_2 concentrations tested. Potentiodynamic polarization studies of the citric acid - H_2O_2 - copper system at high citric acid concentrations do not indicate any passivation of the copper, either with or without abrasion [21]. This suggests that, while low concentrations of citric acid stabilize the passive film, it may in fact dissolve any passive film formed at high concentrations.

Copper, Hydrogen Peroxide and Commercial Slurry

Wang, Tsai and coworkers [11] examined the effect of adding varying concentrations of H_2O_2 to a commercial slurry (Rodel® XJFW8099). In keeping with the results of the studies discussed here, they found that the addition of a small amount of H_2O_2 greatly increased the static etch rate of copper, while larger amounts promoted the formation of a protective passive film that prevented further dissolution. When the same slurries were used for polishing, a 1:1 mixture of 30 wt% H_2O_2 and XJFW8099 showed high polishing rates and excellent surface quality, but significant greater MRRNU, compared to a 1:4 mixture of the same components. AFM images of the copper surface after polishing in these two mixtures are shown in figure 4.7a) and b) respectively. From this figure, it is apparent that the copper surface polished in the 1:1 H_2O_2:slurry mixture is significantly smoother, and has altered the as-deposited grain structure far more, than that polished in the 1:4 H_2O_2:slurry mixture. This suggests that increased concentration of H_2O_2 in this slurry improved the quality of the passive film.

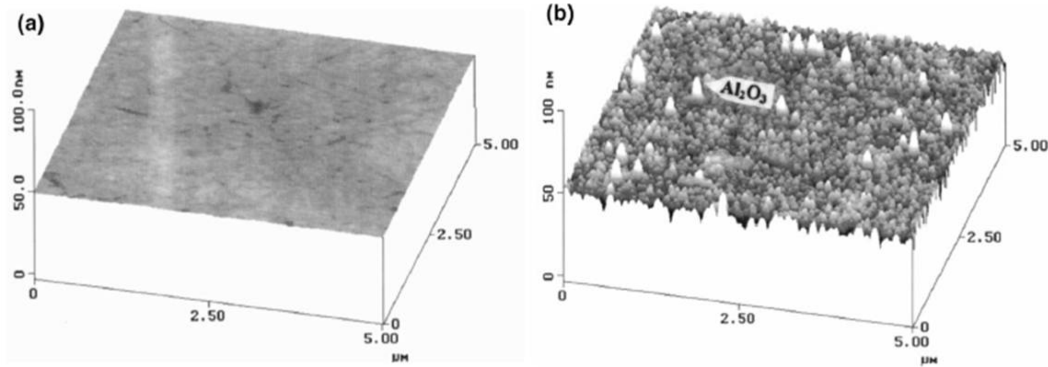

Figure 4.7: AFM images of the copper surface after polishing with 30 wt% H_2O_2 and Rodel® XJFW8099 slurry mixed in a a) 1:1 ratio and b) 1:4 ratio (from [11]).

4.1.3 Effect of Abrasive Concentration on Material Removal Rate

The effect of the abrasive particle size and concentration has been examined for alumina particles in W-CMP by Bielmann, Mahajan and Singh [60]. For W-CMP, the material removal rate increased as the particle concentration increased from 2 wt% to 15 wt% for all abrasive sizes. The relationship between MRR and particle concentration reached a plateau for larger particle sizes, shown in figure 4.8a). Kim, Kwon and coworkers investigated the effect of ceria abrasive and BTA concentration on Cu-CMP [13]. As with tungsten polishing, an increase in the abrasive concentration resulted in an increased MRR, with the rate of MRR increase slowing at higher concentrations. No plateau was detected over the limited abrasive concentration range investigated (0.5 wt% to 3 wt%). The results obtained in this study at a glycine concentration of 0.01M are shown in figure 4.8b).

It is clear that the interactions between the slurry components and the abrasives, and hence the formation and removal of a passive film on the copper, are complex. This work examines the specific role of H_2O_2 concentration in developing a passive film, and silica abrasive concentration in removing it.

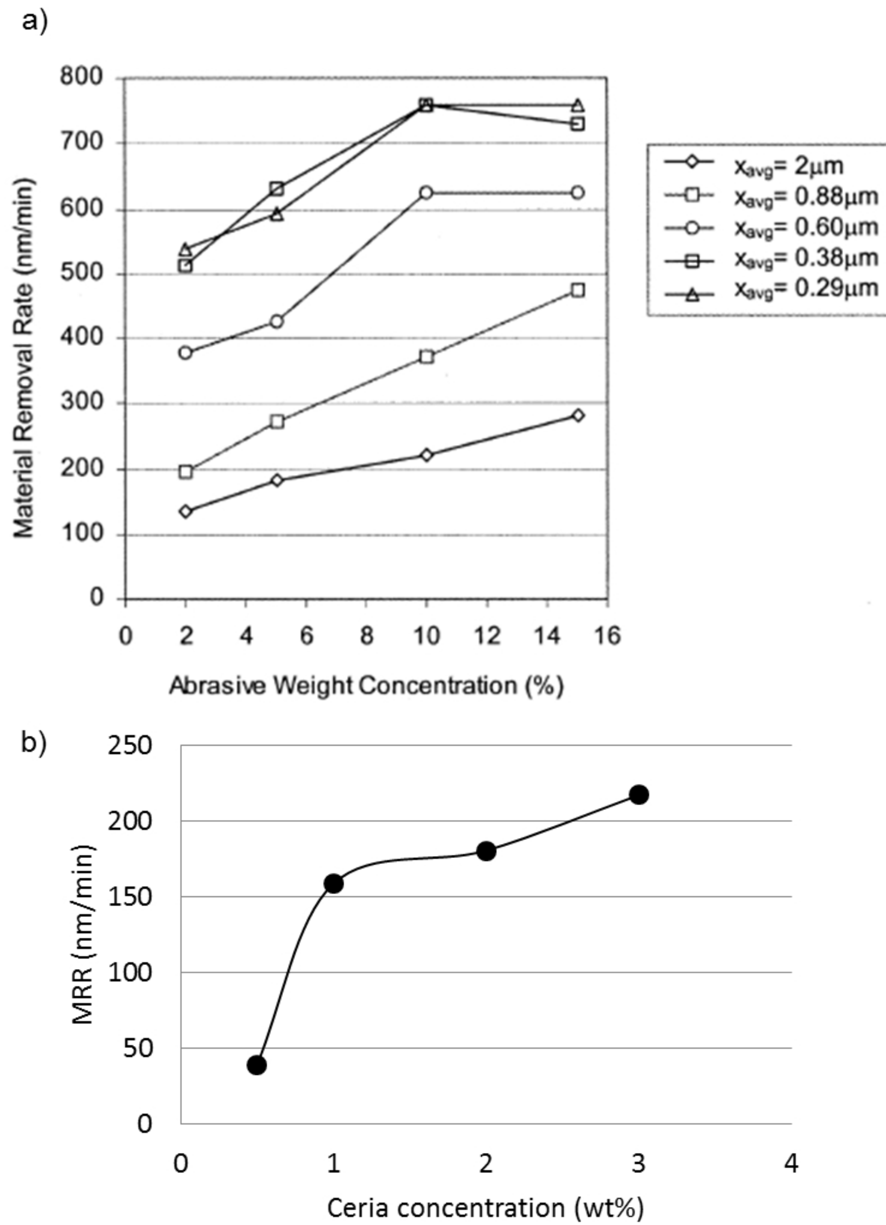

Figure 4.8: Effect of particle concentration on a) W-CMP (from [12]) and b) Cu-CMP (replotted from [13]).

A synergistic ratio of the two components is observed at which the material removal rate is greatly enhanced.

4.2 Experimental Procedures

A matrix of experiments was carried out, in which 144 wafers were polished under 36 conditions comprising six H_2O_2 concentrations, six silica abrasive concentrations, and all combinations thereof. The polishing conditions, labeled A0 through F5, are summarized in table 4.2.

As well as the concentrations of H_2O_2 and SiO_2 noted, each polishing slurry contained 1 wt% glycine, 1mM BTA, and sufficient citric acid to adjust the pH to 3.55, with the balance comprised of deionised water. The abrasive particles were added in the form of a 50 wt% silica suspension and had a mean diameter of 84nm, as determined by dynamic light scattering. The slurry flow rate was 200mL/min for all conditions.

All polishing was conducted using the apparatus described in section 2.1 with a NexPlanar® E7450-30S radially- and concentrically-grooved pad. The pad was conditioned for a minimum of one hour prior to polishing, and continuously during polishing. The thickness of the copper film was measured at nine points across the wafer radius using a Veeco® 4PP, as outlined in section 2.1.1. Following polishing, the wafers were rinsed thoroughly in deionised water and dried with nitrogen gas. A selection of wafers were imaged using a Digital Instruments® Dimension 3100 AFM before and after polishing, and a selection of slurry samples were taken during polishing for TEM analysis, as described in section 2.4.2.

The coefficient of friction was recorded while each wafer was polished using the method outlined in section 2.3.

Table 4.2: Concentrations of H_2O_2 and SiO_2 for polishing conditions A0 to F5. Each set of polishing experiments was carried out at an applied pressure of 4 psi and rotational speed of 60rpm (1.07 m/s), and the slurry additionally contained 1 wt% glycine, 1mM BTA, and sufficient citric acid to adjust the pH to 3.55.

Concentration	0 wt% H_2O_2	0.5 wt% H_2O_2	1 wt% H_2O_2	2 wt% H_2O_2	3 wt% H_2O_2	4 wt% H_2O_2
0 wt% SiO_2	A0	A1	A2	A3	A4	A5
1.9 wt% SiO_2	B0	B1	B2	B3	B4	B5
5.9 wt% SiO_2	C0	C1	C2	C3	C4	C5
9.8 wt% SiO_2	D0	D1	D2	D3	D4	D5
13.7 wt% SiO_2	E0	E1	E2	E3	E4	E5
19.4 wt% SiO_2	F0	F1	F2	F3	F4	F5

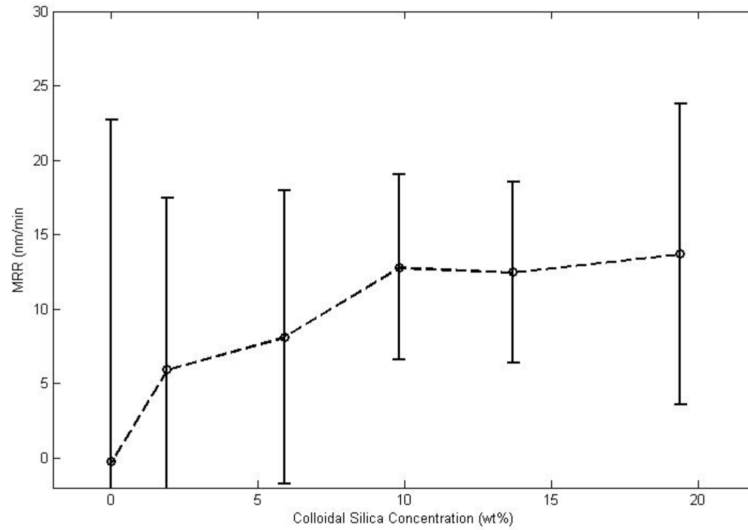

Figure 4.9: Effect of SiO_2 concentration on MRR, without the presence of H_2O_2.

4.3 Results and Discussion

4.3.1 Material Removal Rate MRR

The effect of abrasion concentration on the material removal rate, without the presence of H_2O_2, is shown in figure 4.9. The error bars indicate one standard deviation in the removal rate measured at each point across the wafer surface. The measured error is very large, due to difficulties in accurately measuring very small changes in film thickness. The data is that obtained while polishing under conditions A0 to F0,as described in table 4.2.

It is apparent that without the presence of an oxidiser, the rate of mechanical abrasion by the particles is very low, reaching a maximum of just 14 nm/min at a particle concentration of 19.4 wt%. This supports the theory of Kaufman and coworkers [6] described in section 4.1.1 that removal is by abrasion of an oxide layer, as without the formation of such a film, removal rate is extremely low. By extension, any removal of the copper film that does

occur must be by abrasion of the copper itself. The removal rates recorded are therefore equivalent to the change in copper thickness with time due to mechanical action only. Evidence for such a mechanism is observed in AFM analysis of wafers polished without the presence of an oxidiser, such as those presented in figure 4.10. The wafer shown in figure 4.10a) was polished in a slurry containing 11.8 wt% colloidal SiO_2 only, at an applied pressure of 4psi and a rotational speed of 30rpm (relative linear velocity = 0.53m/s). This wafer was in the as-sputtered state prior to polishing. The root-mean-square line roughness (R_q) of the section shown is 102Å. Several scratches are visible, with depths of 29nm (black cursors) and 9nm (green cursors). Abrasive particles are visible at the ends of a number of the scratches. This suggests that they were created by the 'gouging' action of the abrasives, and that they became wedged in the scratches during polishing. Away from the scratches, the surface resembles that of an as-sputtered wafer, such as the one shown in figure 4.11 for comparison. This surface has a roughness R_q of just 19Å, indicating that the scratches generated during polishing add significantly to the roughness. The wafer shown in figure 4.10b) was also polished from the as-sputtered state in a slurry containing 11.8 wt% SiO_2, but with an applied pressure of 8psi and a rotational speed of 60rpm (relative linear velocity = 1.07m/s). The scratch visible on this surface has a depth of 3nm and the line roughness R_q is 1.4Å. Numerous abrasive particles that remained adhered to the copper surface after polishing are also visible, but do not appear to be anchored at the ends of scratches. For this wafer, it is apparent that polishing action occurred, leading to an overall reduction in surface roughness and a visibly smoother surface, such as that shown in figure 4.7. The difference in polish outcomes illustrated in figure 4.10 may be the result of differences in load distribution that occur with increasing pressure, and supports the notion of a transition from rolling

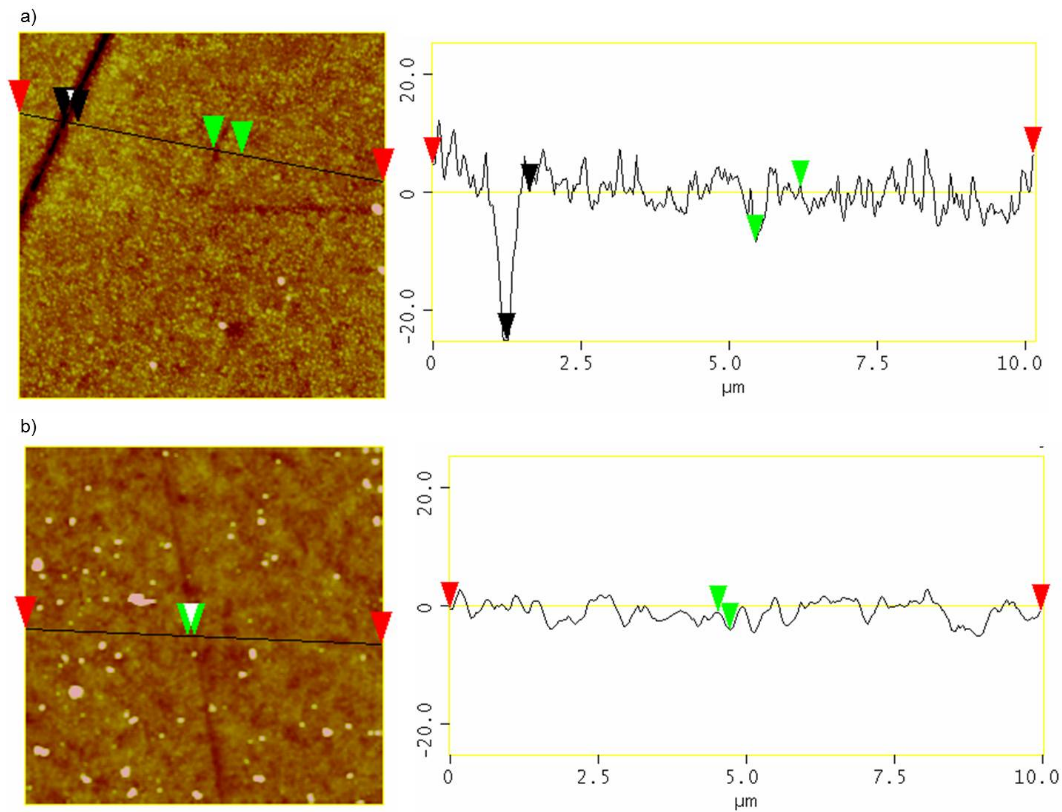

Figure 4.10: AFM images and sections for copper films polished in a slurry containing 11.8 wt% colloidal SiO_2 particles, polished at a) an applied pressure of 4psi and rotational speed of 30rpm (relative velocity = 0.53m/s), and b) an applied pressure of 8psi and rotational speed of 60rpm (relative velocity = 1.07m/s). Each scan is $10\mu m \times 10\mu m$

to sliding wear proposed by Zhao and Shi [28] and discussed in section 1.2.3. Increasing the applied pressure results in a linear increase in the contact area between the pad and the wafer, according to confocal examination of polishing pads [66], and hence a linear increase in the number of particles caught at the pad - wafer interface. The load applied to the wafer *per particle* therefore decreases. In combination with the higher polishing speed used to polish this wafer, a rolling abrasive mechanism for material removal may account for the reduced scratch depth and greatly reduced surface roughness obtained under these conditions.

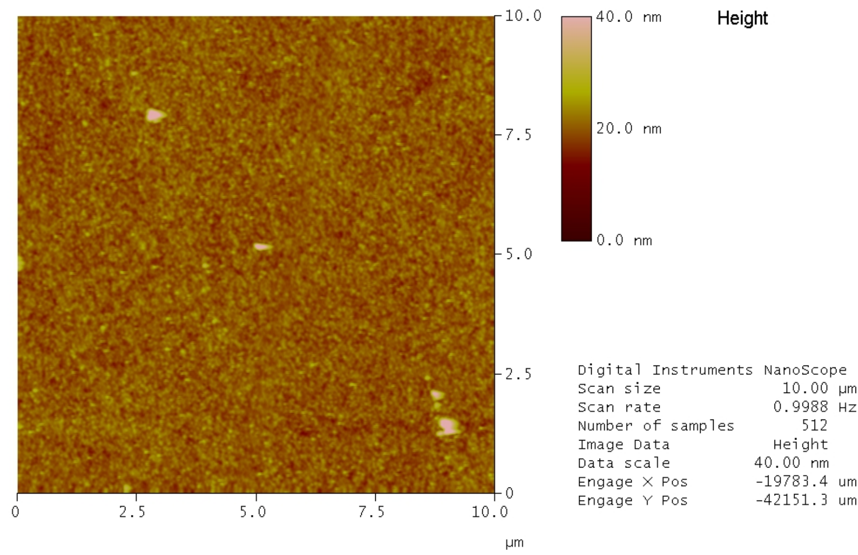

Figure 4.11: AFM image of a wafer in the as-sputtered condition.

A similar mechanism may be responsible for the plateau in removal rate observed at SiO_2 concentrations greater than 9.8 wt% in figure 4.9, and reported by other researchers in figure 4.8. Increasing the concentration of particles in the slurry increases the number of particles trapped at the points of contact between the pad and the wafer in a manner similar to increasing the applied load. This again reduces the load per particle, and may be responsible for the observed plateau in material removal rate.

The effect of H_2O_2 concentration on the material removal rate, without the presence of abrasives, is shown in figure 4.12. The error bars indicate one standard deviation in the removal rate measured at each point across the wafer surface. The data shown is that obtained under conditions A0 to A5, as described in table 4.2. The removal rates achieved are an order of magnitude greater than those obtained using abrasive particles without H_2O_2, reaching a maximum of 174 nm/min.

The results obtained reflect those of other researchers, such as those seen

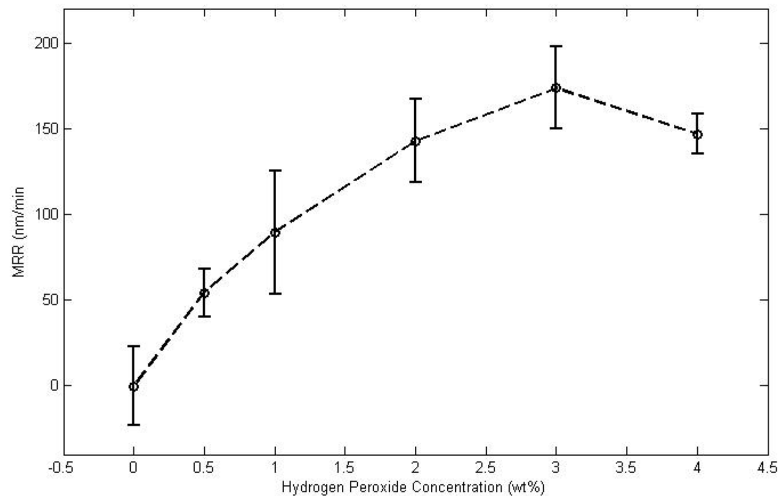

Figure 4.12: Effect of H_2O_2 concentration on MRR, without the presence of abrasives.

in figure 4.5. They suggest that small amounts of H_2O_2, in conjunction with the BTA and glycine present, encourage copper dissolution. Larger amounts result in the formation of a passive film and a decrease in the rate of copper loss from the surface. The rate at which the surface is chemically passivated is therefore a key indicator of the polishing outcomes. This is supported by visual inspection of the wafers after polishing in H_2O_2 without abrasives, which reveals a haze over the wafer surface consistent with an oxide film. An example of a hazed wafer, polished at an applied down pressure of 6 psi and a rotational speed of 30rpm (relative velocity = 0.53m/s) in a solution containing BTA, glycine and citric acid as indicated, and 1 wt% H_2O_2, is shown in figure 4.13.

The removal rates achieved for all concentration combinations of H_2O_2 and abrasives can be seen in figure 4.14. It is apparent that increasing the concentration of both the abrasives and H_2O_2 significantly increases the material removal rate, up to a maximum value. Beyond this peak value, the removal rate drops to a plateau and further additions of abrasives and H_2O_2 do not

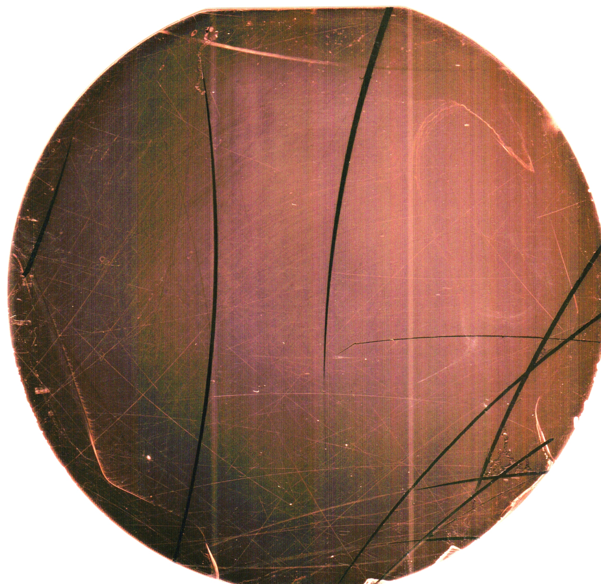

Figure 4.13: Optical image of a wafer polished with an applied down pressure of 6 psi and a rotational speed of 30rpm (relative velocity = 0.53m/s) in a solution containing 1mM BTA, 1 wt% glycine and citric acid as indicated, and 1 wt% H_2O_2.

result in any increase in polishing rate. The maximum polishing rate, 664 nm/min, occurs at a H_2O_2 concentration of 3 wt% and SiO_2 concentration of 9.8 wt%. This rate is nearly four times the removal rate achieved at the same H_2O_2 concentration without abrasives, and more than 50 times the mechanical abrasion rate achieved at the same SiO_2 concentration without H_2O_2. This demonstrates that material removal is the result of a synergistic interaction between chemical reaction rate and mechanical abrasion. The same data is replotted in figure 4.15 as a contour map to aid analysis.

The ratio of H_2O_2 to abrasives at which the material removal rate is the highest varies from approximately 2.5:1 at high H_2O_2 concentrations to 10:1 at high SiO_2 concentrations, forming a ridge in the MRR/concentration map. It is apparent that an increased abrasive concentration shifts the peak polishing rate to a lower H_2O_2 concentration, suggesting that the passive film removed by the abrasives is thinner. This supports the notion that an increase in

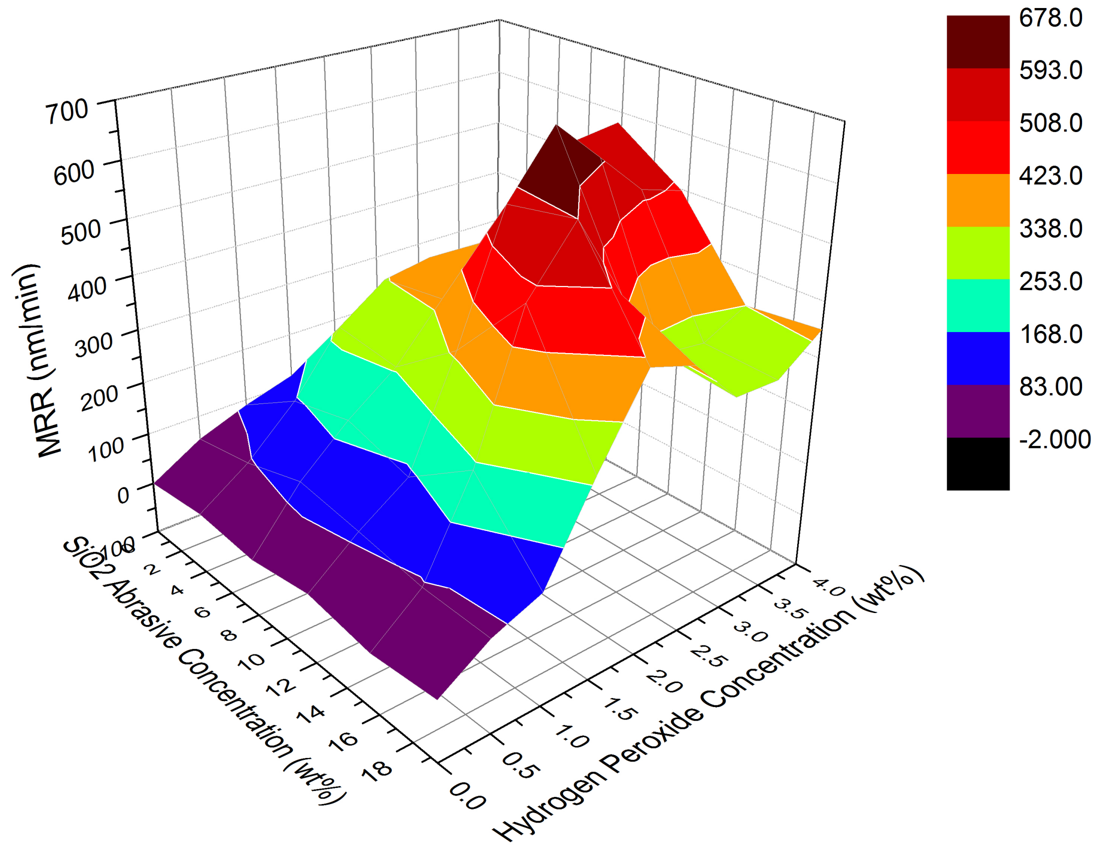

Figure 4.14: Surface plot of measured polishing rate for varying concentrations of H_2O_2 and abrasives. The colour bar represents material removal rate, MRR, in nm/min. All results were obtained at an applied pressure of 4 psi and a rotational speed of 60rpm (1.07m/s).

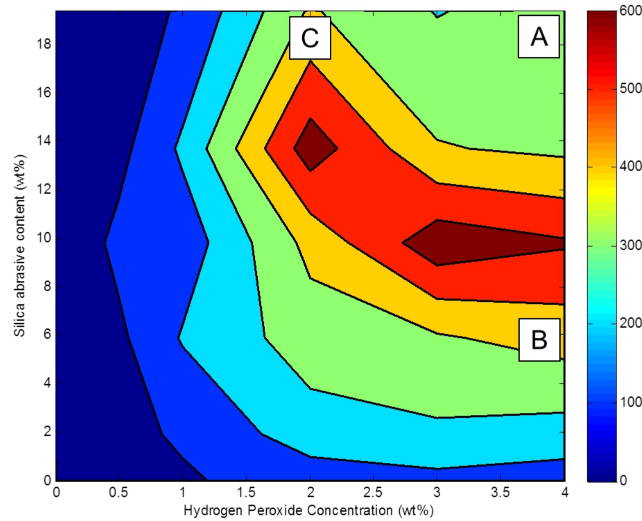

Figure 4.15: Contour map of polishing rate at all concentrations of H_2O_2 and abrasives. The colour bar represents material removal rate, MRR, in nm/min.

particle concentration lowers the load transmitted to the wafer per particle, and hence the polishing action carried out by each particle. In contrast, the presence of a plateau in the polishing rate at concentrations of abrasives and H_2O_2 beyond the peak level suggests that the oxide film has reached a thickness that is beyond that which the abrasives can effectively remove. This allows the surface to remain passivated at all times, slowing further reaction and reducing material removal rate. Three regions can therefore be identified in figure 4.15:

- At concentrations below the peak concentration, the rate of mechanical abrasion outstrips the rate of chemical removal. Removal is therefore *abrasion - dominated*. The particles are always able to remove the passive film and expose the underlying copper. Removal rate therefore increases rapidly with H_2O_2 concentration, as there is no barrier to reaction in the form of a passive film. The relationship between component concentration and MRR is approximately linear in this region.

- At concentrations above the peak concentration, the passive film forms too quickly to be effectively removed by the abrasives. Removal is therefore *passivation - dominated*. Additional abrasives have little effect on removal rate as the load per particle decreases and they are less able to penetrate and remove the passive film. The addition of H_2O_2 also has little effect, as the copper surface remains partially passivated at all times, hindering further reaction.

- The maximum removal rate occurs when the rates of mechanical abrasion and chemical reaction are *synchronised*. The material removal rate resulting from their combined action at this point is significantly enhanced, compared to the removal rates due to chemical or mechanical action only, indicating a synergistic interaction of slurry chemistry and abrasives.

These regions are shown schematically in 4.16.

Final wafer surface quality is related to the region, as described above, in which it was polished. AFM images of wafers polished at locations A, B and C on the MRR/concentration map in figure 4.15 are shown in figure 4.17. The surface of the wafer polished at location A is contaminated with large amounts of polishing particles, but examination of the surface between the particles reveals that it is smooth and flat, with a roughness R_q of 10Å. This is consistent with the development of a thick passive layer that is not fully removed by abrasion. In contrast, the wafer polished at location B has a rough surface (R_q = 20Å). This is not significantly altered from the as-sputtered roughness of 25Å, and is consistent with constant removal of the passive film to expose the copper surface beneath, leading to uneven polishing on the nanoscale. At location C, the wafer surface is smooth (R_q = 13Å), and the grain structure has undergone significant disruption, indicating an effective

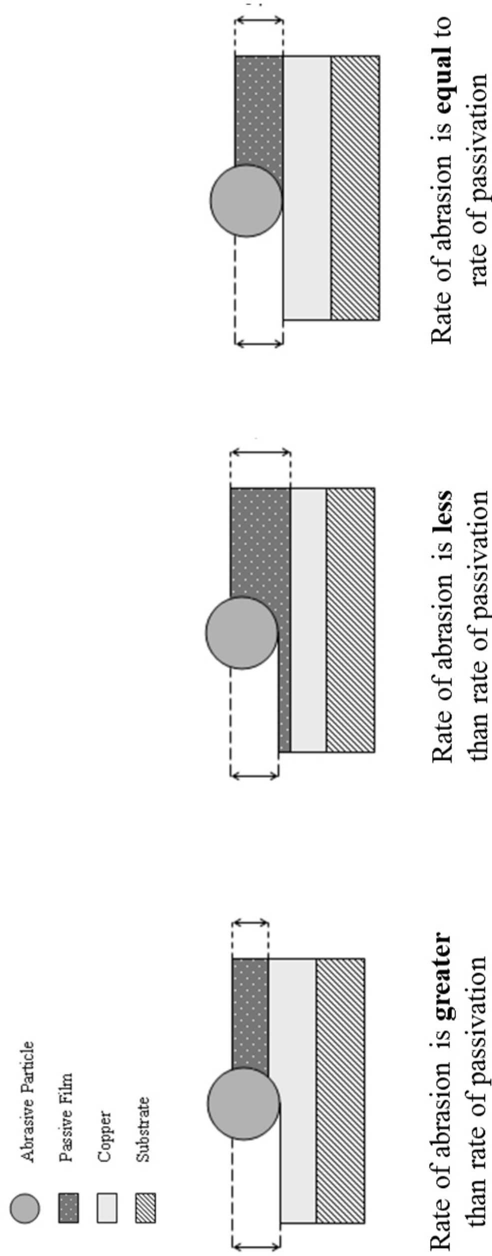

Figure 4.16: Schematic representation of abrasion-dominated, passivation dominated and synchronised polishing mechanisms.

polishing action.

4.3.2 Coefficient of Friction CoF

The highest CoF recorded was 0.79 under conditions F4, and the lowest was 0.31 under conditions A0. While this generally suggests an increase in coefficient of friction with increasing H_2O_2 and abrasive concentration, the results, shown in figure 4.18, were scattered and no strong trends were observed. The correlation between MRR and CoF, shown in figure 4.19a) was poor. This has been noted by a number of authors in the past, such as Li, Ina and coworkers [14]. The relationship between CoF and MRR they reported for a set of Cu-CMP experiments in which several different slurry compositions were used is shown in figure 4.19b).

4.4 Conclusions

The interaction of the abrasive particles and H_2O_2 in Cu-CMP is synergistic in nature. The combined action of these two components leads to polish rates that are far higher than the sum of the polishing rates of the components in isolation. Different mechanisms for material removal are proposed for regions of the MRR - concentration map, resulting in different final surface characteristics. Where the rate of mechanical abrasion is faster than the rate of chemical removal, MRR increases rapidly and linearly with increasing H_2O_2 concentration. However, the surface quality of the polished surface under these circumstances is poor and displays high roughness. This is consistent with the constant removal of the passive layer by abrasion. In contrast, where the chemical reaction rate dominates, the polished surface quality is very good. However, removal rates are lower in this regime and independent of the H_2O_2 concentration. A synergy occurs when the rates of mechanical and chemical

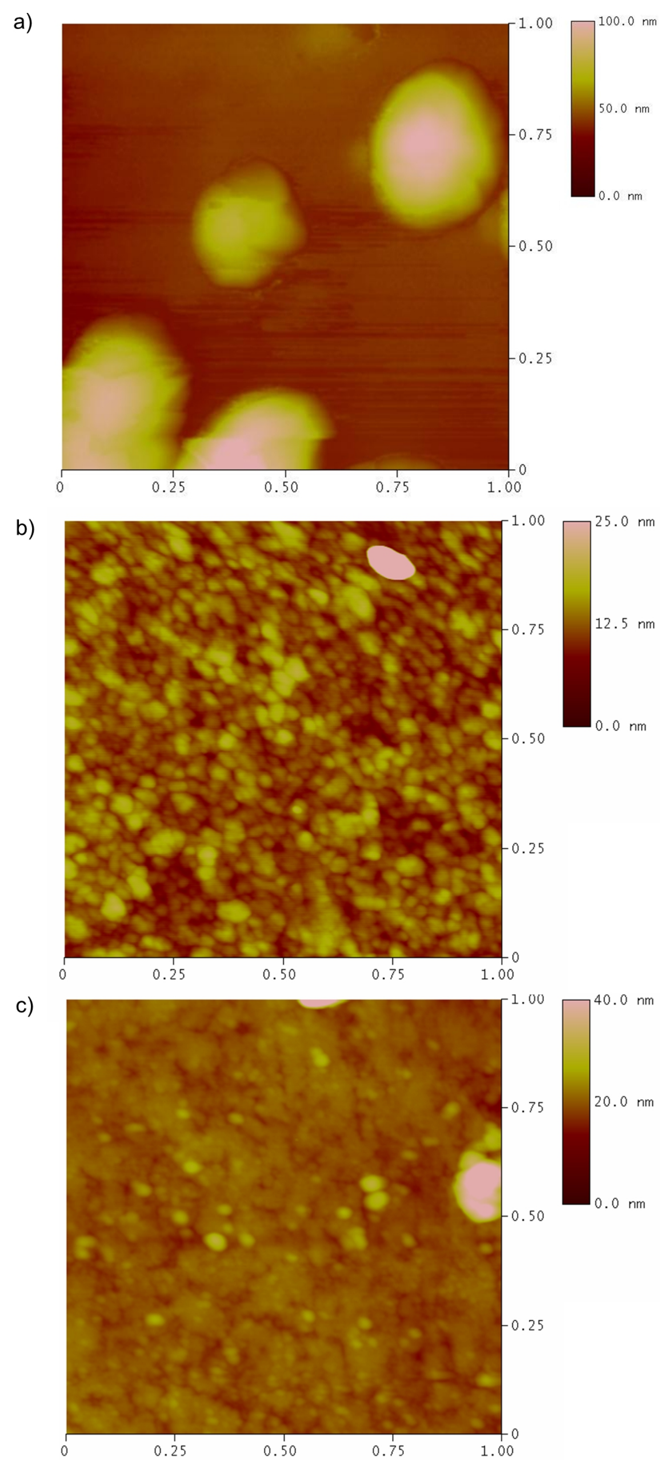

Figure 4.17: AFM images of wafers polished at a) location A, b) location B and c) location C in figure 4.15. All scans are $1\mu m \times 1\mu m$.

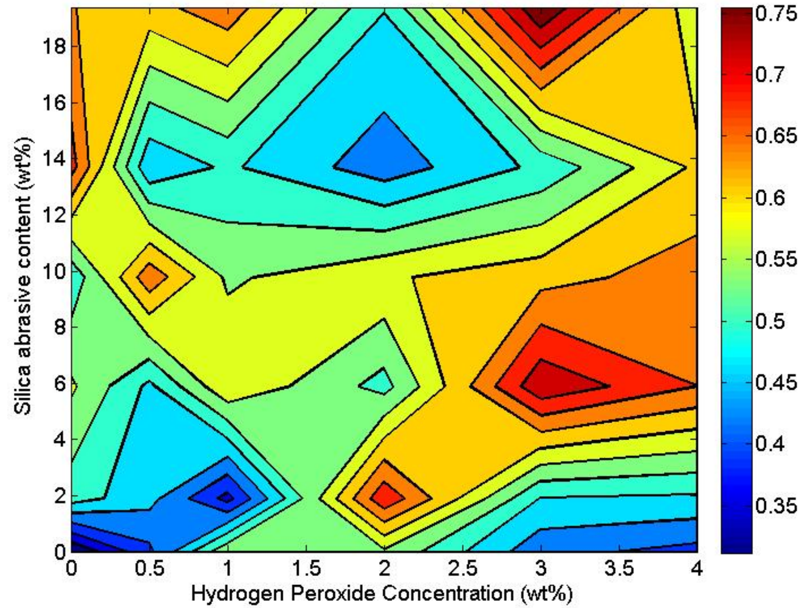

Figure 4.18: Map of measured CoF, represented by the colour bar, for varying concentrations of H_2O_2 and abrasives. No strong trends were observed.

abrasion are approximately equal, at which point the material removal rate is greatly increased. The interactions noted appear to be unrelated to the coefficient of friction, or the polishing mechanism at work.

4.4.1 Future Work

In these experiments, the H_2O_2 and abrasive concentrations were varied while the other components of the slurry, and the polishing conditions used, remained constant. However, the concentration of corrosion inhibitor in the slurry is likely to have a substantial effect on the rate of passivation, while the polishing pressure and down force are likely to affect the abrasion rate. These interactions warrant further investigation.

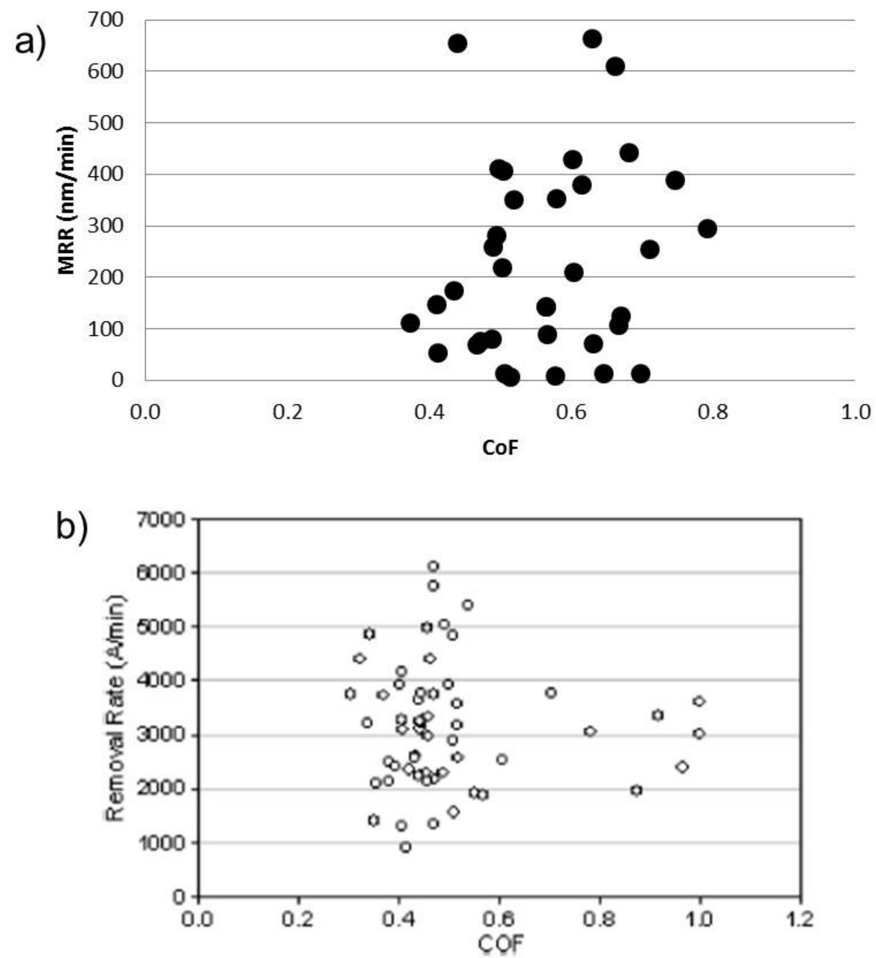

Figure 4.19: Correlation between MRR and CoF for a) conditions A0 to F5 in this work and b) Li, Ina and coworkers [14].

5

Optimal Delivery of Slurry to the Polishing Interface

In this chapter, slurry flow across three commonly-used pad surface types is characterised. The impact of slurry flow on Cu-CMP is found to be negligible, however understanding its characteristics allows the use of slurry in polishing to be optimised.

5.1 Introduction

In most CMP processes, the polishing slurry is poured onto the centre of the pad at a constant rate, then transported to the wafer (a distance of tens of centimetres) by the rotation of the pad or the sweeping action of the conditioner. The relationship between the pad topography, the slurry flow rate and conditioning protocol used, and their effects on polishing outcomes and slurry utilisation, are examined.

Slurry is a high-cost item in CMP, and makes up around 50% of the cost-of-ownership of the process [67]. Some work has been done on reducing this cost through recycling or reusing slurry [67]. Others have investigated the slurry flow characteristics to determine utilization and optimisation parameters for CMP, as will be discussed in the next section, with varied results. In this

study, a simple tracer is used to determine the flow characteristics of the slurry across the polishing pad. The information collected is then used to describe the incursion of slurry into the pad / wafer interface.

5.1.1 Slurry Utilization in CMP

Philipossian and Mitchell [15] investigated the utilization of slurry in CMP by modeling the CMP system as a closed flow reactor, and measuring the progress of a tracer in the slurry input through the pad/wafer interface. They established a relationship between CoF and the abrasive content, from 0% (deionised water) to 20%, for the slurry, then used this relationship as the friction 'signature' for slurries with varying abrasive concentrations as the tracer. While polishing, the slurry was instantaneously switched from deionised water to slurry with an abrasive content of 20%. The CoF was measured and correlated to the slurry abrasive content using the 'signature' established, allowing the authors to determine how much of the initial water had been displaced by slurry in the polishing interface. The fraction of the fluid that had been displaced, from 0 to 1, was plotted over time to produce an F-curve. This was differentiated to obtain an E-curve, representing the distribution of residence times of the fluid elements. Integrating the E-curve with respect to time gives the mean residence time (τ) of the slurry in the pad/wafer interface. If the volume (V) of this interface is known, the flow rate of slurry through the interface can be determined by:

$$q_{interface} = \frac{V}{\tau} \tag{5.1}$$

Dividing the obtained flow rate $q_{interface}$ by the input flow rate at which slurry is delivered on to the pad, q_{input} gives the utilization of the slurry η in the process. The authors estimated the volume of the pad/wafer interface

by summing the volume of the pad grooves, and approximating the fluid film thickness on the surface as the pad roughness. Using this technique with a fumed silica slurry and a Fruedenberg® FX-9 perforated pad, they determined that η was as high as 22% when q_{input} was 40mL/min (the lowest tested), the relative linear velocity was 0.62m/s (the highest tested) and the applied pressure was 2psi (the lowest tested). Conversely, with a colloidal silica slurry and a Rodel® IC-1000 K-grooved pad, η was as low as 2% when q_{input} was 60mL/min, the relative linear velocity was 0.31m/s (the lowest tested) and the applied pressure was 6psi (the highest tested). A summary of their results for the fumed silica slurry is shown in Figure 5.1. This illustrates the general trend that utilization increases with increasing relative linear velocity, and decreases with increasing input flow rate q_{input}. The effect of pressure is less clear, with the values shown in 5.1 independent of pressure within the authors' stated error margin of $\pm$10%. These results are somewhat at odds with an earlier study [68] by one of the authors that uses fluorescing dyes to measure the relative amounts of new and old slurry beneath a wafer, in which the slurry utilization was found to be as high as 90% under similar conditions. In this study, as in the later work of Philipossian and Mitchell, utilization increased with increasing relative velocity, and was independent of pressure. However, the earlier study also found that utilization increased with increasing input flow rate, while Philipossian and Mitchell noted the opposite effect.

Philipossian and Mitchell do not report or discuss the actual flow rate at the pad/wafer interface $q_{interface}$, instead focussing on methods of improving slurry usage presented by their data. However, this can be established from the data presented by multiplying the utilization by the input flow rate. The values of $q_{interface}$ obtained in this manner at 2psi are presented in Figure 5.2. It is apparent from this figure that, at a low relative linear velocity, a

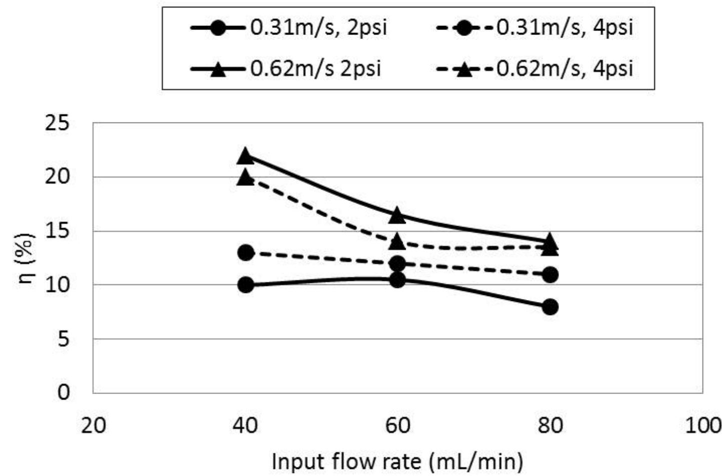

Figure 5.1: Variation of slurry utilization with flow rate for four combinations of high and low relative linear velocity, and high and low applied pressure (redrawn from [15]).

steady flow rate at the pad/wafer interface is obtained when the input flow rate is sufficiently high. No steady flow rate was observed at a high relative linear velocity. Outside of these steady flow rate conditions, $q_{interface}$ is linearly proportional to the velocity.

This suggests that the pad/wafer interface is starved of slurry until the input flow rate is sufficient to produces a 'saturated' film. Increasing the input flow rate beyond saturation does not lead to any increase in $q_{interface}$, and hence the additional slurry on the pad must pass around the wafer. This phenomenon, while not remarked on Philipossian and Mitchell, is commonly termed a 'bow wave' and is visible as a wave around the leading edge of the wafer. An example of a typical bow wave is shown in Figure 5.3.

A follow-up study by the same authors [69] investigates the effect of the mean residence time τ calculated in [15] for the colloidal silica slurry and Rodel® IC-1000 K-grooved pad on removal of an interlayer dielectric film. Unsurprisingly, this study illustrated that removal rate increased with decreasing

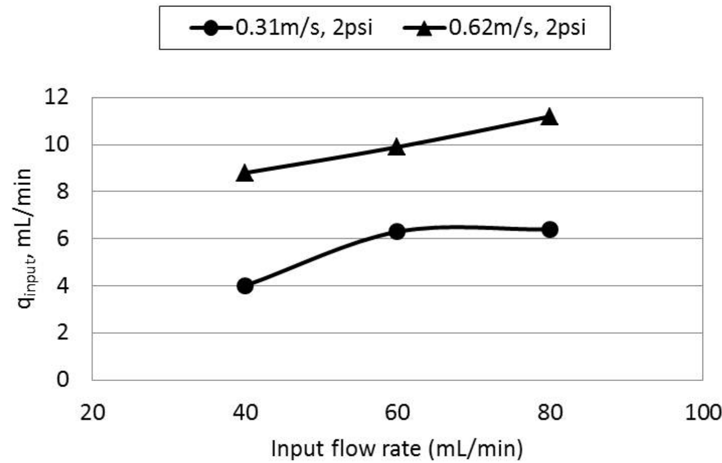

Figure 5.2: Variation of slurry flow rate in the pad/wafer interface with input flow rate with an applied pressure of 2psi.

τ, as a more rapid displacement of water in the pad/wafer interface by slurry led to increased material removal. They also found that the Preston coefficients for their polishing processes decreased with increasing τ, an effect for which they had no explanation.

The transport of slurry from the point at which it is poured on to the pad to the pad/wafer interface was investigated by Mueller, Rogers and co-workers [70]. As with the work of Philipossian and Mitchell, the authors introduced tracers into the fluid stream to visualise its behaviour. Pepper was initially used to gain qualitative information about the slurry flow at pad and wafer rotational speeds of 30rpm and 33rpm respectively for three different pad topographies. The input flow rate q_{input} was constant at 150mL/min. However, the authors found that pepper particles became trapped in the pad topography, and discontinued its use. They then obtained quantitative data by using a fluorescing oil as a tracer and tracking its motion using particle image velocimetry (PIV), a form of digital image analysis that yields instantaneous velocity data. This analysis was limited to pad rotational speeds of 5rpm or

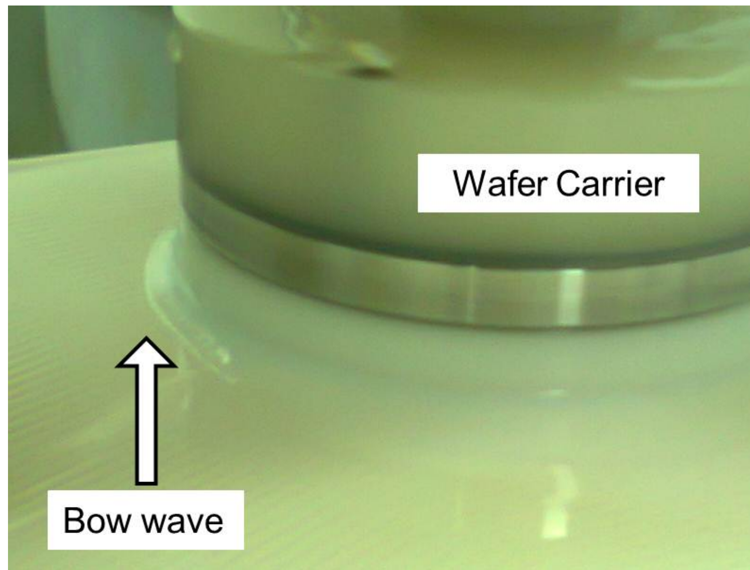

Figure 5.3: Photograph of the wafer carrier during polishing, with the bow wave indicated.

less due to the exposure times needed for the PIV system. Their data was also limited by the fact that both tracers floated on top of the slurry, and hence could not give information on slurry flow at the pad surface.

Mueller, Rogers and their coworkers found that a bow wave, such as that pictured in Figure 5.3, formed for all the experimental conditions they investigated. This suggests that all of their experiments were conducted in the 'saturated' condition, and that the flow of slurry under the wafer $q_{interface}$ was not limited by slurry transport from the centre of the pad to the wafer. This is unsurprising, given that the flow rate q_{input} used was at least double that of Philipossian and Mitchell for the same pad diameter and a smaller wafer diameter.

Their qualitative analysis of the flow obtained using pepper as a tracer focussed on the behaviour of the slurry in and around the bow wave. They found that the slurry in this region was a mix of both new slurry and older slurry that had been present on the pad for at least one pad rotation. They

also found that the type of pad used had a significant and complex impact on the flow fields, as did the position at which the slurry was poured on to the pad. The pressure applied to the wafer was not a significant factor in their results. When fluorescing oil was used as a tracer, the authors found that the flow velocity on top of the slurry, where the oil was floating, was at most 35% of the platen velocity. The flow velocities from the outer edge of the water to the edge of the pad at 3rpm, 4rpm and 5rpm were quantified using PIV. Outside of the bow wave, the slurry velocity increased monotonically until reaching a constant value of between 10% and 30% of the platen speed. No insights into potential impacts on polishing are offered by the authors, who focussed instead on demonstrating the strengths and limitations of PIV techniques in CMP research.

In this work, the slurry flow field across the pad is quantified without conditioning and without the presence of a wafer. An ink tracer and a digital camera were used to visualise the slurry flow for three different pad topographies. The results obtained shed considerable light on the slurry flow characteristics, and the results obtained by the authors cited in this section. Polishing is then carried out using the tested conditions, with and without conditioning.

5.2 Experimental Procedures

5.2.1 Flow Field Characterisation (Ink Tests)

As described in section 2.1, slurry is introduced onto the centre of the polishing pad with peristaltic pumps. The slurry flow rate can be set from 20mL/min to 500mL/min with an accuracy of ±2% over one minute. In order to examine the effects of flow rate on slurry transport across the pad, a tracer was introduced to the slurry and its path tracked using a digital camera. Water was used as the slurry, and Sheaffer Skrip® writing ink as the tracer. Ink was introduced

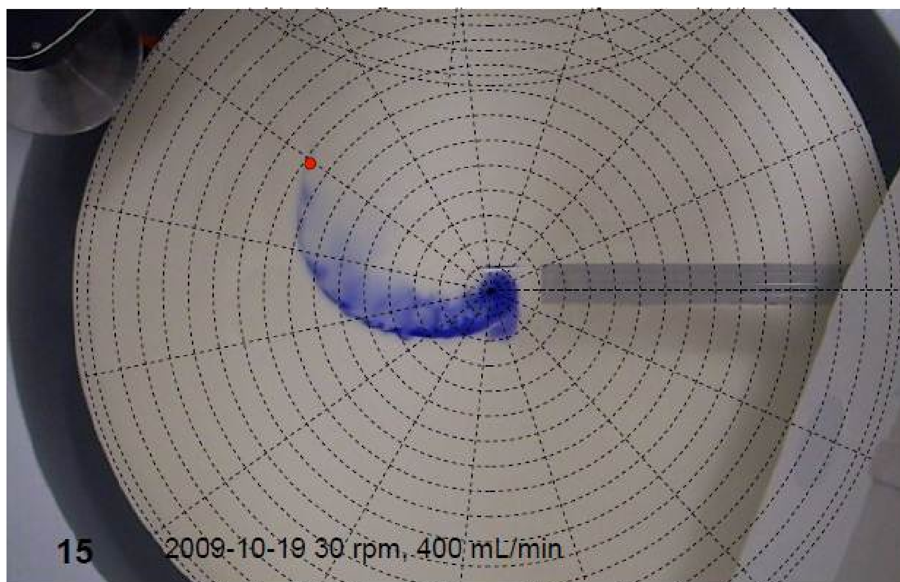

Figure 5.4: Sample data point for Pad 1, 30rpm, 400mL/min, approximately one second after ink was injected into the slurry stream. The frame has been overlaid with a polar grid and the position of the ink tracer noted.

into the wafer stream with a pipette immediately after it reached the pad. The path of the ink tracer was recorded with either a Microsoft® LifeCam Cinema® high-definition webcam or a Kodak® EasyShare® M893 IS digital camera operating in video mode. These cameras had resolutions of 720p and 8.1 megapixels respectively, and captured images at a rate of 15 frames per second. The recordings were split into their constituent frames using either the webcam or camera software. Each frame was then digitally overlaid with a polar grid and the position of the ink trace manually recorded. The position of the pad was also noted to ensure consistent results. Due to difficulties in accurately determining the tangential position near the centre of the pad, the first second of tangential data was neglected in analysis. An example of a single frame of data, with the polar grid overlaid and the ink position marked, is shown in Figure 5.4.

This procedure was carried out on two different polishing pads and on the

Table 5.1: Summary of polishing conditions

Conditions	Pressure (psi)	Velocity (m/s)	Flow Rate (mL/min)	Conditioning Protocol
N1	5	1.07	500	Ex situ
N2	5	1.07	200	Ex situ
N3	2	1.07	500	Ex situ
N4	2	1.07	200	Ex situ
P1	2	1.07	200	In situ
P2	2	1.07	300	In situ
P3	2	1.07	400	In situ
P4	2	1.07	500	In situ

underlying brushed aluminium platen, representing a flat, ungrooved pad. The two pads used, called Pad 1 and Pad 2, were respectively a Cabot Microelectronics® concentrically grooved pad and a NexPlanar® E7450-30S radially and concentrically grooved pad. Pad rotational speeds of 30rpm and 60rpm were used, and flow rates q_{input} of 100, 200, 300, 400 and 500mL/min. The pad conditioner was not used during testing. The displacement vs. time data acquired from this process was analysed in Microsoft Excel® and MATLAB®.

5.2.2 Polishing Tests

Based on the results obtained from the ink tests, a series of copper films were polished using the apparatus described in section 2.1 and Pad 2. Sixteen wafers were polished without conditioning and a further sixteen with conditioning using the parameters described in Table 5.1. Note that conditions N1-N4 are the same as those described in Table 3.2, and the results used for both experiments.

For all the experiments described in Table 5.1, a slurry containing hydrogen peroxide, glycine, BTA, colloidal silica abrasives and sufficient citric acid to adjust the pH to 3.55 was used. At 200mL/min, the concentration of these components was as described in Table 5.2. However, it was diluted in the ratios 2:1, 2:2 and 2:3 for use at 300, 400 and 500mL/min, so that the input of

Table 5.2: Slurry composition used at 200mL/min and diluted as described at higher flow rates

Component	Concentration
Colloidal Silica, mean diameter 84nm	3wt%
Hydrogen peroxide	1wt%
Glycine	1wt%
BTA	1mM
Citric Acid	To adjust pH to 3.55
Deionised water	Balance

reactants on to the polishing pad was constant for all flow rates. Before and after polishing, the thickness of the copper film on the wafers was measured at nine points across the wafer radius using a 4-point probe, as described in section 2.1.1.

5.3 Results and Discussion

5.3.1 Flow Field Characteristics (Ink Tests)

The ink tracer proved to be an effective method of tracking the position of the fluid over time, with repeatable results obtained over all the conditions tested in this work. Visualisation of the slurry flow revealed a number of qualitative points before any quantitative analysis was carried out. The first of these is that the force generated by rotation is not always sufficient to propel the slurry to the edge of the pad. Where this occurs, the extent of the slurry flow field is analysed using the quantitative data collected. It also became apparent that the flow was 'split' by the pad topography for Pad 2, which is both radially and concentrically grooved. Part of the ink trace traveled over the pad in a similar manner to Pad 1, while the other part traveled through the radial groove system, greatly accelerating its radial velocity. To account for this phenomenon, each of these traces were separately tracked using the method noted in section 5.2.1. The results for each part are referred to as 'Pad 2 (Plane)' and 'Pad 2 (Groove)' for flow across the pad surface and through

the grooves respectively.

Because both the radial and tangential position of the ink tracer was recorded, the displacement vs. time data can be analysed in both directions. Examples of the fluid tangential position vs. time (θ(t)) data for all three surfaces and both rotational speeds are shown in Figures 5.5 and 5.6.

The data can be fit to a linear equation of the form

$$\theta = mt + b \tag{5.2}$$

with R^2 values of at least 0.964, and generally better than 0.99. Notably, the tangential velocity (the first derivative of Equation 5.2 with respect to time) equals the rotational velocity of the pad to within ±3% at all flow rates, for all the surfaces, at both 30rpm (π radians/s) and 60rpm (2π radians/s). On this basis, the fluid tangential velocity is taken to be equal to the pad rotational velocity in all cases. Additionally, the tangential acceleration (the second derivative of displacement with respect to time) is zero.

In contrast, the radial velocity of the fluid varied significantly with surface type, rotational speed, and flow rate. The radial displacement vs. time (*r(t)*) data collected for the bare platen, Pad 1, Pad 2 (Plane) and Pad 2 (Groove) are shown in Figures 5.7 to 5.10.

From these data, it is apparent that the radial flow characteristics of the slurry are strongly dependent on the pad rotational speed, the slurry flow rate and the pad topography. Increasing the pad rotational speed increases the radial velocity in all cases. Increasing the slurry flow rate also increases the radial velocity, but the rate of increase slows with increasing flow rate until a plateau is reached. This is more pronounced, and occurs at lower flow rates, at higher rotational speeds. The pad topography also has a significant impact on the radial flow characteristics. As expected, the fluid travels fastest (at

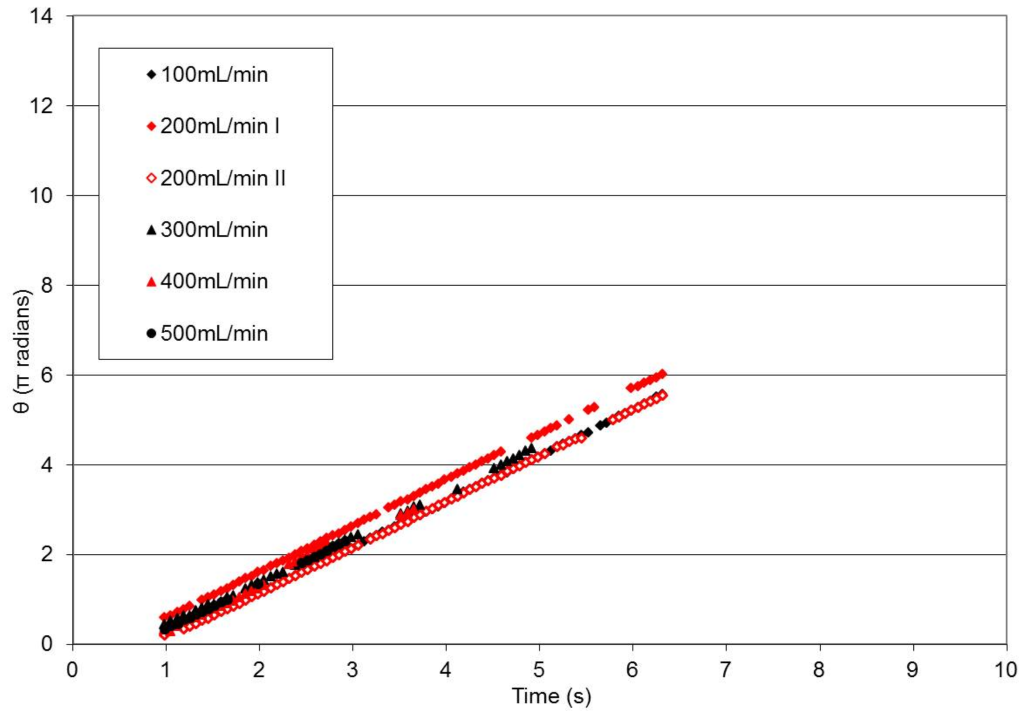

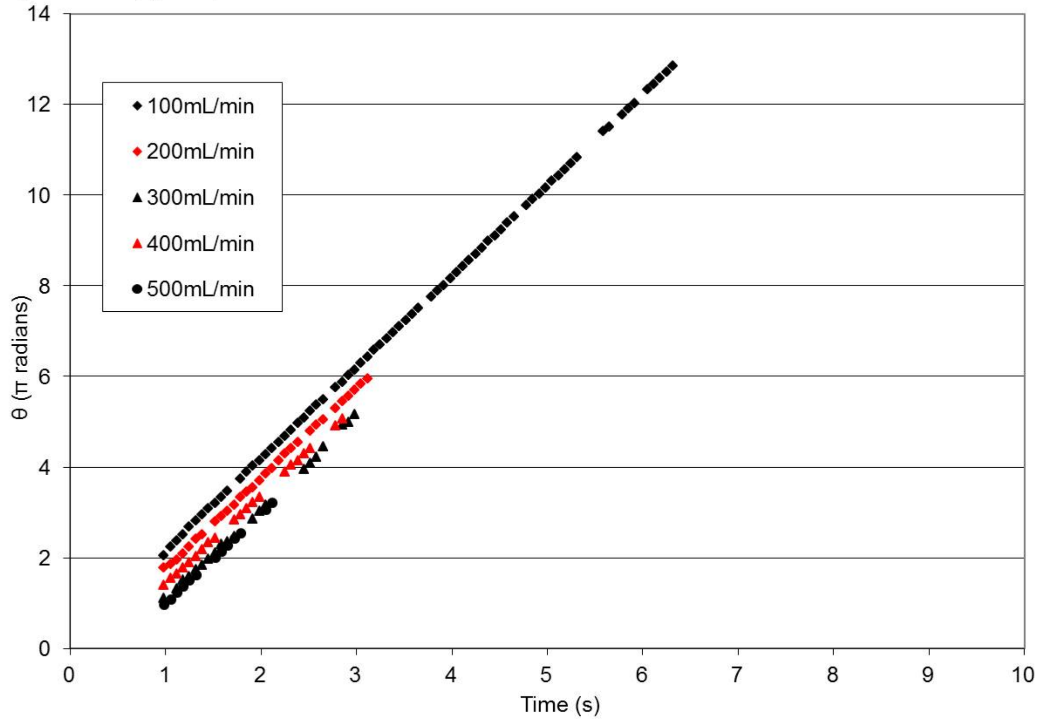

Figure 5.5: θ(t) data for a) pad 1 at 30rpm and b) pad 1 at 60rpm. All data are shown on the same axes to aid comparison.

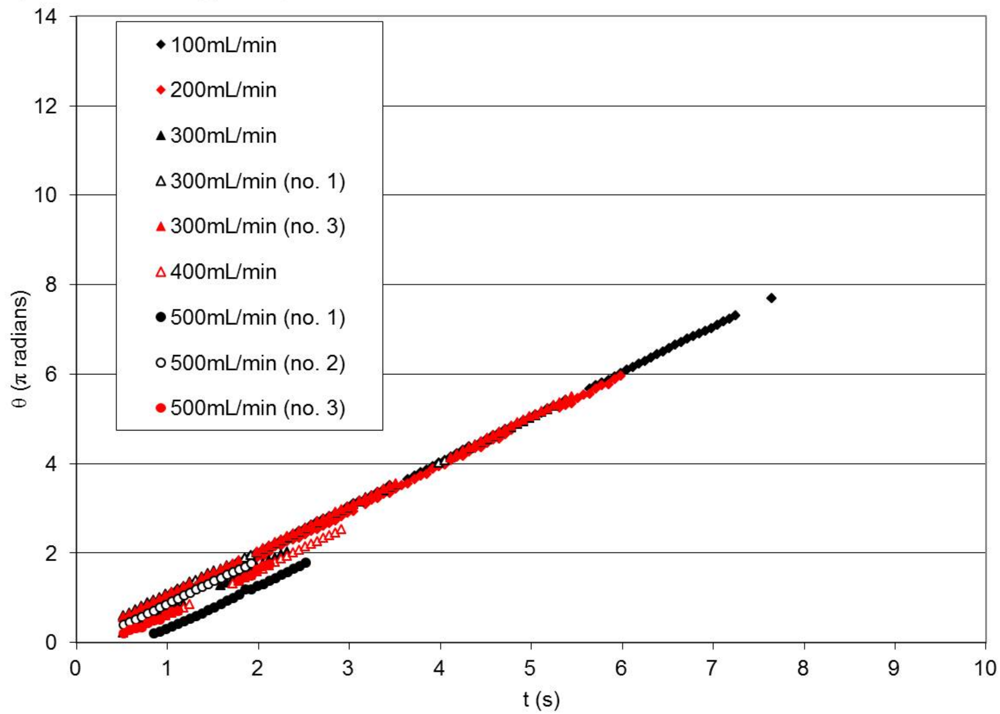

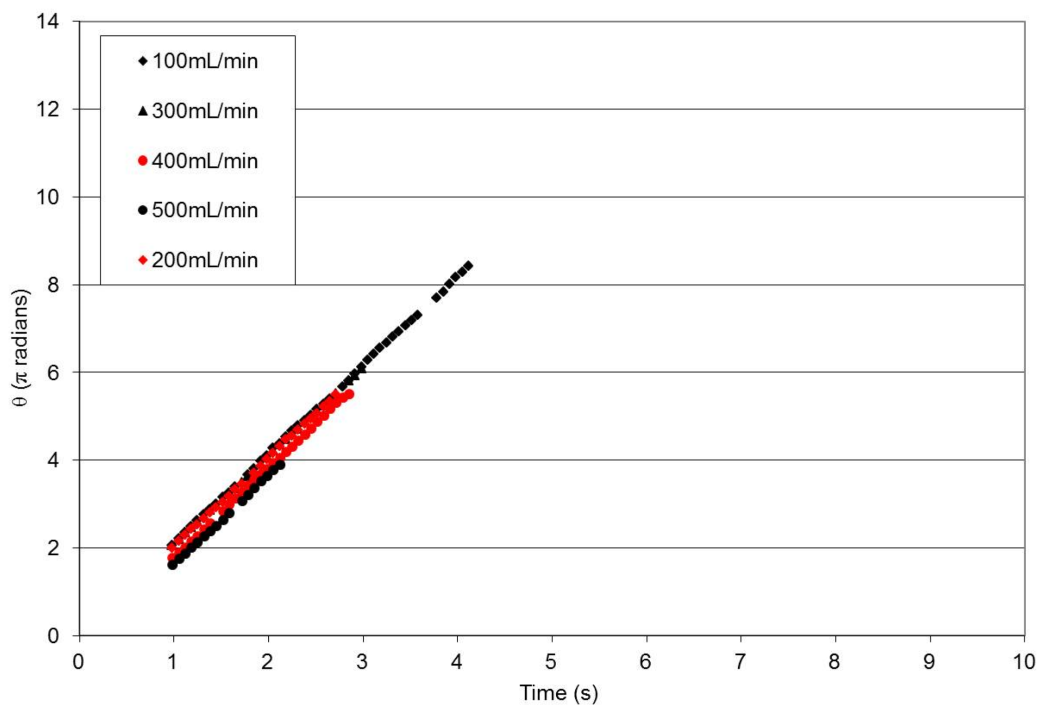

Figure 5.6: θ(t) data for c) the bare platen (plane) at 30rpm and d) pad 2 at 60rpm. All data are shown on the same axes to aid comparison.

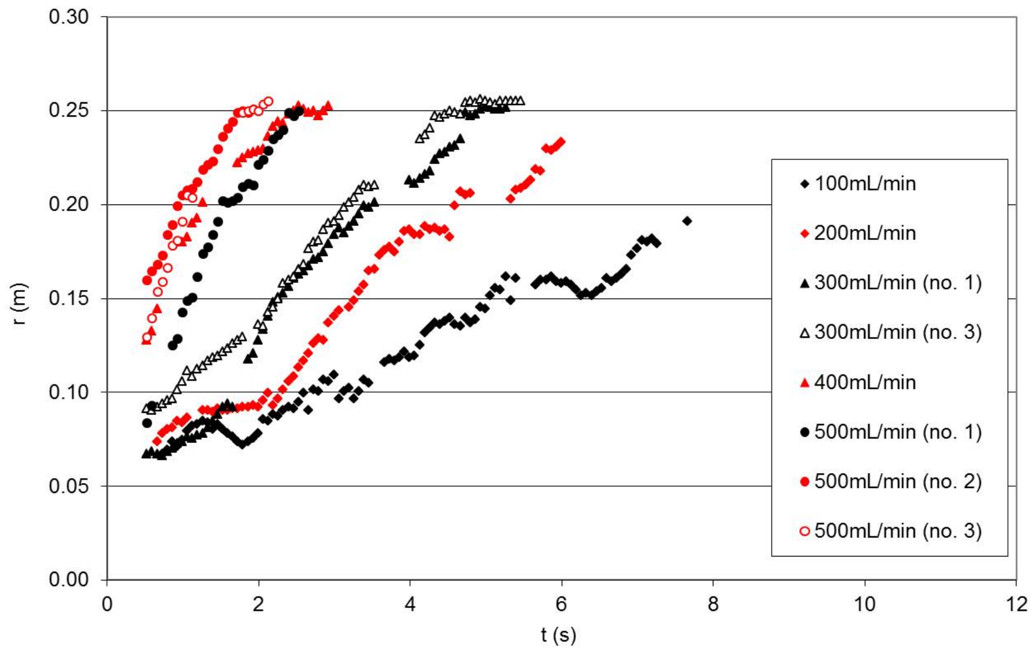

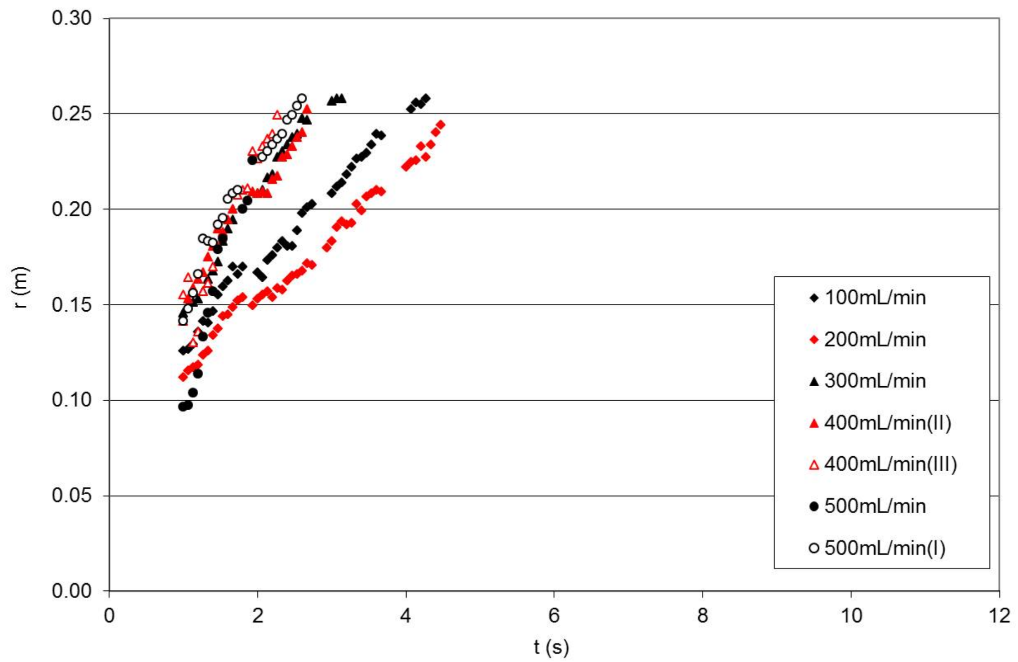

Figure 5.7: r(t) data for the bare platen at a) 30rpm and b) 60rpm. The axes are the same on both plots to allow for comparison.

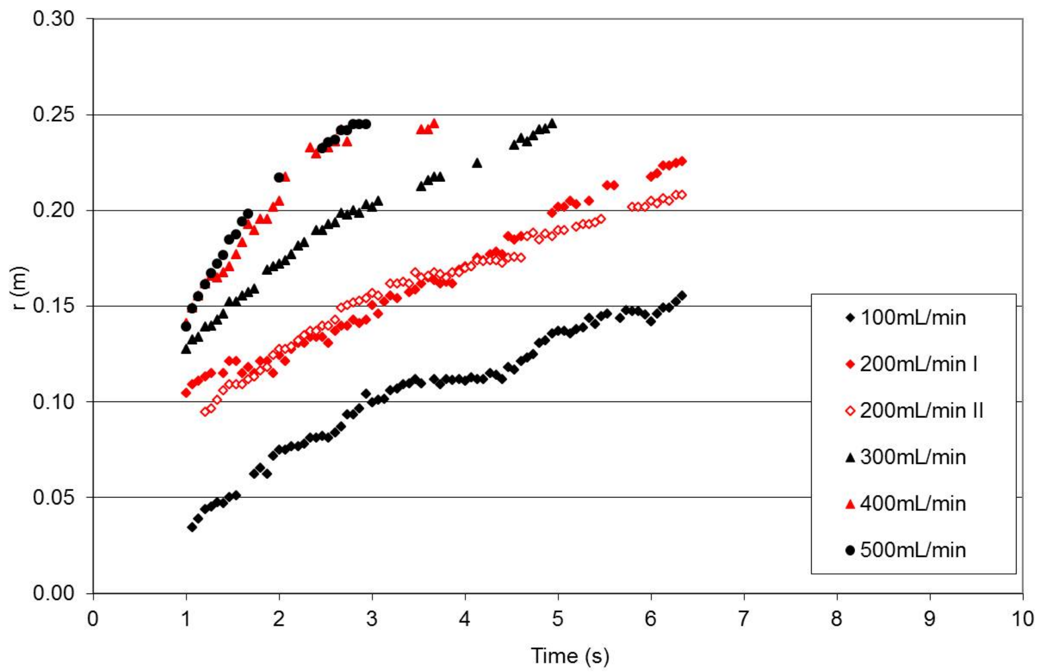

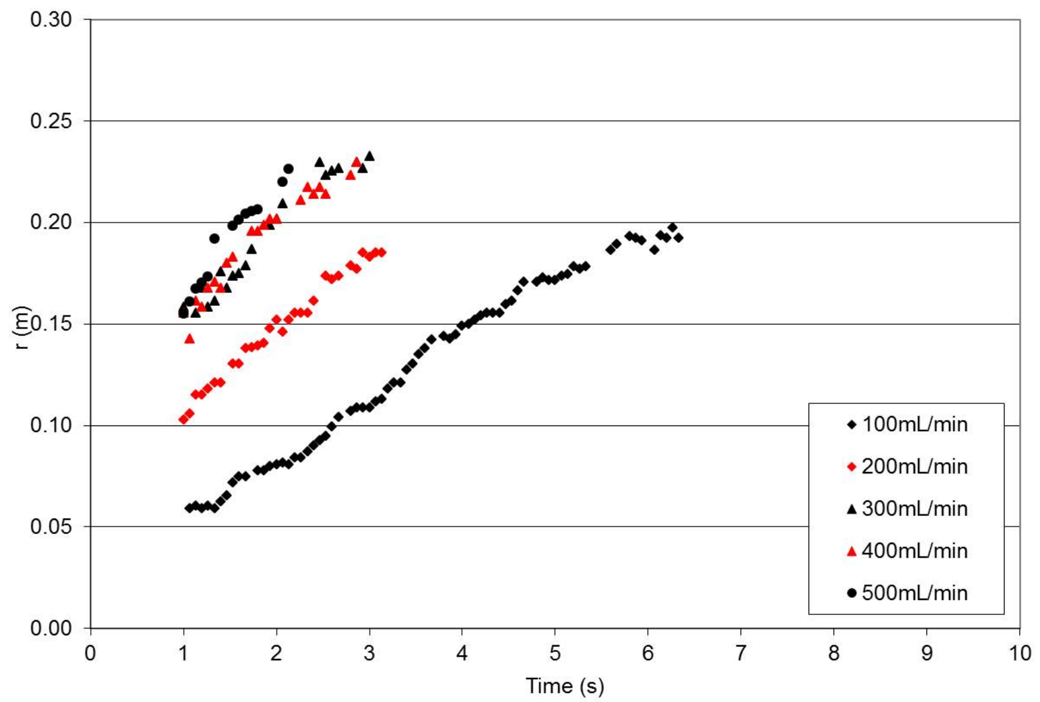

Figure 5.8: r(t) data for Pad 1 at a) 30rpm and b) 60rpm. The axes are the same on both plots to allow for comparison.

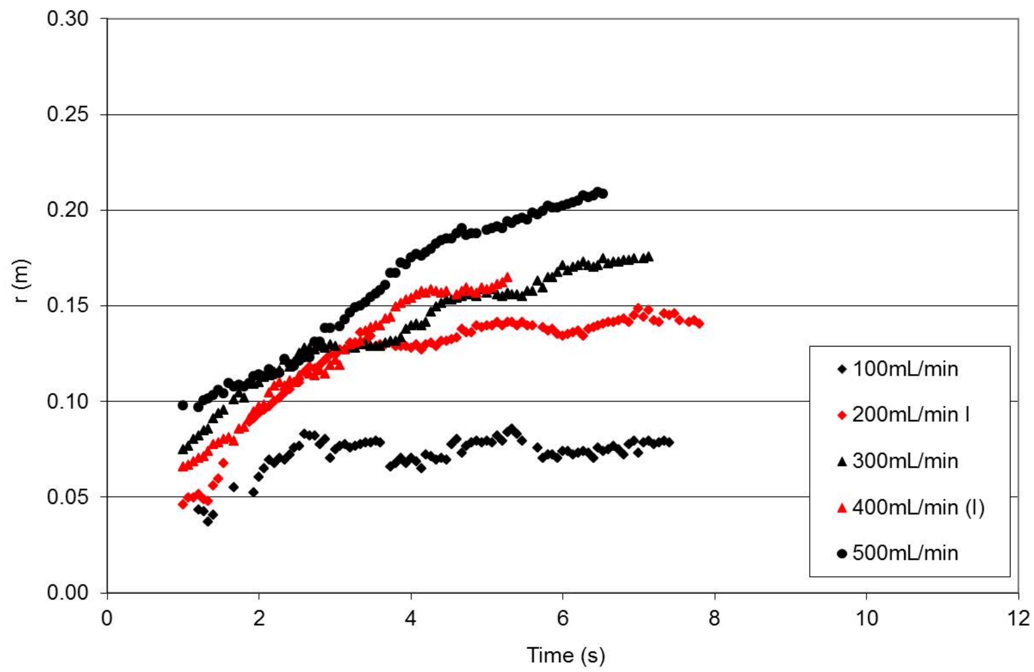

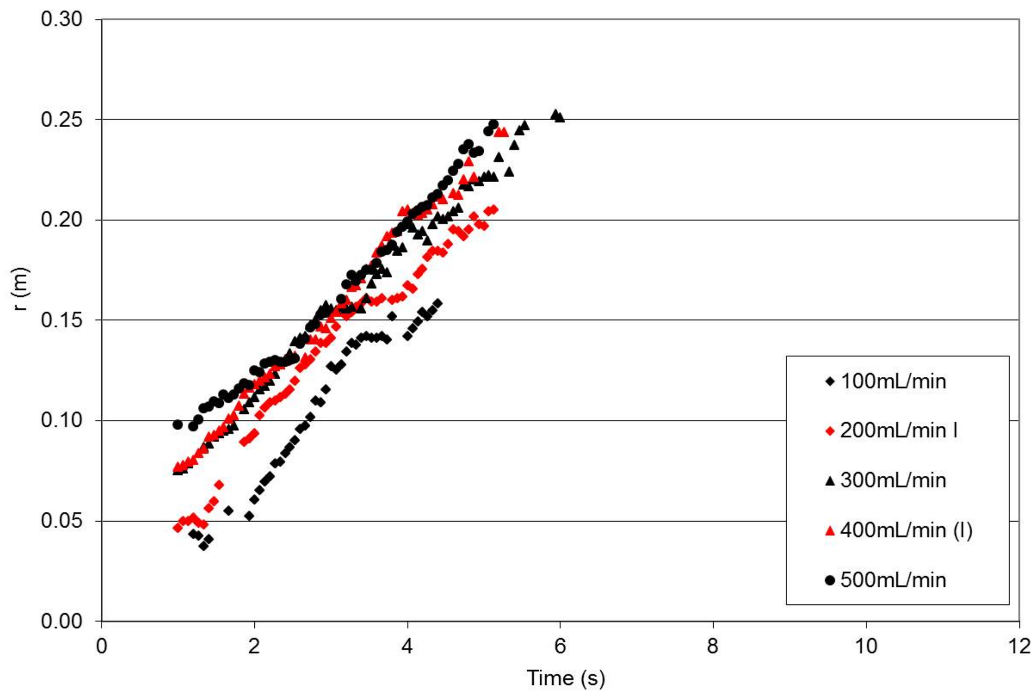

Figure 5.9: r(t) data at 30rpm for a) Pad 2: Plane and b) Pad 2: Groove. The axes are the same on both plots to allow for comparison.

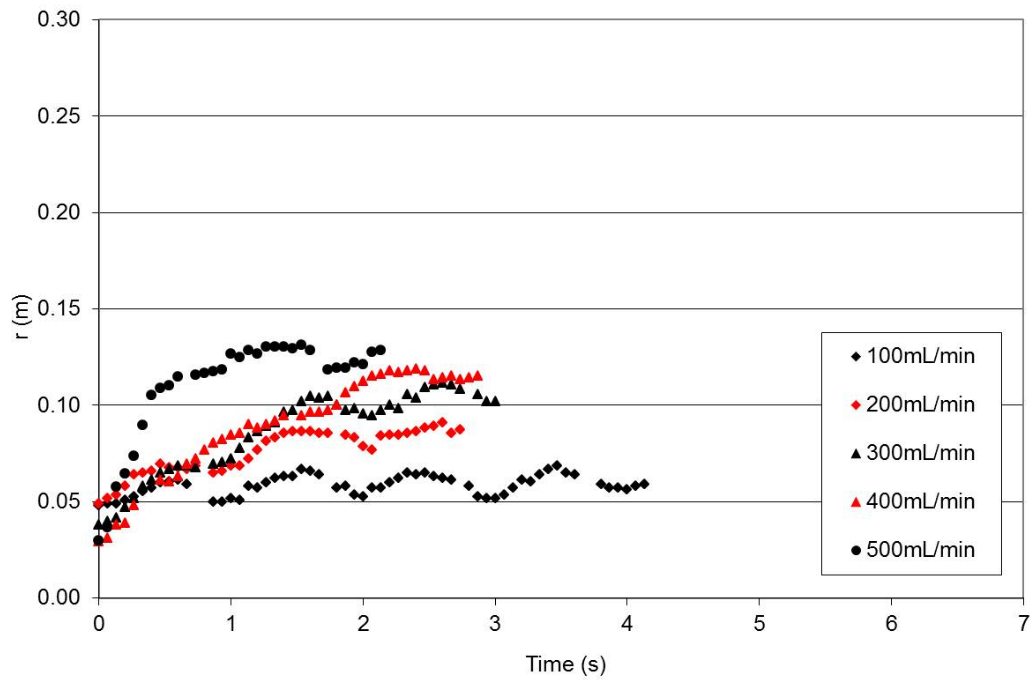

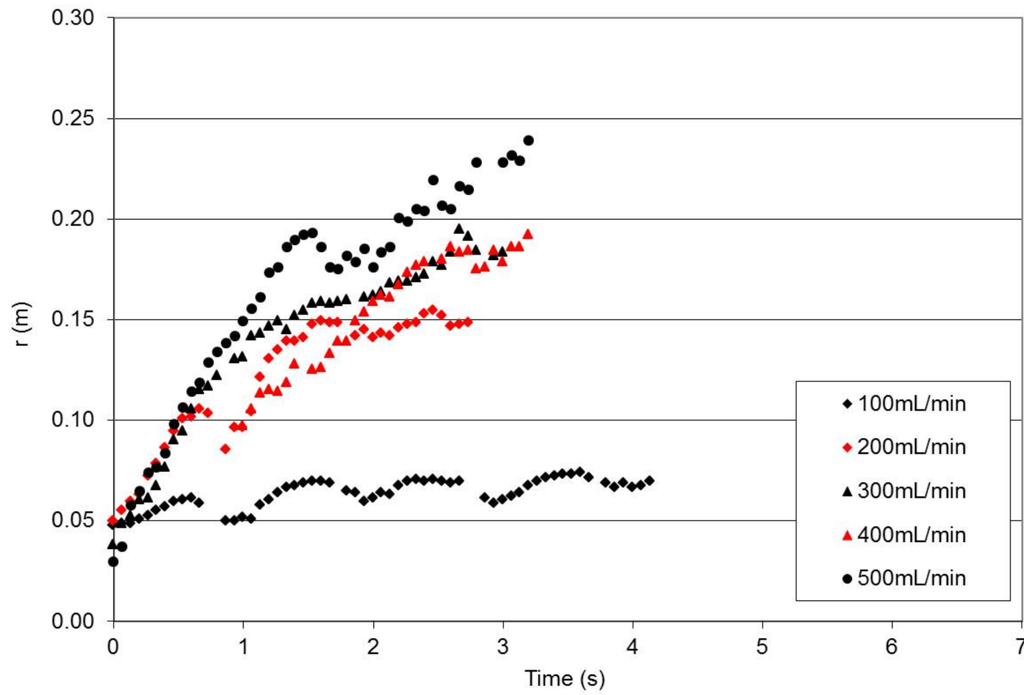

Figure 5.10: r(t) data at 60rpm for a) Pad 2: Plane and b) Pad 2: Groove. The axes are the same on both plots to allow for comparison.

velocities of nearly 10 cm/s) on the flat surface of the bare platen, which has the least topographical resistance to radial fluid motion. Similar velocities are observed in the radial grooves of Pad 2. In contrast, the concentric grooving of Pad 1 and Pad 2 (Plane) hinders fluid motion significantly. The radial fluid data can be fit to a quadratic equation of the form

$$r = at^2 + bt + c \tag{5.3}$$

with R^2 values of at least 0.8795, and typically near 0.98, apart from the data from Pad 2 (both plane and groove) at 60rpm and 100mL/min. These two series displayed poor fit using the Microsoft Excel® built-in error analysis. The correlation coefficients were therefore calculated using MATLAB® and found to be 0.7999 for the Pad 2 (Groove) data and 0.4923 for the Pad 2 (Plane) data. The Pad 2 (Plane) data was therefore excluded from further analysis. As is the case for the tangential data, the radial velocity is then the first derivative of Equation 5.3 with respect to time, and the acceleration is the second derivative. The velocity therefore varies with time, while the acceleration is constant. The variation of initial radial velocity v_{r0} and acceleration a_r with flow rate is shown in Figures 5.11 and 5.12 respectively.

These figures confirm that velocity increases with increasing flow rate, and that a plateau velocity is reached, for Pad 1 and the bare platen at 30rpm, and for all four surfaces considered at 60rpm. At 30rpm, the radial velocity of slurry on Pad 2 (Groove) is approximately constant. The radial acceleration acts mainly in the negative direction, towards the centre of the pad, becoming more negative with increasing flow rate, except for Pad 2 (Groove) where it remains constant or becomes slightly positive with increasing flow rate. The effect of pad rotation is less pronounced.

The radius of the pad is 0.254m. In the case of the bare platen, and the

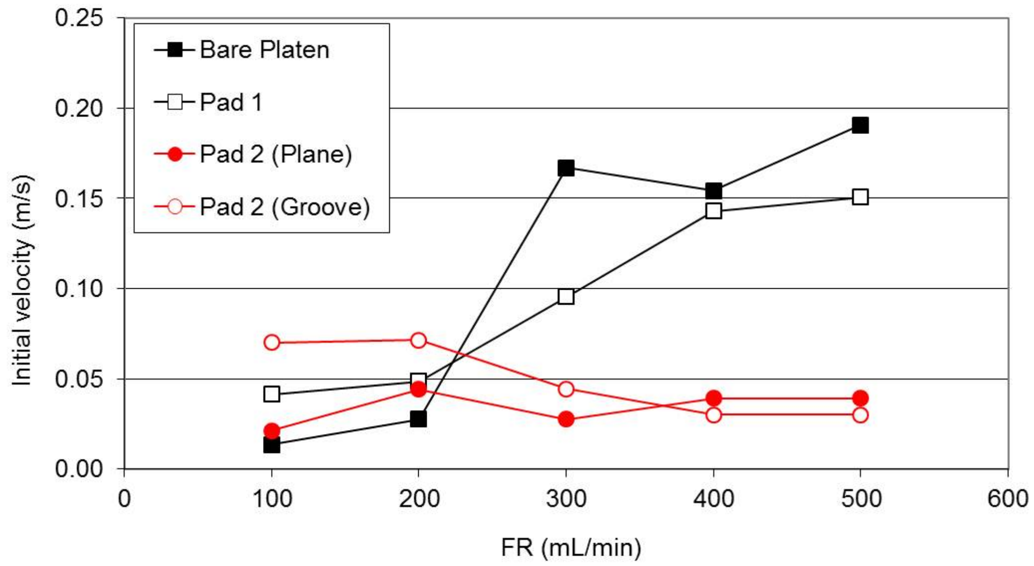

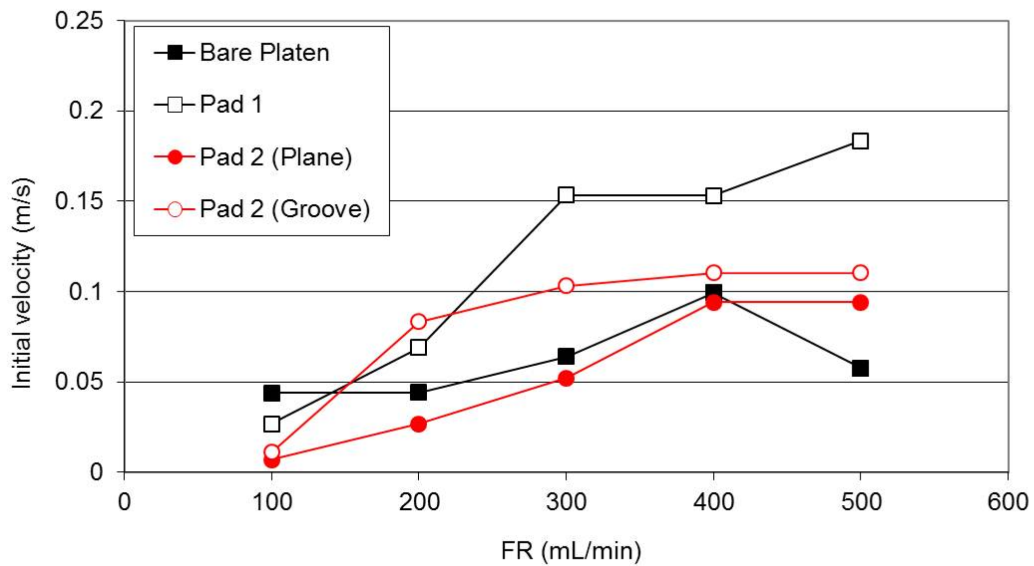

Figure 5.11: Initial radial velocity $v_{r,0}$ as a function of flow rate at a) 30rpm and b) 60rpm.

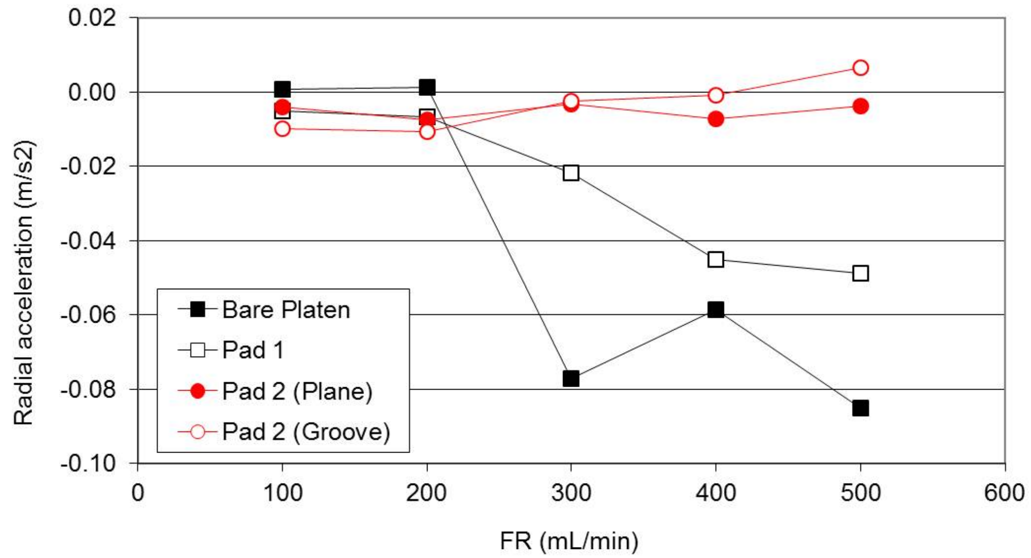

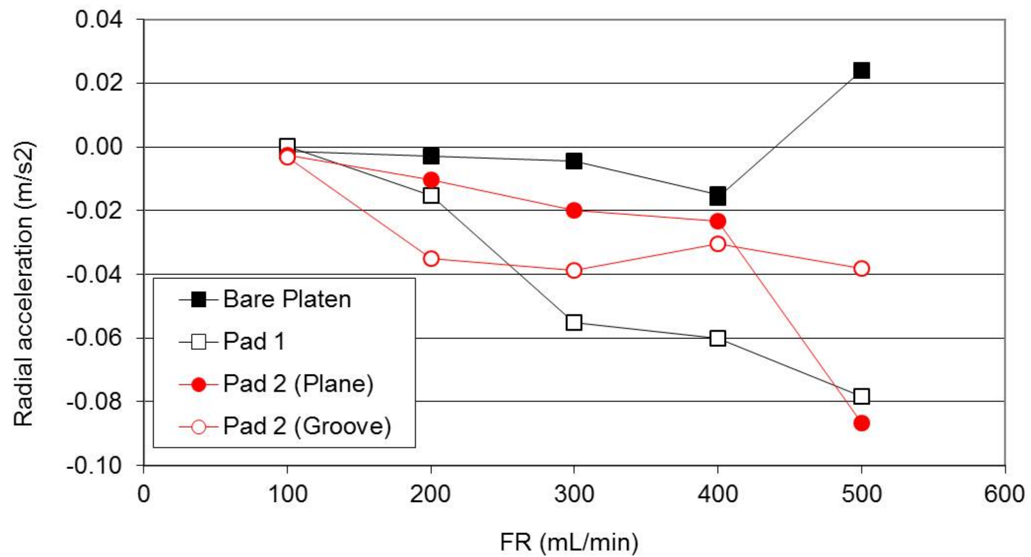

Figure 5.12: Radial acceleration a_r as a function of flow rate at a) 30rpm and b) 60rpm.

high flow rate data from Pad 1 and Pad 2 (Groove) at 30rpm, this is also the maximum displacement reached by the fluid, as seen in Figures 5.7 to 5.10. However, for the remaining scenarios, a maximum fluid displacement is reached at an intermediate radius. The fluid therefore does not flow across the entire polishing pad under its own inertia in these scenarios. The role of the conditioner in such situations is therefore to distribute slurry on the pad, as well as to maintain a consistent pad surface. These maxima in the r(t) data obtained allow a force balance to be carried out. The forces acting on the fluid are the centripetal force F_c, acting outwards from the centre of the pad, and the fluid drag force F_D, acting inwards. The Coriolis force can be neglected here as the data were collected in an inertial frame of reference. At the maxima, these two forces must exactly balance and oppose each other, preventing further radial fluid motion. This is most clearly illustrated in the r(t) data presented in Figure 5.10a), in which the fluid radial position reaches a maximum and remains at that value until the end of the test. In other cases, the maximum radial value is not observed in the experimental data due to the length of the tests, but can be inferred from the data fit to Equation 5.3. Equating the centripetal and drag forces on the fluid allows the shear force on the pad τ, normalised by the thickness of the fluid, to be calculated. To a first approximation, the thickness of the fluid film is assumed to be constant across the pad [71]. For a fluid element of dimensions $dA \times t$, where dA is an infinitely small area of the pad and t is the thickness of the fluid film, the force balance can be derived from the following relationships:

$$mr\omega^2 = -\tau dA$$

$$dAt\rho r\omega^2 = -\tau dA$$

This leads to the expression:

$$\frac{\tau}{t} = -\rho r \omega^2 \tag{5.4}$$

As the slurry density ρ, pad rotational velocity ω, and radial distance r at which the force balance is achieved are known, the value of τ normalised by the thickness t can be calculated. The results obtained for the bare platen and for Pad 2 (Groove) at 30rpm using this method are very scattered, as the fit to the r(t) data is skewed by the fact that the fluid path is interrupted by the edge of the pad and a maximum radial distance is not observed in the data set. These points are therefore removed from the results, and the remainder are presented in Figure 5.13. From this data, it is apparent that:

- For Pad 1, and Pad 2 (Plane) at 30rpm, a constant value of $\frac{\tau}{t}$ is reached within the flow rates investigated. This suggests that the thickness of slurry on the pad is independent of flow rate at higher flow rates.

- Comparing the data for Pad 1 and Pad 2 (Plane) at 30rpm, it is apparent that Pad 1 either presents a greater degree of resistance to radial fluid motion than Pad 2 (Plane) or retains a thinner slurry film than Pad 2 (Plane), as $\frac{\tau}{t}$ is higher for Pad 1 for all flow rates.

- For Pad 2 (Groove) and Pad 2 (Plane) at 60rpm, the value of $\frac{\tau}{t}$ increases over the range of flow rates investigated. This may be the result of lower fluid retention (and hence a thinner slurry film) with increasing flow rate, or may indicate that the shear force exerted by the pad on the fluid is increasing. Both alternatives are plausible; the Reynolds number for the flows examined here ranges from 3230 to 20740, depending on the fluid velocity, and hence the drag force may vary with fluid velocity. As described previously, the fluid velocity increases with increasing flow rate

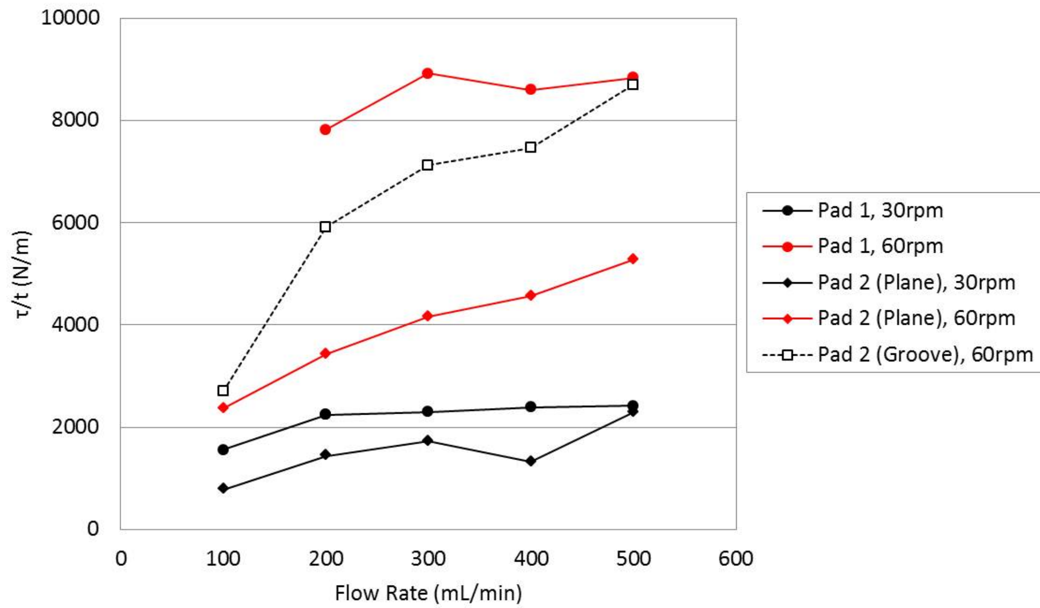

Figure 5.13: Shear force τ across the pad surface, normalised by the film thickness t.

and thus would result in increased drag at higher flow rates. The parameter $\frac{\tau}{t}$, as described in Equation 5.4, is thus a useful tool for comparing the fluid-carrying characteristics of polishing pads.

The incursion of 'fresh' slurry into the pad/wafer interface can also be calculated from the radial displacement data gathered. This is shown schematically in Figure 5.14; at any point in time, the slurry at point 'A' is 'fresh', and has not previously been in contact with the wafer. After one revolution, if the slurry has traveled a radial distance less than the diameter of the wafer (e.g. to point 'B'), part of the wafer is being polished in slurry that has previously been in contact with it. On the other hand, if the slurry travels a radial distance greater than the diameter of the wafer (e.g. to point 'C'), all the slurry reaching the wafer is 'fresh' and has not previously been used in polishing. Once the slurry stream reaches the wafer, it is assumed to either be ejected into the bow wave, if polishing under saturated conditions, or pass directly

under the wafer at the same speed and in the same direction as the relative linear velocity of the two surfaces [72]. This has significant implications for the utilization of slurry. In unsaturated conditions, such that no bow wave is formed, slurry that takes the path A to C is not used at all in the polishing process. In contrast, under the same unsaturated conditions, a slurry path from A to B implies that all slurry is used in polishing, and that utilization therefore approaches 100%. Polishing with fresh or used slurry is not thought to make a significant difference in overall reaction rates, based on the diffusion-limited behaviour noted in Chapter 4. However, fresh slurry is less likely to contain debris from polishing, and hence may result in better surface quality. In this study, the wafer is located with its centre at 0.17m from the centre of the pad, and its inner and outer edges at 0.12m and 0.22m from the centre of the pad respectively. Of the pads assessed here, only Pad 1 at 30rpm and 500mL/min or the bare platen at 30rpm and 300mL/min or more meet this criteria, and introduce only fresh slurry to the polishing interface.

5.3.2 Impact of Flow Rate on Polishing Outcomes

As described in section 5.2.2, eight sets of polishing tests, outlined in Table 5.1 were conducted on Pad 2 to assess the impact of flow rate and conditioning on Cu-CMP. A bow wave was observed when the flow rate was 300mL/min or greater. An approximation of the slurry flow rate in the pad/wafer interface can be made by assuming the fluid flows through a square volume of the same dimension as the interface, and thus has a constant cross-sectional area. The flow rate in the interface $q_{interface}$ can then be approximated as:

$$q_{interface} = V \times A \tag{5.5}$$

where V is the velocity of the fluid in the interface and A is the area of the

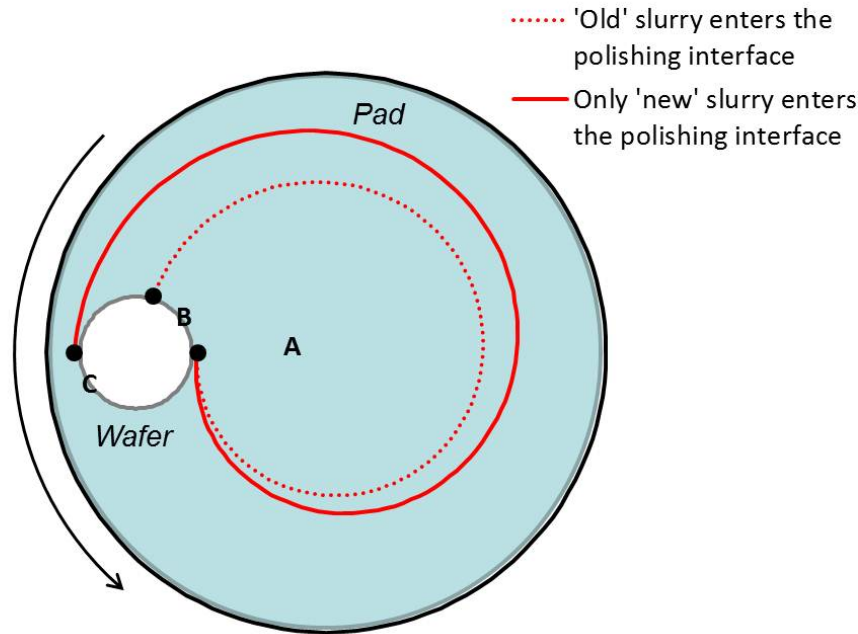

Figure 5.14: Schematic of alternative slurry paths, demonstrating the incursion of fresh or old slurry into the polishing interface.

cross section through which it flows. For conditions P3, the height of the slurry film between the wafer and the pad is approximately 40μm, as determined by the modeling procedure outlined in section 3.3.1. The dimension of a square of equal area to the wafer is 0.0886m, and the fluid velocity is 1.07m/s. This yields a volumetric flow rate $q_{interface}$ of 228mL/min. Given that when the input flow rate q_{input} is greater than $q_{interface}$, the polishing conditions will be at saturation, a saturation condition is expected for flow rates of 300mL/min or more and saturation is not expected at 200mL/min. The observation of a bow wave at flow rates of 300mL/min and greater corresponds well to this prediction. Additionally, a mixture of fresh and old slurry in the polishing interface is expected for all the conditions tested here.

The material removal rates obtained are shown in Table 5.3. Given that removal rates are directly proportional to slurry concentration at low concen-

trations, as discussed in section 4.3.1, the material removal rate normalised by the slurry concentration is also given.

It is apparent that the flow rate has no effect on MRR when conditioning is carried out during polishing. This suggests that, as well as renewing the pad surface, conditioning plays an important role in distributing slurry evenly across the pad. This may be a valuable tool in optimising both conditioning and q_{input} in the future. When conditioning is not carried out during polishing, increasing the flow rate q_{input} from 200mL/min to 500mL/min increases the polishing rate by 4% at a high applied pressure (5psi) and 13% at a low applied pressure (2psi). This may be due to saturation effects as increasing the applied pressure reduces the separation between the pad and the wafer, altering the flow rate $q_{interface}$ calculated in Equation 5.5. As previously discussed, $q_{interface}$ for conditions N3 and N4 (which have the same applied pressure as P3) is around 228mL/min. This means that N4 was carried out under unsaturated conditions while N3 was saturated. This may explain the 13% increase in normalised MRR when the flow rate was increased beyond saturation. In contrast, the saturation flow rate calculated for conditions P1 and P2 is 159mL/min. Both sets of experiments were therefore saturated, leading to a small difference in normalised MRR. The calculated flow rate $q_{interface}$ may thus be a valuable design tool in ensuring that sufficient slurry is used to maintain high polish rates, while preventing wastage.

5.4 Conclusions

Optimising the use of slurry in CMP is important due to its high cost. This work demonstrates that choosing the correct flow rate can improve slurry outcomes by minimising waste and maximising the polishing rate.

Table 5.3: Summary of polishing conditions

Conditions	Flow Rate (mL/min)	Conditioning Protocol	$\overline{MRR}$ (nm/min)	Normalised $\overline{MRR}$
N1	500	Ex situ	192	1.00
N2	200	Ex situ	459	0.96
N3	500	Ex situ	142	1.00
N4	200	Ex situ	310	0.87
P1	200	In situ	267	1.00
P2	300	In situ	156	1.02
P3	400	In situ	134	1.00
P4	500	In situ	108	1.01

6

Maximising Rate and Uniformity in Cu-CMP

In this chapter, the findings outlined in Chapters 3, 4 and 5 are combined to produce an optimal Cu-CMP process. The method of determining the optimal conditions and the outcome of the polishing process are reported here.

6.1 Introduction

Achieving copper polish rates that are simultaneously high and uniform is an important outcome of CMP, leading to increased yield, greater efficiency and lower process costs. To be able to predict *a priori* the combination of chemistry, pressure and velocity that results in this outcome is of great benefit to the CMP community.

In Chapter 4, both the polishing rate and the final wafer quality are shown to depend on the relative rates of mechanical abrasion and chemical passivation, determined by the ratio of hydrogen peroxide to abrasive loading. In Chapter 3, the polish rate uniformity MRRNU achieved for a given chemistry is shown to depend on the lubrication characteristics of the polishing couple, expressed by the dimensionless Sommerfield number So. Finally, polishing is shown in Chapter 5 to be independent of the rate of slurry use during the

Table 6.1: Slurry composition

Component	Concentration
Colloidal Silica, mean diameter 84nm	9.8 wt%
Hydrogen peroxide	3 wt%
Glycine	1 wt%
BTA	1mM
Citric Acid	To adjust pH to 3.55
Deionised water	Balance

process, q_{input}, above a certain rate that can be determined for each combination of pressure and velocity used. This allows the amount of slurry used to be minimised, reducing costs, without affecting the CMP process. These principles were combined here to design an optimised Cu-CMP process.

6.2 Design Method

6.2.1 Slurry Chemistry

As the optimal slurry flow rate is dependent on the pressure and velocity of polishing and the polish rate uniformity MRRNU is dependent on slurry chemistry, a preferred chemistry is selected first based on the relative rates of chemical and mechanical action on the wafer surface. From Figure 4.14, the maximum polish rate is achieved with conditions D4, at a H_2O_2 concentration of 3 wt% and SiO_2 concentration of 9.8 wt% for a given concentration of glycine, BTA and citric acid. The complete slurry composition is given in Table 6.1.

In Chapter 4, a material removal rate of 664 nm/min was achieved using this slurry in combination with a NexPlanar® E7450-30S polishing pad at an applied pressure of 4psi and a rotational speed of 60rpm (relative linear velocity of 1.07 m/s).

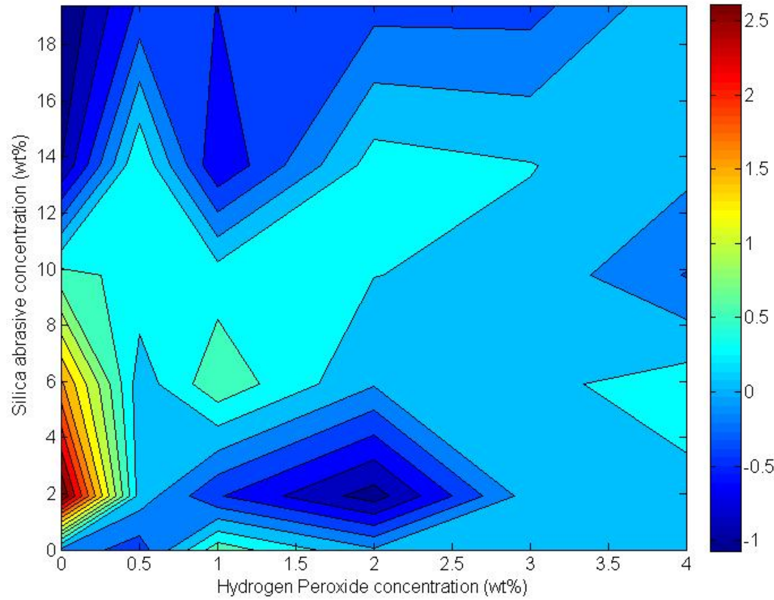

Figure 6.1: Contour map of MRRNU at varying concentrations of H_2O_2 and abrasives. The colour bar represents MRRNU. All results were obtained as outlined in Chapter 4.

6.2.2 Applied Pressure and Velocity - MRRNU

The investigations of Chapter 3 demonstrate that the relationship between MRRNU, the polish rate non-uniformity, and the lubrication characteristics as described by the Sommerfield number So, is strongly dependent on the composition of the polishing slurry. This is apparent in the varying gradients of the MRRNU - So curves shown in Figure 3.12b) for polishing copper with different slurries, including different particle sizes. The effects of varying H_2O_2 and SiO_2 concentrations are shown in Figure 6.1, in which the variation of MRRNU with H_2O_2 and SiO_2 content for the experiments conducted in Chapter 4 is shown.

From this figure, it can be seen that the MRRNU values achieved range from approximately +2.5, indicating severe dishing, to -1, indicating doming. Both

conditions are present within the range of chemistry tested. This is consistent with the maxima and minima observed in analogous curves by Yi, Yuling and coworkers [53].

At the slurry chemistry that maximises the polish rate, outlined in section 6.2.1, the observed MRRNU was -0.229 at a Sommerfield number of 17.03 $\times 10^{-4}$. The mean dome height for the wafers polished at these conditions was 26.2 nm. The wafer therefore underwent doming, with a material removal rate at the centre of the wafer 23% less than the mean removal rate, $\overline{MRRNU}$. A polishing process could be designed for this process by polishing wafers at successively higher Sommerfield numbers, and collating the results as a MRRNU - So curve such as that shown in 3.12a). The desired MRRNU conditions can then be obtained by polishing at the corresponding Sommerfield number. However, this was not possible due to equipment constraints. Instead, the validity of the relationship was assessed by polishing wafers under different conditions characterised by the same Sommerfield number of 17.03 $\times 10^{-4}$, and comparing the resultant values of MRRNU.

6.2.3 Slurry Flow Rate q_{input}

As described in Chapter 5, the flow rate of slurry in the interface between the pad and the wafer, $q_{interface}$ can be approximated if the slurry height between the two surfaces is known. This value is calculated using the Chen and Fang model [44], as described in 3.1.2, using the initial non-uniformity of the wafers h_D and the pressure and velocity applied by the user. A flow rate q_{input} is then selected that is higher than $q_{interface}$, to ensure that the polishing process is in the saturated condition.

6.3 Experimental Method

A total of eight wafers were polished under two sets of conditions designed to have approximately the same Sommerfield number. The two conditions, T1 and T2, are summarised in Table 6.2. All wafers were polished using the procedure outlined in section 2.1, with the exception that the total polish duration was 60s instead of 90s. The slurry described in Table 6.1 was used at a rate q_{input} of 200mL/min and the NexPlanar® E7450-30S pad was conditioned continuously during polishing.

Immediately before and after polishing, the thickness of the copper film was measured in the nine locations indicated in Figure 2.2 with a four-point probe. The wafers were rinsed thoroughly in deionised water and dried in nitrogen gas after polishing.

6.4 Results and Discussion

The average polish rate over all measurement locations for conditions T1 was 499 nm/min. This is approximately 25% less than that achieved for conditions D4, as discussed in Chapter 4. There are several possible explanations for this discrepancy. One is that the H_2O_2 solution used to mix the slurries degraded between the times the D4 and T1 slurries were mixed, a period of approximately one month. Another is that material removal during Cu-CMP is nonlinear over time. The polish time for the T1 conditions was 60s, compared to 90s for the D4 conditions. During polishing, significant heat is generated, which may impact the chemical reaction rate at the slurry / wafer interface [73]. This would result in increased MRR as the polishing procedure progresses, consistent with a nonlinear removal rate and the results shown here. In all other respects, conditions D4 and T1 are identical.

Table 6.2: Polishing conditions used in this study, including mean measured wafer dome heights h_D and corresponding calculated slurry film thicknesses.

Design So: 17.03×10^{-4}

Conditions	Mean h_D (nm)	Calculated h_m (μm)	P (psi)	V (m/s)	$q_{interface}$ (mL/min)	So
T1	14.16	20.6	4	1.07	117	16.73×10^{-4}
T2	13.92	30.4	1.5	0.51	82	14.35×10^{-4}

The polish rate profiles obtained under conditions T1 and T2 are shown in Figure 6.2. This figure demonstrates that, while the overall magnitude of the polishing rate is significantly different for the two conditions, the shape of the profile is qualitatively very similar. This is confirmed by the MRRNU values of -0.293 and -0.336 obtained for conditions T1 and T2 respectively. The discrepancy between these MRRNU values, and between these and the value of -0.229 obtained previously, is accounted for by the variation in Sommerfield numbers for these conditions. A plot of log(So) against MRRNU, analogous to the one presented in Figure 3.12, is shown in Figure 6.3. The line of best fit displayed has a correlation coefficient of 0.86 to the data, comparable to the degree of fit shown by the larger data set displayed in Figure 3.12. The range of Sommerfield numbers, and hence values of MRRNU, is due to differences in the film thickness between the wafer and the pad. This highlights both the importance and utility of modeling techniques in quantifying the film thickness.

Using the procedure outlined in Chapter 5, the flow rate of slurry between the pad and wafer, $q_{interface}$, was estimated to be 117 mL/min and 89 mL/min for conditions T1 and T2 respectively. As polishing was carried out for both these conditions with an input flow rate q_{input} of 200mL/min, both wafers were polished under saturated conditions. As such, q_{input} was not expected to affect the polishing outcome of either condition. However, this does suggest that q_{input} could be significantly reduced, by more than 50% in the case of the T2 condition. This warrants further investigation in the future.

6.5 Conclusions

Achieving high rates and high uniformity through *a priori* process design is of great interest to the Cu-CMP community. The experiments outlined in this chapter demonstrate that it is also both possible and practical. As shown here,

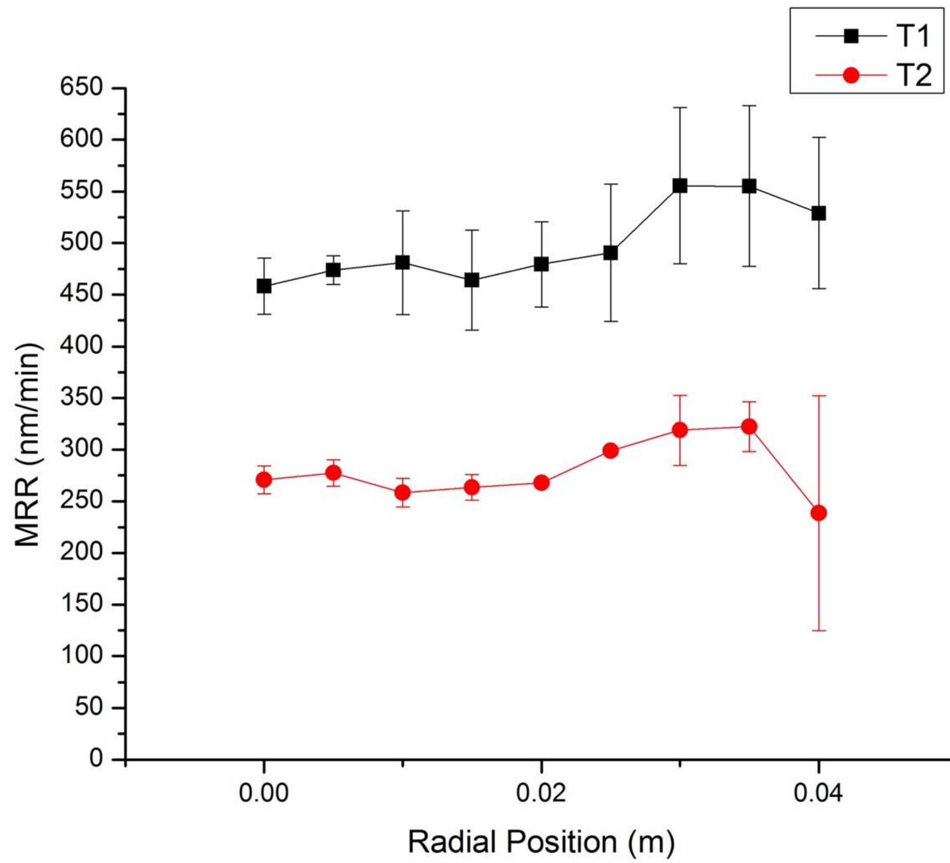

Figure 6.2: Polish rate profiles obtained for conditions T1 and T2. The error bars represent ± 1 standard deviation.

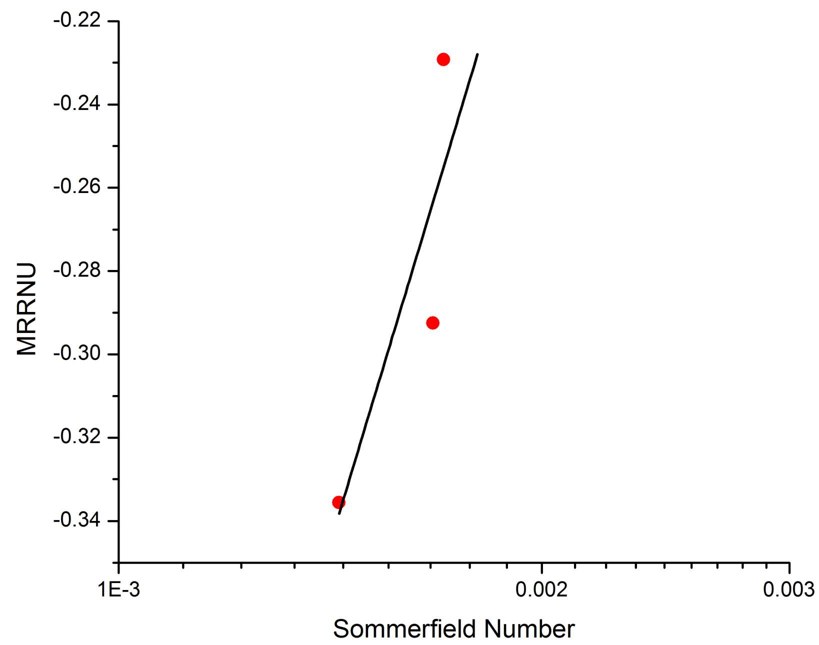

Figure 6.3: MRRNU vs. logSo for conditions T1, T2 and D4. The line shown is a logarithmic fit to the data, with a correlation coefficient of 0.86.

once a relationship between So and MRRNU is established for a given slurry chemistry, So can be used to predict MRRNU prior to the commencement of polishing with a good degree of correlation and repeatability. Additionally, the thickness of the slurry film between the pad and the wafer needed to determine So may be calculated from hydrodynamic models, such as the one developed by Chen and Fang [44], with good results.

7

Conclusions

It is the aim of this thesis to present a unified approach to Cu-CMP that combines the chemical and mechanical aspects of the process, and that enables the Cu-CMP user to design high rate, high uniformity polishing processes from first principles.

The presence of different zones of material removal explains the relationship between MRRNU and the lubrication conditions of the polishing couple as expressed by So. For the acidic slurry chemistry used in this work, polishing at less lubricating conditions (typified by lower Sommerfield numbers) results in high, negative values of MRRNU due to the presence of the edge and suppression zones in the pad / wafer interface. Polishing under highly lubricating conditions (typified by high Sommerfield numbers) results in high, positive values of MRRNU as the polishing couple becomes fully hydrodynamic and the material removal rate is proportional to the hydrodynamic pressure developed. The good agreement between the observed polish rate and that predicted by Preston's equation in this zone implies that Preston's equation describes hydrodynamic polishing conditions. This is a major clarification of its use. Additionally, an intermediate value of Sommerfield number with zero MRRNU can be deduced from the MRRNU vs. So curves produced.

The relationship between MRRNU and Sommerfield number can also be

applied to polishing oxides, as shown in Figure 3.17, and may be applicable to other materials as well. This relationship may additionally explain the apparently contradictory experimental results presented in the literature, such as those shown in Figure 1.4, by allowing the polish rate at the centre of a wafer and the average polishing rate to be considered separately.

Second, a model for the relative actions of chemical dissolution and mechanical abrasion in material removal is proposed. This model is verified through experiments, and demonstrates that synchronised chemical and mechanical action can greatly enhance material removal rates. The surface quality of the polished wafer is also examined, and related to the proposed model. The interaction of the abrasive particles and H_2O_2 was found to result in polish rates that are far higher than the sum of the polishing rates of the components in isolation. Different mechanisms for material removal are proposed for regions of the MRR - concentration map, resulting in different final surface characteristics. Where the rate of mechanical abrasion is faster than the rate of chemical removal, MRR increases rapidly and linearly with increasing H_2O_2 and abrasive concentration. However, the surface quality of the polished surface under these circumstances is poor and displays high roughness. This is consistent with the constant removal of the passive layer by abrasion. In contrast, where the chemical reaction rate dominates, the polished surface quality is very good. However, removal rates are lower in this regime and independent of the H_2O_2 concentration. A synergy occurs when the rates of mechanical and chemical abrasion are approximately equal, at which point the material removal rate is greatly increased. The interactions noted appear to be unrelated to the coefficient of friction, or the polishing mechanism at work.

Third, the role of slurry transport across the pad to the polishing interface is described in detail. The impacts on polishing are found to be small, allowing

costs to the user to be reduced by reducing total slurry usage. This work demonstrates that choosing the correct flow rate can improve slurry outcomes by minimising waste and maximising the polishing rate.

Finally, achieving high rates and high uniformity through *a priori* process design is of great interest to the Cu-CMP community. The testing carried out in Chapter 6 demonstrates that it is also both possible and practical. As shown in this chapter, once a relationship between So and MRRNU is established for a given slurry chemistry, So can be used to predict MRRNU prior to the commencement of polishing with a good degree of correlation and repeatability. Additionally, the thickness of the slurry film between the pad and the wafer needed to determine So may be calculated from hydrodynamic models, such as the one developed by Chen and Fang [44], with good results.

7.1 Future Work

The relationships developed in this work, while successful, have not been tested beyond the scope of equipment available at the University of Alberta. Further investigation of the phenomena described in this chapter could clarify the link between lubrication regime and non-uniformity in polishing. The work carried out here utilised only one polishing pad and wafer size, and a limited range of slurry compositions, but was sufficient to indicate that these factors have a significant impact on the relationship between lubrication conditions and MR-RNU. Systematic quantification of these effects would clarify the relationship, expanding the relevance of the MRRNU - So curves to the CMP community. In particular, the applicability of these findings to larger wafer sizes should be confirmed as industrial semiconductor processors typically use wafers with diameters of 200mm or more.

Further work should also be carried out to elucidate the mechanisms be-

hind the hydrodynamic, edge and suppression zones described in 3.3.3. An improved understanding of polishing behaviour in these zones could lead to greatly improved modeling methods for Cu-CMP.

In demonstrating the synergistic relationship between oxidation and abrasion rates, the H_2O_2 and abrasive concentrations were varied while the other components of the slurry, and the polishing conditions used, remained constant. The concentration of corrosion inhibitor in the slurry is likely to have a substantial effect on the rate of passivation of the surface, while the polishing pressure and down force are likely to affect the rate of abrasion. These interactions also warrant further investigation.

Bibliography

[1] Nolan L, Cadien K. Chemical Mechanical Polish for Nanotechnology. In: Stepanova M, Dew S, editors. Nanofabrication. Springer-Verlag/Wien; 2012. p. 239–274.

[2] Philipossian A, Olsen S. Fundamental Tribological and Removal Rate Studies of Inter-Layer Dielectric Chemical Mechanical Planarization. Japanese Journal of Applied Physics. 2003;42 part 1(10):6371Ű6379.

[3] Rosales-Yeomans D, DeNardis D, Borucki L, Philipossian A. Design and Evaluation of Pad Grooves for Copper CMP. Journal of The Electrochemical Society. 2008;10:H797–H806.

[4] Osorno A, Tereshko S, Yoon I, Danyluk S. Dynamics of the Formation of the Subambient Pressure Distribution During Chemical-Mechanical Polishing. In: Proceedings of ASME/STLE International Joint Tribology Conference. vol. IJTC2007-44441. ASME; 2007. .

[5] Shan L, Zhou C, Danyluk S. Mechanical Interactions and Their Effects on Chemical Mechanical Polishing. IEEE Transactions on Semiconductor Manufacturing. 2001;14(3):207–213. ©[2001], IEEE. Figure 3.17 reprinted with permission.

[6] Kaufman FB, Thompson DB, Broadie RE, Jaso MA, Guthrie WL, Pearson DJ, et al. Chemical-Mechanical Polishing for Fabricating Patterned W Metal Features as Chip Interconnects. Journal of The Electrochemical Society. 1991;138(11):3460–3465.

[7] Tromans D. Aqueous Potential-pH Equilibria in Copper-Benzotriazole Systems. Journal of The Electrochemical Society. 1998;145(3):L42–L45.

[8] Ein-Eli Y, Abelev E, Starosvetsky D. Electrochemical Behavior of Copper in Conductive Peroxide Solutions. Journal of The Electrochemical Society. 2004;151(4):G236–G240.

[9] Du T, Tamboli D, Desai V. Electrochemical characterization of copper chemical mechanical polishing. Microelectronic Engineering. 2003;69:1–9.

[10] Ein-Eli Y, Starosvetsky D. Review on copper chemical mechanical polishing (CMP) and post-CMP cleaning in ultra large system integrated (ULSI): An electrochemical perspective. Electrochimica Acta. 2007;52:1825Ű1838.

[11] Wang MT, Tsai MS, Liu C, Tseng WT, Chang TC, Chen LJ, et al. Effects of corrosion environments on the surface finishing of copper chemical mechanical polishing. Thin Solid Films. 1997;308-309:518–522.

[12] Luo J, Dornfeld DA. Effects of Abrasive Size Distribution in Chemical Mechanical Planarization: Modeling and Verification. IEEE Transactions on Semiconductor Manufacturing. 2003;16(3):469–476. ©[2003], IEEE. Figure 4.8 reprinted with permission.

[13] Kim YJ, Kwon OJ, Kang MC, Suh MW, Im Y, Kim JJ. Development of a Copper Chemical Mechanical Polishing Slurry at Neutral pH Based on Ceria Slurry. Journal of The Electrochemical Society. 2010;157(10):H952–H958.

[14] Li Z, Ina K, Lefevre P, Koshiyama I, Philipossian A. Determining the Effects of Slurry Surfactant, Abrasive Size, and Abrasive Content on the Tribology and Kinetics of Copper CMP. Journal of The Electrochemical Society. 2005;152(4):G299–G304.

[15] Philipossian A, Mitchell E. Slurry Utilization Efficiency Studies in Chemical Mechanical Planarization. Japanese Journal of Applied Physics. 2003;42(12):7259–7264.

[16] Beyer K. The Inception of Chemical-Mechanical Polishing for Device Applications at IBM. IBM MicroNews. 1999;5:4–6.

[17] Preston FW. The Theory and Design of Plate Glass Polishing Machines. Journal of the Society of Glass Technology. 1927;XI:214–256.

[18] Cook LM. Chemical Processes in Glass Polishing. Journal of Non-Crystalline Solids. 1990;120:152–171.

[19] Xu G, Liang H, Zhao J, Li Y. Investigation of Copper Removal Mechanisms during CMP. Journal of the Electrochemistry Society. 2004;151(10):G688–G692.

[20] Chen JC, Tsai WT. Effects of hydrogen peroxide and alumina on surface characteristics of copper chemicalŨmechanical polishing in citric acid slurries. Materials Chemistry and Physics. 2004;87:387–393.

[21] Wu YF, Tsai TH. Effect of organic acids on copper chemical mechanical polishing. Microelectronic Engineering. 2007;84:2790–2798.

[22] Ishikawa A, Matsuo H, Kikkawa T. Influence of Slurry Chemistry on Frictional Force in Copper Chemical Mechanical Polishing. Journal of The Electrochemical Society. 2005;152(9):G695–G697.

[23] Burtovyy R, Liu Y, Zdyrko B, Tregub A, Moinpour M, Buehler M, et al. AFM Measurements of Interactions Between CMP Slurry Particles and Substrate. Journal of The Electrochemical Society. 2007;154(6):H476–H485.

[24] Cooper K, Gupta A, Beaudoin S. Simulation of Particle Adhesion: Implications in Chemical Mechanical Polishing and Post Chemical Mechanical Polishing Cleaning. Journal of The Electrochemical Society. 2001;148(11):G662–G667.

[25] Matijevic E, Babu SV. Colloid aspects of chemicalŰmechanical planarization. Journal of Colloid and Interface Science. 2008;320:219–237.

[26] Hong Y, Patri UB, Ramakrishnan S, Roy D, Babu SV. Utility of dodecyl sulfate surfactants as dissolution inhibitors in chemical mechanical planarization of copper. Journal of Materials Research. 2005;20(12):3413–3424.

[27] Luo Q, Ramarajan S, Babu SV. Modifcation of the Preston equation for the chemical-mechanical polishing of copper. Thin Solid Films. 1998;335:160–167.

[28] Zhao B, Shi FG. Chemical Mechanical Polishing: Threshold Pressure and Mechanism. Electrochemical and Solid-State Letters. 1999;2(3):145–147.

[29] Che W, Guo Y, Chandra A, Bastawros A. A Scratch Intersection Model of Material Removal During Chemical Mechanical Planarization (CMP). Journal of Manufacturing Science and Engineering. 2005;127:545–554.

[30] ASTM F1711-96: Standard Practice for Measuring Sheet Resistance of Thin Film Conductors for Flat Panel Display Manufacturing Using a Four-Point Probe Method; Revised 2008.

[31] Adams JH, Ammons M. Properties and Selection: Nonferrous Alloys and Special-Purpose Materials. In: ASM Handbook. vol. 2. ASM International; 2010. .

[32] Stintz M, Barthel H, Moinpour M. Particle Metrology in CMP Slurries - Potential and Limitations of Relevant Measuring Methods. In: Materials Research Society Symposium Proceedings. vol. 991; 2007. p. 0991–C04–02.

[33] Mingard K, Morrell R, Jackson P, Lawson S, Patel S, Buxton R. Measurement Good Practice Guide No. 111: Good Practice Guide for Improving the Consistency of Particle Size Measurement. National Physical Laboratory (U.K.); 2009.

[34] Xie X, Boning D. Relating Friction in CMP to Topography Evolution. In: Proceedings of WTC2005 (World Tribology Congress III). ASME; 2005. p. WTC2005–641.

[35] Tamai K, Morinaga H, Doi TK, Kurokawa S, Ohnishi O. Analysis of Chemical and Mechanical Factors in CMP Processes for Improving Material Removal Rate. Journal of The Electrochemical Society. 2011;158(3):H333–H337.

[36] Mullany B, Byrne G. The effect of slurry viscosity on chemicalŰmechanical polishing of silicon wafers. Journal of Materials Processing Technology. 2003;132:28–34.

[37] Harnoy A. Bearing Design in Machinery: Engineering Tribology and Lubrication. CRC Press; 2002.

[38] Kato K, Adachi K. Chapter 7. Wear Mechanisms. In: Bhushan B, editor. Modern Tribology Handbook. vol. 1. CRC Press; 2000. .

[39] Lu J, Rogers C, Manno VP, Philipossian A, Anjur S, Moinpour M. Measurements of Slurry Film Thickness and Wafer Drag during CMP. Journal of The Electrochemical Society. 2004;151(4):G241–G247.

[40] Li Z, Lee H, Borucki L, Rogers C, Kikuma R, Rikita N, et al. Effects of Disk Design and Kinematics of Conditioners on Process Hydrodynamics during Copper CMP. Journal of The Electrochemical Society. 2006;153(5):G399–G404.

[41] Schlichting H. Boundary-Layer Theory. 6th ed. McGraw-Hill; 1968.

[42] Runnels SR, Eyman LM. Tribology Analysis of Chemical-Mechanical Polishing. Journal of The Electrochemical Society. 1994;141(6):1698–1701.

[43] Cho CH, Park SS, Ahn Y. Three-dimensional wafer scale hydrodynamic modeling for chemical mechanical polishing. Thin Solid Films. 2001;389:254–260.

[44] Chen JM, Fang YC. Hydrodynamic Characteristics of the Thin Fluid Film in ChemicalŰMechanical Polishing. IEEE Transactions on Semiconductor Manufacturing. 2002;15(1):39–44.

[45] Thakurta DG, Borsta CL, Schwendeman DW, Gutmann RJ, Gill WN. Pad porosity, compressibility and slurry delivery effects in chemical-mechanical planarization: modeling and experiments. Thin Solid Films. 2000;366:181–190.

[46] Higgs III CF, Ng SH, Borucki L, Yoon I, Danyluk S. A Mixed-Lubrication Approach to Predicting CMP Fluid Pressure Modeling and Experiments. Journal of The Electrochemical Society. 2005;152(3):G193–G198.

[47] Higgs CF, Terrell EJ, Kuo M, Bonivel J, Biltz S. On a Particle-Augmented Mixed Lubrication Approach to Predicting CMP. Materials Research Society Symposium Proceedings. 2007;991:0991–C13–01.

[48] Bullen D, Scarfo A, Koch A, Bramono DPY, Coppeta J, Racz L. In Situ Technique for Dynamic Fluid Film Pressure Measurement during Chemical Mechanical Polishing. Journal of The Electrochemical Society. 2000;147(7):2741–2743.

[49] Osorno A. Dynamic, In-Situ Pressure Measurements During CMP [Master's Thesis]. Georgia Institute of Technology; 2005.

[50] Guo Y, Lee Y, Lee H, Jeong H. Research on CMP Characteristics Attribute to Groove Size. Advanced Materials Research. 2011;189–193:4112–4115.

[51] Park K, Oh J, Jeong H. Pad Characterization and Experimental Analysis of Pad Wear Effect on Material Removal Uniformity in Chemical Mechanical Polishing. Japanese Journal of Applied Physics. 2008;47(10):7812–7817.

[52] Miranda PA, Imonigie JA, Moll AJ. Chemical Mechanical Planarization for Cu Through-Wafer Interconnects: An Investigation of Slurry Chemistry Interaction Effects Using a Design of Experiments Approach. Journal of The Electrochemical Society. 2006;153(3):G211–G217.

[53] Yi H, Yuling L, Xiaoyan L, Liran W, Yangang H. Effect of copper slurry on polishing characteristics. Journal of Semiconductors. 2011;32(11):116001–1–116001–5.

[54] Lee H, Park B, Jeong H. Influence of slurry components on uniformity in copper chemical mechanical planarization. Microelectronic Engineering. 2008;85:689–696.

[55] Xin J. Coffee Stain Ring Effect and Nonuniform Material Removal in Chemical Mechanical Polishing. Journal of Tribology. 2010;132:041605–1–041605–6.

[56] Hu TC, Chiu SY, Dai BT, Tsai MS, Tung IC, Feng MS. Nitric acid-based slurry with citric acid as an inhibitor for copper chemical mechanical polishing. Materials Chemistry and Physics. 1999;61:169–171.

[57] Wang D, Lee J, Holland K, Bibby T, Beaudoin S, Cale T. Von Mises Stress in Chemical-Mechanical Polishing Processes. Journal of The Electrochemical Society. 1997;144(3):1121–1127.

[58] Chekina OG, Keer LM, Liang H. Wear-Contact Problems and Modeling of Chemical Mechanical Polishing. Journal of The Electrochemical Society. 1998;6(2100–2106).

[59] Seok J, Sukam CP, Kim AT, Tichy JA, Cale TS. Multiscale material removal modeling of chemical mechanical polishing. Wear. 2003;254:307Ű320.

[60] Bielmann M, Mahajan U, Singh RK. Effect of Particle Size during Tungsten Chemical Mechanical Polishing. Electrochemical and Solid-State Letters. 1999;2(8):401–403.

[61] Tamilmani S, Huang W, Raghavan S. Galvanic Corrosion Between Copper and Tantalum under CMP Conditions. Journal of The Electrochemical Society. 2006;153(4):F53–F59.

[62] Lytle DA, Nadagouda MN. A comprehensive investigation of copper pitting corrosion in a drinking water distribution system. Corrosion Science. 2010;52:1927–1938.

[63] Aksu S, Doyle FM. The Role of Glycine in the Chemical Mechanical Planarization of Copper. Journal of The Electrochemical Society. 2002;149(6):G352–G361.

[64] Aksu S, Wang L, Doyle FM. Effect of Hydrogen Peroxide on Oxidation of Copper in CMP Slurries Containing Glycine. Journal of The Electrochemical Society. 2003;150(11):G718–G723.

[65] Chen JC, Lin SR, Tsai WT. Effects of oxidizing agent and hydrodynamic condition on copper dissolution in chemical mechanical polishing electrolytes. Applied Surface Science. 2004;233:80–90.

[66] Sun T, Zhang Y, Borucki L, Philipossian A. Characterization of Pad-Wafer Contact and Surface Topography in Chemical Mechanical Planarization Using Laser Confocal Microscopy. Japanese Journal of Applied Physics. 2010;49:066501–1–066501–4.

[67] Seo YJ. Oxide-chemical mechanical polishing characteristics using silica slurry retreated by mixing of original and used slurry. Microelectronic Engineering. 2005;77:263–269.

[68] Coppeta J, Rogers C, Racz L, Philipossian A, Kaufman FB. Investigating Slurry Transport Beneath a Wafer during Chemical Mechanical Polishing Processes. Journal of The Electrochemical Society. 2000;147(5):1903–1909.

[69] Philipossian A, Mitchell E. Mean Residence Time and Removal Rate Studies in ILD CMP. Journal of The Electrochemical Society. 2004;151(6):G402–G407.

[70] Mueller N, Rogers C, Manno VP, White R, Moinpour M. In Situ Investigation of Slurry Flow Fields during CMP. Journal of The Electrochemical Society. 2009;156(12):H908–H912.

[71] Emslie AG, Bonner FT, Peck LG. Flow of viscous liquid on rotating disk. Journal of Applied Physics. 1958;29(5):858–862.

[72] Rogers C, Coppeta J, Racz L, Philipossian A, Kaufman FB, Bramono D. Analysis of flow between a wafer and pad during CMP processes. Journal of Electronic Materials. 1998;27(10):1082–1087.

[73] Borucki L, Li Z, Philipossian A. Experimental and Theoretical Investigation of Heating and Convection in Copper Polishing. Journal of The Electrochemical Society. 2004;151(9):G559–G563.

Appendix A

MATLAB Code for Relative Velocity Calculations

```
% Script M-file calculates the magnitude of the↙
relative linear velocity
% between platern and wafer. Platern and wafer↙
rotations are entered,
% output is a 3D colour plot

% Developed July 30th 2009 (Notes vol.2), based on .↙
txt sequence developed
% August 15th 2008

close all
clear all
%hold off

% Inputs
omw = input('\nCarrier rotational velocity↙
(clockwise) in rpm: \n');
omp = input('Platern rotational velocity (clockwise)↙
in rpm: \n');
e = input('Centre-to-centre offset between the↙
platern \nand the carrier (in mm): \n');
rad = input('Wafer radius (in mm): \n');

ww=omw*2*pi/60;
wp=omp*2*pi/60;

% Define grid and convert from polar to cartesian
r=0:5:rad;
theta=(0:0.1:2)*pi;

% Wafer calcs:

[Rw, Tw] = meshgrid(r, theta);
```

```
x=Rw.*cos(Tw);
y=Rw.*sin(Tw);

uw=ww*Rw.*sin(Tw+pi);
vw=ww*Rw.*cos(Tw);

% Platern calcs

xp=x-e;
Tp=atan(y./xp);
Rp=sqrt(xp.^2+y.^2);

up=wp*Rp.*sin(Tp);
vp=wp*Rp.*cos(Tp+pi);

% Summation

u=-uw+up;
v=-vw+vp;

V=sqrt(u.^2+v.^2)*0.001;

% Plot

quiver(x,y,u,v,'k', 'filled'); axis equal; hold all;
H = surf(x, y, V); axis image; axis equal; view(2);
title('Relative linear velocity across wafer at↙
platern-wafer interface (m/s)','FontSize', 14)
set(H, 'FaceAlpha', 0.5); colorbar;

% Report max and min

M=max(V); Max=max(M)
N=min(V); Min=min(N)
```

Appendix B

Motor and Gearbox Data Sheets

ELECTRIC MOTORS, GEARMOTORS AND DRIVES

Product Features

List Price : $ 873

Catalog No	098032.00	**Model**	C42D17FK7
Product type	DC	**Stock**	Stock
Description	3/4HP.1750RPM.USS56C.TEFC.90V.CONT.40C.1.0SF.RIGID C.DC NEM/		

Information shown is for current motor's design

Engineering Data

RPM	1750	**HP**	3/4
KW		**Form Factor**	1.38
KW2		**Form Factor 2**	
Volts	90	**Frame**	56C
Max Amb	40	**Duty**	CONT
Insul Class	F	**Enclosure**	TEFC
Protection	NOT	**Protector**	
EFF	84.2%	**Torque**	27 LB-IN
UL	Yes	**CSA**	Yes
Motor Wt.	39 LB	**Nameplate**	081259
Carton Label	Leeson Gen Purpose		
Assembly		**Mounting**	C-Face Rigid
Winding	D472293	**Ext. Diag.**	
GROUP:	1 A	**Shaft Dia.**	5/8 IN
Sub Group	A	**Paint**	305000.01
Test Card	01	**Outline**	027620

RMS Amps

		RMS Amps	
AB Code		**Peak**	
Resistance		**Peak@DegC**	
Connection			**Const Torque Speed Range**
Rework Status		**Rework TYPE**	

Explosion Proof Brake Mot

Temp Op Code

Class		GROUP:	
Class		GROUP:	
			Brake Co

Performance

Torque UOM	405 LB-IN		Inertia (WK²)	12.5
Torque	0	27		
CURRENT (amps)	.8	7.7		
Efficiency (%)	0	.842		.
PowerFactor				

Load Curve Data

Output Pwr (HP)	RPM	AMP	Torque (LB-IN)	Eff	Watts
0	1968	.8	0	0	70
.78	1830	7.7	27	.842	585
1.46	1702	15	54	.808	1088

SA, SF, DSA and DSF Series

18SA Net wt. 13 lbs.

Net wt. 13 lbs. 18SF

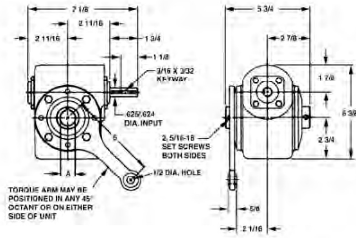

1.75" C.D.

A (BORE)		KEYWAY
.750	.751	3/16 x 3/32
.875	.876	3/16 x 3/32
.9375	.9385	1/4 x 1/8
1.000	1.001	1/4 x 1/8

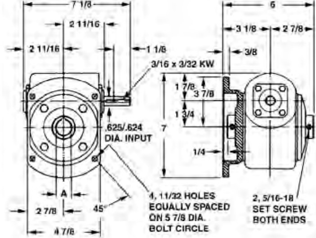

1.00 Service Factor* - Single Reduction Wormgear - Models 18SA and 18SF

TORQUE and HORSEPOWER RATINGS

RATIO	AT 1750 RPM INPUT			AT 1150 RPM INPUT			AT 870 RPM INPUT			AT 580 RPM INPUT			AT 300 RPM INPUT			AT 100 RPM INPUT		
	Input HP	Output R.P.M.	Output ▲Torque	Input HP	Output R.P.M.	Output ▲Torque	Input HP	Output R.P.M.	Output ▲Torque	Input HP	Output R.P.M.	Output ▲Torque	Input HP	Output R.P.M.	Output ▲Torque	Input HP	Output R.P.M.	Output ▲Torque
5	2.17	350.0	359	1.73	230.0	430	1.44	174.0	468	1.06	116.0	509	.61	60.0	551	.22	20.0	580
7.5	1.71	233.3	415	1.35	153.3	490	1.12	116.0	530	.82	77.3	571	.47	40.0	614	.17	13.3	643
10	1.42	175.0	447	1.12	115.0	527	.93	87.0	567	.68	58.0	610	.39	30.0	654	.14	10.0	682
15	1.06	116.6	479	.84	76.6	531	.70	58.0	603	.52	38.7	648	.30	20.0	693	.11	6.6	727
20	.85	87.5	490	.67	57.5	570	.56	43.5	611	.41	29.0	654	.24	15.0	698	.09	5.0	722
25	.71	70.0	494	.56	46.0	570	.47	34.8	608	.35	23.2	649	.20	12.0	688	.08	4.0	715
30	.63	58.4	494	.51	38.4	578	.43	29.0	620	.32	19.3	667	.19	10.0	711	.07	3.3	745
40	.50	43.7	489	.41	28.7	567	.34	21.8	607	.26	14.5	648	.15	7.5	694	.06	2.5	715
50	.41	35.0	471	.33	23.0	543	.28	17.4	578	.21	11.6	616	.13	6.0	658	.05	2.0	679
60	.34	29.2	446	.28	19.2	512	.24	14.5	545	.18	9.7	578	.11	5.0	615	.04	1.6	630

18DSA Net wt. 18 lbs.

1.75" C.D.

Net wt. 18 lbs. 18DSF

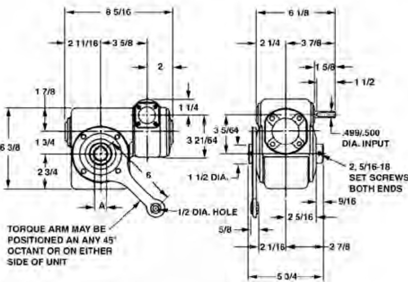

A (BORE)		KEYWAY
.750	.751	3/16 x 3/32
.875	.876	3/16 x 3/32
.9375	.9385	1/4 x 1/8
1.000	1.001	1/4 x 1/8

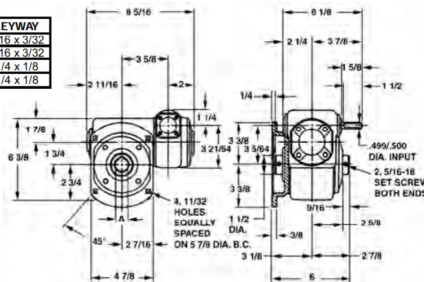

1.00 Service Factor* - Double Reduction Wormgear - Models 18DSA and 18DSF
1.33" Centers Primary - 1.75" Centers Secondary

TORQUE and HORSEPOWER RATINGS

RATIO	Primary Ratio	Secondary Ratio	AT 1750 RPM INPUT			AT 1150 RPM INPUT			AT 870 RPM INPUT			AT 580 RPM INPUT		
			Input HP	Output R.P.M.	Output ▲Torque	Input HP	Output R.P.M.	Output ▲Torque	Input HP	Output R.P.M.	Output ▲Torque	Input HP	Output R.P.M.	Output ▲Torque
75	5	15	.37	23.33	687	.26	15.33	706	.21	11.60	716	.15	7.73	725
100	5	20	.30	17.50	691	.21	11.50	710	.17	8.70	719	.12	5.80	728
125	5	25	.25	14.00	684	.18	9.20	702	.14	6.96	710	.10	4.64	719
150	10	15	.21	11.67	715	.15	7.67	725	12	5.80	730	.08	3.87	735
200	10	20	.17	8.75	718	.12	5.75	728	.10	4.35	732	.07	2.90	737
250	10	25	.15	7.00	710	.10	4.60	719	.08	3.48	723	.06	2.32	727
300	15	20	.13	5.83	728	.09	3.83	734	.07	2.90	737	.05	1.93	740
400	20	20	.10	4.38	732	.07	2.88	737	.06	2.18	739	.04	1.45	742
500	25	20	.09	3.50	735	.06	2.30	739	.05	1.74	741	.03	1.16	742
600	30	20	.08	2.92	737	.06	1.92	740	.05	1.45	742	.03	.97	743
800	40	20	.07	2.19	739	.05	1.44	742	.04	1.09	743	.03	.73	744
1000	50	20	.06	1.75	741	.04	1.15	742	.03	.87	743	.02	.58	744
1200	60	20	.05	1.46	741	.04	.96	743	.03	.73	744	.02	.48	745
1500	25	60	.04	1.17	645	.03	.77	648	.02	.58	650	.02	.39	651
1800	30	60	.04	.97	647	.03	.64	649	.02	.48	650	.02	.32	652
2400	40	60	.03	.73	648	.02	.48	650	.02	.36	651	.01	.24	652
3000	50	60	.03	.58	650	.02	.38	651	.02	.29	652	.01	.19	653
3600	60	60	.02	.49	650	.02	.32	652	.02	.24	652	.01	.16	653

▲ Inch-pounds

* Refer to page 386 for other service factors. Refer to pages 388 and 389 for torque arm and flange arrangements. Shaft mounted units will be furnished with torque arm or mounting flange on the side shown unless otherwise specified on order.
Consult Application Engineering (1 800 626 2093) for OHL and thrust load values.

Appendix C

MATLAB Code for Evaluating Model of Pressure Distribution

```
%This program is written for the sole purpose of
solving the hydrodymamic
%model for polish pressuse distribution developed by
Chen and Fang, IEEE
%TRANSACTIONS ON SEMICONDUCTOR MANUFACTURING, VOL.
15, NO. 1, FEBRUARY 2002
%pp39-44.

%Lucy Nolan, February 2011

close all; clear all

start1=tic;

% Define model parameters:
v=60;%rpm
hd=26.2; hd=hd*1e-9;

%These are all in metres, degrees, Pa or Pa.s
e=.17; u=0.0214; rho=1.300; a=0.0008;
hm=23.3*1e-6; r0=0.05;

% Chen&Fang Model

a=a/180*pi; %Convert tilt angle from deg to rad

%Calculate remaining model parameters
ep=hd/r0;
wp=v/30*pi;
if ep==0
    h0=hm+r0*sin(a);
else
    h0=hm+(sin(a)./(4*ep))*r0.*sin(a);
end
```

```
%Define r
syms r C

%Define model step interval (metres)
s=0.001;

%Find constant of integration

r=r0;
C = -(- log(18.*h0.^2.*r0.^4.*sin(a).^6 + 27.*r.^2.↙
*r0.^4.*sin(a).^8 + 24.*ep.^3.*h0.^5.*r0 ...
    + 24.*ep.^4.*h0.^4.*r.^2 + 84.*ep.*h0.^3.*r0.^3.↙
*sin(a).^4 ...
    + 6.*h0.^2.*r0.^3.*sin(a).^5.*(9.*r0.^2.*sin(a).↙
^2 + 24.*ep.*h0.*r0).^(1/2) ...
    + 106.*ep.^2.*h0.^4.*r0.^2.*sin(a).^2 + 9.*r.^2.↙
*r0.^3.*sin(a).^7.*(9.*r0.^2.*sin(a).^2 ...
    + 24.*ep.*h0.*r0).^(1/2) + 162.*ep.*h0.*r.^2.↙
*r0.^3.*sin(a).^6 ...
    + 20.*ep.^3.*h0.^3.*r.^2.*sin(a).*(9.*r0.^2.*sin↙
(a).^2 + 24.*ep.*h0.*r0).^(1/2) ...
    + 20.*ep.*h0.^3.*r0.^2.*sin(a).^3.*(9.*r0.^2.↙
*sin(a).^2 + 24.*ep.*h0.*r0).^(1/2) ...
    + 208.*ep.^3.*h0^3.*r.^2.*r0.*sin(a).^2 + 315.↙
*ep.^2.*h0.^2.*r.^2.*r0.^2.*sin(a).^4 ...
    + 14.*ep.^2.*h0^4.*r0.*sin(a).*(9.*r0.^2.*sin↙
(a).^2 + 24.*ep.*h0.*r0).^(1/2) ...
    + 57.*ep.^2.*h0.^2.*r.^2.*r0.*sin(a).^3.*(9.*r0.↙
^2.*sin(a).^2 + 24.*ep.*h0.*r0)^(1/2)...
    + 42.*ep.*h0.*r.^2.*r0^2.*sin(a).^5.*(9.*r0.^2.↙
*sin(a).^2 ...
    + 24.*ep.*h0.*r0).^(1/2)).*((e.*u.*wp)/(2000.↙
*h0.*sin(a)) ...
```

```
    + (3.^(1/2).*e.*u.*wp.*sin(a).*(3.*r0.^2.*sin↙
(a).^2 ...
    + 8.*ep.*h0.*r0).^(1/2))/(16000.*ep.*h0.^2.*sin↙
(a) + 6000.*r0.*h0.*sin(a).^3)) ...
    - log(18.*h0.^2.*r0.^4.*sin(a).^6 + 27.*r.^2.↙
*r0.^4.*sin(a).^8 + 24.*ep.^3.*h0.^5.*r0 ...
    + 24.*ep.^4.*h0.^4.*r.^2 + 84.*ep.*h0.^3.*r0.^3.↙
*sin(a).^4 ...
    - 6.*h0.^2.*r0.^3.*sin(a).^5.*(9.*r0.^2.*sin(a).↙
^2 + 24.*ep.*h0.*r0).^(1/2) ...
    + 106.*ep.^2.*h0.^4.*r0.^2.*sin(a).^2 - 9.*r.^2.↙
*r0.^3.*sin(a).^7.*(9.*r0.^2.*sin(a).^2 ...
    + 24.*ep.*h0.*r0).^(1/2) + 162.*ep.*h0.*r.^2.↙
*r0.^3.*sin(a).^6 ...
    - 20.*ep.^3.*h0.^3.*r.^2.*sin(a).*(9.*r0.^2.*sin↙
(a).^2 ...
    + 24.*ep.*h0.*r0).^(1/2) - 20.*ep.*h0.^3.*r0.^2.↙
*sin(a).^3.*(9.*r0.^2.*sin(a).^2 ...
    + 24.*ep.*h0.*r0)^(1/2) + 208.*ep^3.*h0.^3.*r.↙
^2.*r0.*sin(a)^2 ...
    + 315.*ep.^2.*h0.^2.*r.^2.*r0.^2.*sin(a).^4 ...
    - 14.*ep.^2.*h0.^4.*r0.*sin(a).*(9.*r0.^2.*sin↙
(a).^2 + 24.*ep.*h0.*r0)^(1/2) ...
    - 57.*ep^2.*h0^2.*r.^2.*r0.*sin(a).^3.*(9.*r0.↙
^2.*sin(a).^2 ...
    + 24.*ep.*h0.*r0).^(1/2) - 42.*ep.*h0.*r.^2.*r0.↙
^2.*sin(a).^5.*(9.*r0.^2.*sin(a).^2 ...
    + 24.*ep.*h0.*r0).^(1/2)).*((e.*u.*wp)/(2000.↙
*h0.*sin(a)) ...
    - (3.^(1/2).*e.*u.*wp.*sin(a).*(3.*r0.^2.*sin↙
(a).^2 ...
    + 8.*ep.*h0.*r0).^(1/2))/(16000.*ep.*h0.^2.*sin↙
(a) + 6000.*r0.*h0.*sin(a).^3)) ...
    + (e.*u.*wp.*log(ep.*r.^2 + h0.*r0))/(1000.*h0.↙
```

```
*sin(a)));

%Calculate pressure GRADIENT (kPa/m)

r=(0:s:(r0-s));
grad=(-12.*.001.*e.*wp.*sin(a).*r.*u)./(4.*(h0+ep.*↙
(r.^2/r0)).^3+...
    6.*r.^2.*sin(a).^2.*(h0+ep.*(r.^2/r0)));

%Calculate pressure (kPa)

p = C - log(18.*h0.^2.*r0.^4.*sin(a).^6 + 27.*r.^2.↙
*r0.^4.*sin(a).^8 + 24.*ep.^3.*h0.^5.*r0 ...
    + 24.*ep.^4.*h0.^4.*r.^2 + 84.*ep.*h0.^3.*r0.^3.↙
*sin(a).^4 ...
    + 6.*h0.^2.*r0.^3.*sin(a).^5.*(9.*r0.^2.*sin(a).↙
^2 + 24.*ep.*h0.*r0).^(1/2) ...
    + 106.*ep.^2.*h0.^4.*r0.^2.*sin(a).^2 + 9.*r.^2.↙
*r0.^3.*sin(a).^7.*(9.*r0.^2.*sin(a).^2 ...
    + 24.*ep.*h0.*r0).^(1/2) + 162.*ep.*h0.*r.^2.↙
*r0.^3.*sin(a).^6 ...
    + 20.*ep.^3.*h0.^3.*r.^2.*sin(a).*(9.*r0.^2.*sin↙
(a).^2 + 24.*ep.*h0.*r0).^(1/2) ...
    + 20.*ep.*h0.^3.*r0.^2.*sin(a).^3.*(9.*r0.^2.↙
*sin(a).^2 + 24.*ep.*h0.*r0).^(1/2) ...
    + 208.*ep.^3.*h0^3.*r.^2.*r0.*sin(a).^2 + 315.↙
*ep.^2.*h0.^2.*r.^2.*r0.^2.*sin(a).^4 ...
    + 14.*ep.^2.*h0^4.*r0.*sin(a).*(9.*r0.^2.*sin↙
(a).^2 + 24.*ep.*h0.*r0).^(1/2) ...
    + 57.*ep.^2.*h0.^2.*r.^2.*r0.*sin(a).^3.*(9.*r0.↙
^2.*sin(a).^2 + 24.*ep.*h0.*r0)^(1/2)...
    + 42.*ep.*h0.*r.^2.*r0^2.*sin(a).^5.*(9.*r0.^2.↙
*sin(a).^2 ...
    + 24.*ep.*h0.*r0).^(1/2)).*((e.*u.*wp)/(2000.↙
```

```
*h0.*sin(a)) ...
    + (3.^(1/2).*e.*u.*wp.*sin(a).*(3.*r0.^2.*sin↙
(a).^2 ...
    + 8.*ep.*h0.*r0).^(1/2))/(16000.*ep.*h0.^2.*sin↙
(a) + 6000.*r0.*h0.*sin(a).^3)) ...
    - log(18.*h0.^2.*r0.^4.*sin(a).^6 + 27.*r.^2.↙
*r0.^4.*sin(a).^8 + 24.*ep.^3.*h0.^5.*r0 ...
    + 24.*ep.^4.*h0.^4.*r.^2 + 84.*ep.*h0.^3.*r0.^3.↙
*sin(a).^4 ...
    - 6.*h0.^2.*r0.^3.*sin(a).^5.*(9.*r0.^2.*sin(a).↙
^2 + 24.*ep.*h0.*r0).^(1/2) ...
    + 106.*ep.^2.*h0.^4.*r0.^2.*sin(a).^2 - 9.*r.^2.↙
*r0.^3.*sin(a).^7.*(9.*r0.^2.*sin(a).^2 ...
    + 24.*ep.*h0.*r0).^(1/2) + 162.*ep.*h0.*r.^2.↙
*r0.^3.*sin(a).^6 ...
    - 20.*ep.^3.*h0.^3.*r.^2.*sin(a).*(9.*r0.^2.*sin↙
(a).^2 ...
    + 24.*ep.*h0.*r0).^(1/2) - 20.*ep.*h0.^3.*r0.^2.↙
*sin(a).^3.*(9.*r0.^2.*sin(a).^2 ...
    + 24.*ep.*h0.*r0)^(1/2) + 208.*ep^3.*h0.^3.*r.↙
^2.*r0.*sin(a)^2 ...
    + 315.*ep.^2.*h0.^2.*r.^2.*r0.^2.*sin(a).^4 ...
    - 14.*ep.^2.*h0.^4.*r0.*sin(a).*(9.*r0.^2.*sin↙
(a).^2 + 24.*ep.*h0.*r0)^(1/2) ...
    - 57.*ep^2.*h0^2.*r.^2.*r0.*sin(a).^3.*(9.*r0.↙
^2.*sin(a).^2 ...
    + 24.*ep.*h0.*r0).^(1/2) - 42.*ep.*h0.*r.^2.*r0.↙
^2.*sin(a).^5.*(9.*r0.^2.*sin(a).^2 ...
    + 24.*ep.*h0.*r0).^(1/2)).*((e.*u.*wp)/(2000.↙
*h0.*sin(a)) ...
    - (3.^(1/2).*e.*u.*wp.*sin(a).*(3.*r0.^2.*sin↙
(a).^2 ...
    + 8.*ep.*h0.*r0).^(1/2))/(16000.*ep.*h0.^2.*sin↙
(a) + 6000.*r0.*h0.*sin(a).^3)) ...
```

```
    + (e.*u.*wp.*log(ep.*r.^2 + h0.*r0))/(1000.*h0.↙
*sin(a));

%Find applied pressure by fitting a 2nd order↙
polynomial to r
%along the P(r) profile and then integrating that↙
profile by shells
syms b


F=polyfit(r,p,2);
G=int(F(1)*b^3+F(2)*b^2+F(3)*b,0,r0);

press=(2*pi*G)/(0.99*r0^2*pi)*0.145038;
psi=double(press)


toc(start1);
```